Catalysis Science & Technology

ROYAL SOCIETY OF CHEMISTRY

REVIEW

View Article Online
View Journal

Cite this: DOI: 10.1039/d5cy01579k

Supported carbon catalysts for the oxidative esterification of aldehydes, alcohols, and olefins

Krishnan Ravi,[a] Jacky Advani,[b] Sivashunmugam Sankaranarayanan,[c] Adam F. Lee,*[d] Karen Wilson*[e] and Martin Muhler *[af]

Received 22nd December 2025,
Accepted 16th April 2026

DOI: 10.1039/d5cy01579k

rsc.li/catalysis

Esters play a critical role in industrial chemistry, serving as key components in the production of fine chemicals, polymers, and liquid fuels. Although traditionally synthesised by acid esterification, esters can also be prepared by the direct oxidative esterification of diverse starting materials, including aldehydes, alcohols and olefins. Metal oxides are promising heterogeneous catalysts for oxidative esterification, and their use in conjunction with a support phase affords synergies that can promote performance. Carbon supports are ubiquitous in catalysis due to their tuneable porosity, acid–base properties, high conductivity and chemical stability. This review discusses recent advances in the oxidative esterification of alcohols, aldehydes, alkenes, and alkynes over carbon-supported catalysts, outlining the commercial importance of esters and traditional esterification methods, and potential advantages of oxidative esterification. Methods to synthesise carbon catalysts and bifunctional heteroatom-doped analogues are introduced, with resulting structure–activity relationships for oxidative esterification highlighted, including the role of radicals. The resulting insight helps to identify strategies to circumvent current challenges in oxidative esterification and future opportunities to apply this methodology.

1. Introduction

Esters are essential compounds in various fields of chemistry, serving as key components in the production of liquid biofuels/fuel additives and flavours and fragrances, including fatty acid alkyl esters (biodiesel), methyl valerate, methyl crotonate, and methyl decanoate.[1] They are also widely used as solvents, *e.g.*, ethyl acetate, methyl acetate, and ethyl levulinate, and as pharmaceuticals such as eugenol acetate, known for its antioxidant and antimicrobial properties,[2–4] and methyl salicylate, commonly used as a pain reliever and in wintergreen formulations.[5–7] Esters also find applications as plasticizers, such as bis(2-ethylhexyl) terephthalate (from the reaction of p-terephthalic acid and 2-ethylhexyl alcohol),[8,9] surfactants, food additives, and other industrially significant compounds (Fig. 1).[10] Their pleasant aroma/flavour and solvent properties render esters valuable in diverse industrial applications where they convey unique functionality that enhances the efficacy and consumer appeal of products.[11–14]

Ester production is economically significant within the global chemical industry, with the market predicted to grow from USD 104.6 billion (b) in 2025 to USD 178.7b by 2035.[15] Manufacturers including Lanxess, BASF SE, Cargill Incorporated, Exxon Mobil Corporation, Croda International Plc, NYCO, Ashland, DowDuPont, and Esterchem produce vast quantities of esters annually to meet the demand for pharmaceuticals, foods, and consumer goods.[16] The market price for methyl benzoate is ~USD 150 million (m), while ethyl acetate commands a significantly higher value at ~USD 4700m.[17] Bio-derived esters are also gaining traction, with methyl levulinate and ethyl levulinate estimated at ~USD 1500m and USD 55m, respectively.[17–20] Innovation in ester production through advanced catalytic processes is required to meet growing global demand while addressing sustainability concerns. Historically, ester synthesis has relied on acid-catalysed reactions between alcohols and carboxylic acids[21–23] or activated acid derivatives such as acyl chlorides and acid anhydrides (Scheme 1).[23,24] Homogeneous carbonylation of aryl halides can also produce acyl intermediates *in situ* that can be subsequently esterified with alcohols.[25] Historically, oxidative esterification employed

[a] *Laboratory of Industrial Chemistry, Department of Chemistry and Biochemistry, Ruhr-Universität Bochum, Universitätsstr. 150, 44801 Bochum, Germany. E-mail: martin.muhler@ruhr-uni-bochum.de*
[b] *Nanotechnology Centre, CEET, VŠB-Technical University of Ostrava, 17. Listopadu 2172/15, Ostrava-Poruba 708 00, Czech Republic*
[c] *Scientific and Technological Bioresource Nucleus (BIOREN), Universidad de La Frontera, Av. Francisco Salazar 01145, Temuco 4780000, Chile*
[d] *Institute of Materials Research and Engineering, Agency for Science Technology and Research, Singapore 138632, Singapore. E-mail: Adam_Lee_from.tp@a-star.edu.sg*
[e] *Centre for Catalysis and Clean Energy, Griffith University, Gold Coast QLD 4222, Australia. E-mail: karen.wilson6@griffith.edu.au*
[f] *Max Planck Institute for Chemical Energy Conversion, 45470 Mülheim an der Ruhr, Germany*

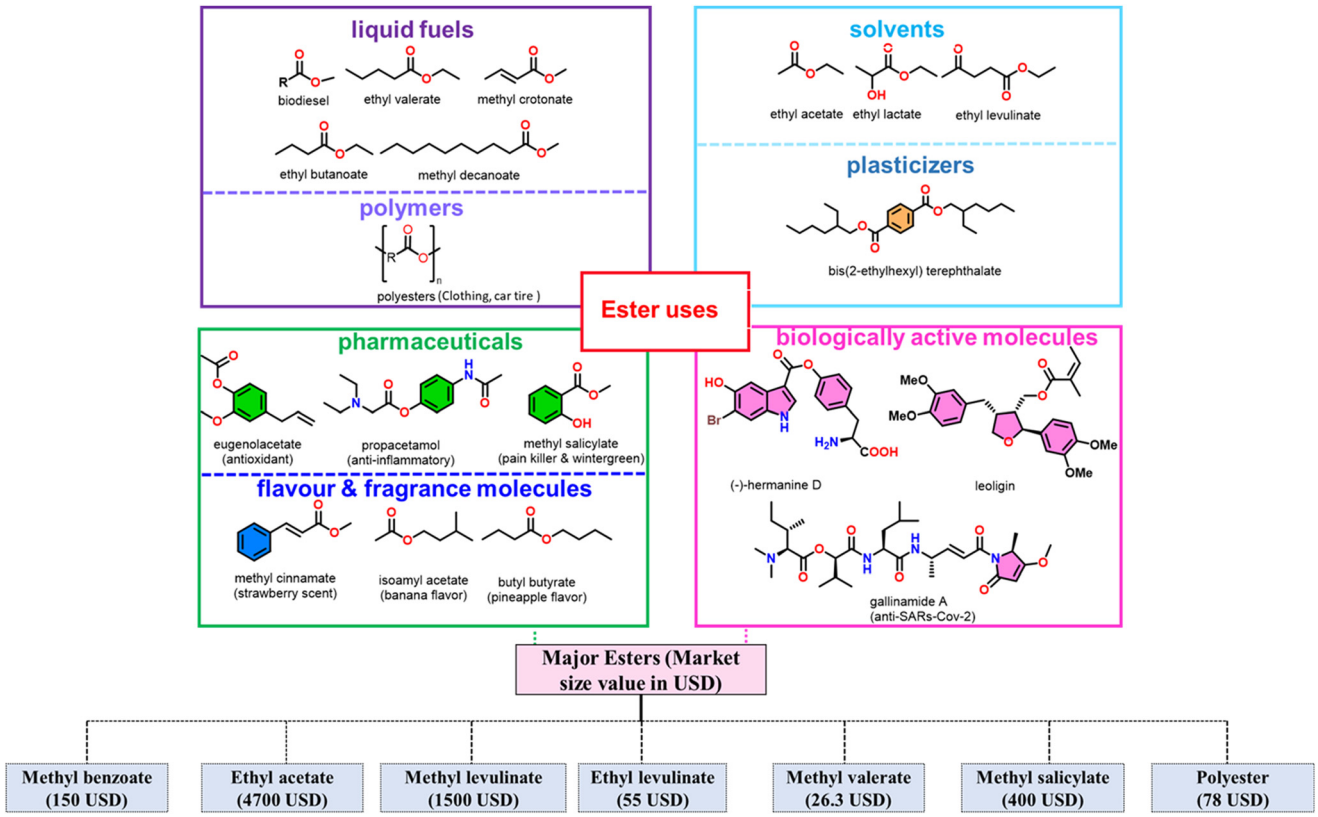

Fig. 1 Industrially important esters and their 2024 market values.[17–20]

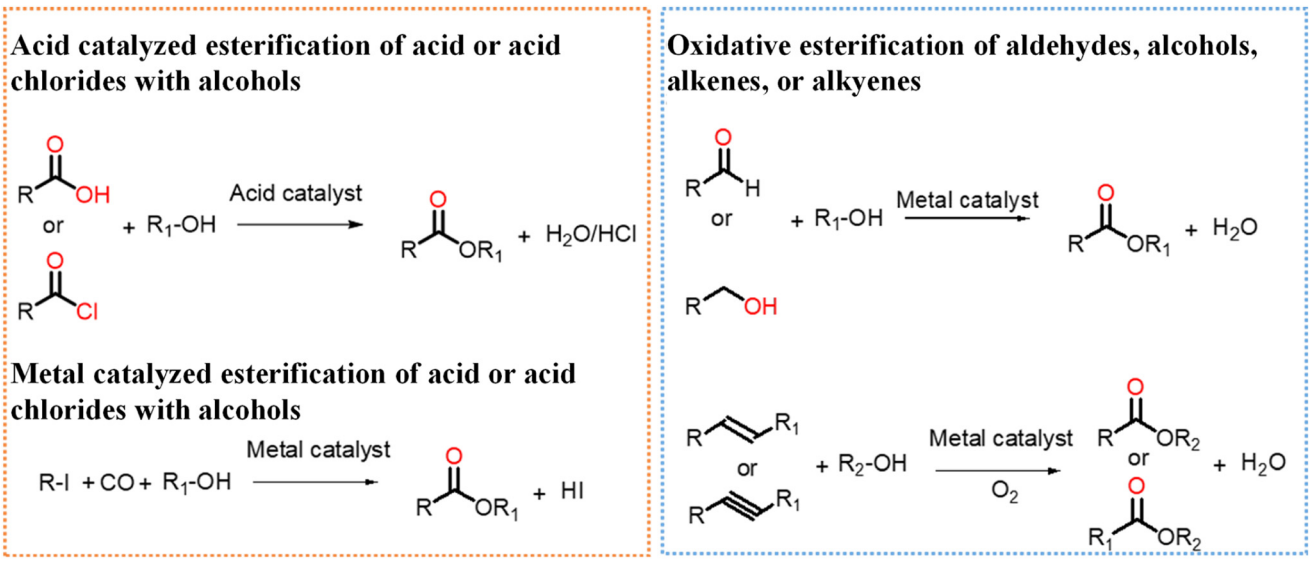

Scheme 1 (Left) Acid and metal catalysed esterification routes, and (right) oxidative esterification of diverse substrates to prepare esters.

homogeneous catalysts in combination with stoichiometric oxidants such as potassium permanganate ($KMnO_4$),[26] ozone (O_3),[27] oxone ($2KHSO_5{\cdot}KHSO_4{\cdot}K_2SO_4$),[28] tertiary butyl hydroperoxide (TBHP)[29] or hydrogen peroxide (H_2O_2).[30] Unfortunately, these generate significant waste by-products (including aqueous waste from quenching of soluble reagents and catalysts), employ hazardous conditions (*e.g.* associated with corrosive halogen species in carbonylation), and/or are energy intensive, necessitating more sustainable routes involving heterogeneous catalysts and dioxygen.[31] Although the use of O_2 as an oxidant would improve the atom-economy of oxidative esterification and simplify product

separation and catalyst reuse, the stable triplet O_2 ground state[11] must first be activated through energy or charge transfer processes.[32]

In most heterogeneous catalysts, the active phase primarily responsible for bond making/breaking is dispersed over and/or throughout a support matrix to increase the number and stability of surface active sites, by modifying the reactivity of existing active sites in the support, or introducing additional active sites or cooperative effects. Common supports include carbons and polymers, and mono- or mixed-metal oxides such as TiO_2, SiO_2, Al_2O_3, CeO_2, zeolites, and layered double hydroxides (Fig. 2).[33,34] Activated carbon, graphene, heteroatom-doped carbon, and mesoporous carbon are popular choices due to their advantageous properties outlined above, accessibility from abundant biomass feedstocks, and ease of surface functionalisation. Such attributes make carbon supports an attractive option for oxidative esterification and biomass valorisation,[35] for which their performance and economic feasibility can surpass simple oxides, as exemplified by the Au catalysed conversion of furfural to methyl 2-furoate (Scheme 2).[36] Gold nanoparticles dispersed over an ordered mesoporous silica (SBA-15), a carbon analogue created by carbonising sucrose with sulfuric acid in a SBA-15 template (CMK-3), or an unspecified titania phase (TiO_2) were all active for the oxidative esterification using excess TBHP oxidant. However, Au/TiO_2 and Au/SBA-15 respectively exhibited lower selectivity (80% *versus* 97%) and lower conversion (73% *versus* 78%) for the desired methyl 2-furoate than Au/CMK-3, which is thus more favourable for applications requiring a high purity ester. The superior performance of Au/CMK-3 was attributed to the combination of mesoporosity and high surface area which facilitate better dispersion of Au nanoparticles and faster mass transport. Electron transfer between the conductive CMK-3 support and Au nanoparticles was also suggested to confer a synergy that stabilises reaction intermediates. CMK-3 also exhibits excellent stability in the presence of a strong base, enabling the use of 1 bar O_2 as the oxidant in the presence of a Cs_2CO_3 cocatalyst to achieve a 72% yield of methyl 2-furoate. Previous reviews on the

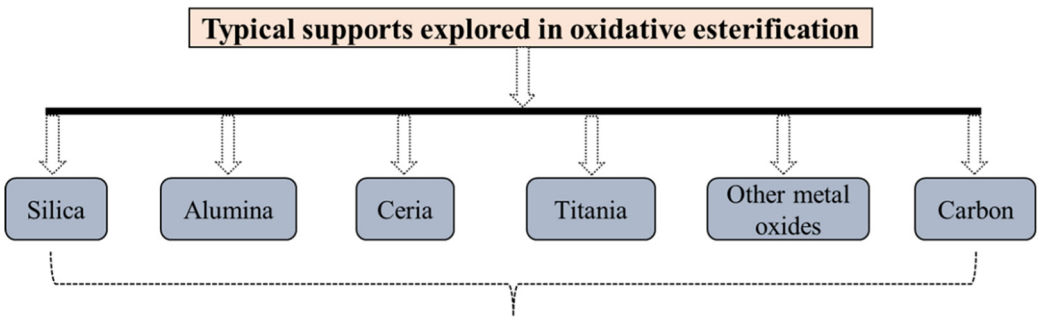

Comparative properties of carbon and other supports

Properties	Carbon	Other supports
Surface tunability	High	Moderate to low
Redox properties	Tunable via doping/support	Often intrinsic and fixed
Hydrophobicity	Tunable	Mostly hydrophilic
Metal dispersion	High	Moderate (aggregation)
Cost	Low	High

Catalytic oxidative esterification of furfural to methyl furoate over Au/different supports[36]

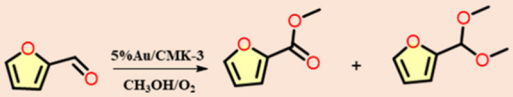

Catalyst	Conversion (%)	Selectivity (%)	Catalytic activity (mmol g cat^{-1}h^{-1})
Au/CMK-3	77.7	96.8	18.1
Au/SBA-15	73.0	99.8	17.5
Au/TiO_2	93.9	79.6	18.1

Reaction conditions: furfural (300 μL), TBHP (3 equiv.), 50 mg of catalyst with 5 wt.% Au loading in 20 mL methanol at 393 K for 3 h. CMK: Carbon Mesostructured from SBA-15 template, SBA-15: Santa Barbara Amorphous-15

Fig. 2 Comparison of carbon and oxide supports and their application to Au-catalysed oxidative esterification of furfural.[36]

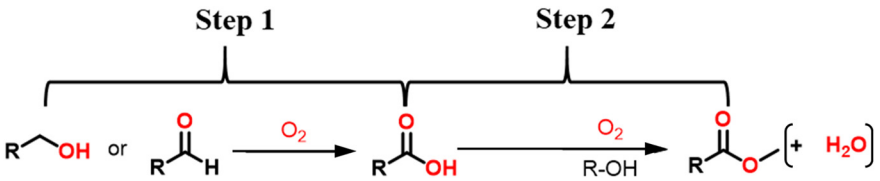

Scheme 2 Two-step oxidative esterification of alcohols or aldehydes.

oxidative esterification of alcohols with aldehydes have focused on direct conversion pathways using homogeneous metal complexes such as V_2O_5, $Fe(ClO_4)_3{\cdot}xH_2O$, $HAuCl_4$,[22] metal oxides,[23,37] (non)-noble metal catalysts including homogeneous (Ru(II) hydride),[38] and heterogeneous gold-based catalysts.[39] Other related reviews target either a narrow range of substrates[21,22,39–41] or a specific product such as furan-2,5-dimethylcarboxylate (from 5-hydroxy methyl furfural).[42] In contrast, this review critically examines the utility of carbon supported noble and base metal catalysts for the oxidative esterification of diverse substrates.

In oxidative esterification clearly demonstrate that carbon-based supports often outperform conventional oxide supports due to their unique textural and electronic properties. For example, in Pd-catalyzed oxidative esterification of benzyl alcohol, Pd supported on activated carbon (Pd/C) achieves nearly complete conversion and excellent ester selectivity under mild conditions, whereas homogeneous Pd salts or oxide-supported analogues typically show lower selectivity.[43] This enhancement is attributed to the high surface area and electron-rich nature of carbon, which improves metal dispersion and facilitates oxygen activation. Furthermore, carbon-based solid acid shows high turnover frequencies (TOF), demonstrating the superior intrinsic activity of carbon frameworks. Structural effects are also pronounced: two-dimensional carbon materials. The carbon supports not only enhance conversion and selectivity but also significantly improve intrinsic activity (TOF) relative to oxide and polymer supports, primarily due to better dispersion of active species, tunable surface chemistry, and improved reactant–catalyst interactions.[44]

2. Oxidative esterification

2.1. History and traditional methods

Oxidative esterification dates back to the early days of organic chemistry (Scheme 2) and was typically performed by the oxidation of alcohols or aldehydes to acids, hemiacetals, or other intermediates, which were then esterified.[45–48] In the late 1970s, oxidative esterification of various alcohols was reported using cyanide in combination with 3,4,5-trimethylthiazolium salts as oxidizing reagent systems. Subsequently, in 1988, bromine was employed as an oxidizing agent for the synthesis of esters.[22] More recently, homogeneous catalysis has been exploited, with significant progress made in 1980–90s on the development of metal-based catalysts for oxidative esterification.[49] In 1983, the homogeneous noble metal catalysts tetrakis(triphenylphosphine)palladium and palladium acetate were reported to facilitate the oxidative esterification of primary and secondary alcohols to esters.[49] Noble metals such as Pd,[50] Ir,[51] and Au (ref. 52) supported on various substrates became popular due to their high catalytic activity and selectivity[53] for the direct oxidative esterification of alcohols and aldehydes, often using O_2 as the oxidant. Later in the 2000, Au supported on CeO_2 and TiO_2 was reported for the aerobic oxidation of primary alcohols to esters.[54–56] This period also saw the introduction of bimetallic catalysts and the use of non-precious metals such as Cu (ref. 57) and Co (ref. 58) as cost-effective alternatives. At the beginning of the 21st century, the principles of green chemistry played a more prominent role in oxidative esterification research, with a focus on catalysts that could operate under milder conditions and with greener oxidants, such as molecular oxygen or air to minimise environmental impacts.[59] Different types of supported metal catalysts have been explored with metal–support interactions significantly influencing their catalytic performance.[60]

Porous solid acids such as zeolites[61] and metal–organic frameworks (MOFs)[62] are increasingly popular in commodity/fine chemicals manufacturing due to their high surface area and tuneable properties, and solid bases such as MgO,[63] hydrotalcite (HT),[64] layered double hydroxides (LDH),[65] and carbons also show promise.[66–68] In 2015, Jain and co-workers reported the oxidative esterification of aldehydes to the corresponding esters using graphene-supported Co_3O_4 with TBHP as the oxidant.[69] Most interest in the use of carbons for oxidative esterification[11,70,71] focuses on the role of oxygen-containing surface functions (*e.g.*, hydroxyl, carbonyl, and carboxyl groups) in enhancing the anchoring and dispersion of transition metal species and promoting catalytic activity through synergistic interactions. In 2019, tailored carbons, especially those derived from renewable sources like lignin, can also be engineered *via* doping (*e.g.*, with nitrogen or metals) and pyrolysis to form single-atom catalysts (SACs).[72] These SACs often exhibit enhanced catalytic efficiency and selectivity in oxidative esterification under mild conditions, with the different carbon functionalities acting as ligands to complex transition metal atoms.[72] Recent innovations have focused on tailoring carbon supports to improve the efficiency and sustainability of oxidative esterification[73,74] including the use of non-precious metals, and hybrid materials that combine metal and carbon

properties, and developing catalytic systems that can operate under ambient conditions.[75] Advanced techniques such as *in situ* spectroscopies can help elucidate catalyst behaviour and reaction mechanisms to identify active sites and thus guide the design of next-generation catalysts.[76,77] Such advances could lead to more efficient industrial processes with better environmental outcomes, promoting the adoption of oxidative esterification in fine chemical, pharmaceutical, and agrochemical production.[78] The oxidative esterification of aldehydes or alcohols is facilitated in the presence of a base, which neutralizes acidic by-products, stabilizes reaction intermediates, enhances the reaction rate, and promotes the nucleophilic activation of alcohols through alkoxide formation. This effect can be understood by comparing reactions carried out in the presence of sodium bicarbonate ($NaHCO_3$) as a base with different catalyst supports, including γ-A_2O_3, MgO, and hydrotalcite (HT).[37,48,61,79–90]

Compared with other supports (γ-A_2O_3, MgO, hydrotalcite (HT), MCM-41 and ZrO_2) carbons offer tuneable surface properties, enabling them to function as either acid or base supports depending on the specific requirements or reaction conditions.[80,81,88–90] The incorporation of heteroatoms such as phosphorus and boron into carbon frameworks imparts acidic character, whereas nitrogen doping introduces basicity.[68,91–93] Nitrogen-doped carbons have been extensively studied for oxidative esterification while phosphorus and boron functionalised acidic carbons have received limited attention, which may reflect the challenge in precisely controlling the acidity of such materials. Consequently, the development and application of acidic carbon-based catalysts in oxidative esterification remains an emerging area with significant potential for further exploration.

In oxidation reactions using carbon-based catalysts (such as activated carbon, graphene-derived materials, or doped carbon), the choice between flow and batch systems significantly influences catalytic performance, selectivity, and scalability.[94] In batch processes, reactants and catalysts are combined in a closed vessel, allowing extended contact time and straightforward control over reaction conditions; however, limitations such as poor mass transfer, catalyst deactivation due to product accumulation, and difficulty in heat management often arise, especially for gas–liquid or liquid–solid oxidations.[95] In contrast, flow systems (*e.g.*, fixed-bed or continuous-flow reactors) offer enhanced mass and heat transfer, continuous removal of products, and improved control over reaction parameters, which can lead to higher selectivity and prolonged catalyst lifetime. Carbon catalysts, particularly those functionalized with heteroatoms (N, S, or B doping), benefit from flow conditions because their active sites are more efficiently utilized and less prone to fouling. Additionally, flow setups facilitate safer handling of oxidants such as oxygen or hydrogen peroxide by minimizing their accumulation, making them preferable for industrial-scale oxidation processes. Despite these advantages, challenges in flow systems include reactor design complexity, catalyst packing issues, and potential pressure drop across the reactor bed. Overall, while batch systems remain valuable for mechanistic studies and small-scale synthesis, flow reactors are increasingly favoured for sustainable and scalable oxidation processes involving carbon-based catalysts.[94,96]

2.2. Carbon material development

The first use of carbons in catalysis can be traced back to the 1960s and 1970s,[97] with activated carbon (AC) and carbon black gaining prominence in the 1970s and 1980s[98] as high area supports for metal catalysts.[10] The focus during this period for oxidative esterification was mainly on homogeneous catalysts, which despite their high activity were problematic for separation and reuse. The transition from homogeneous to heterogeneous catalysis gained momentum in the 1990s,[99] when carbons such as AC, carbon black, and graphite were explored as supports for esterification and oxidation (Fig. 3).[100,101]

The thermal stability, chemical inertness, and tuneable surface properties of carbons render them attractive in catalysis.[104,105] The emergence of N-doped carbons, wherein the incorporation of nitrogen into carbon skeletons introduces basic sites through electron-donation, is beneficial for various oxidation reactions.[106–108] The early 2000s saw significant advances in the synthesis and application of N-doped carbons,[109] with methods developed to control the type and distribution of nitrogen species within the carbon matrix and hence optimise catalytic performance. Chemical vapor deposition (CVD), pyrolysis of N-containing precursors, and hydrothermal synthesis were used to produce such materials.[110] Consequently the use of N-doped carbon materials in oxidative esterification of aldehydes and alcohols gained traction.[111]

Use of AC supported metal catalysts for the oxidation of alcohols and aldehydes to esters[112–114] under harsh oxidation conditions and with homogeneous bases is undesirable. The 1990s therefore saw a shift towards designing more sustainable and environmentally friendly processes,[115] with the possibility to tune the surface functionality of carbon materials offering opportunities for bifunctional catalysis. During this period, various carbons, including mesoporous carbon and carbon nanotubes, were explored in oxidative esterification reactions.[77,116] These materials allowed better control of pore structure and surface properties, improving active site accessibility and catalytic performance. The emergence of N-doped carbons with varied doping levels and types of nitrogen species[117] offered significant improvements over traditional carbon catalysts with basic sites increasing catalytic activity and selectivity in oxidative esterification,[118,119] by facilitating activation of molecular oxygen. The last decade has also seen rapid progress in the development of more sophisticated carbons such as graphene oxide, carbon quantum dots, and MOFs derived carbons.[120] These materials have been used in various oxidative esterification processes and demonstrated high catalytic

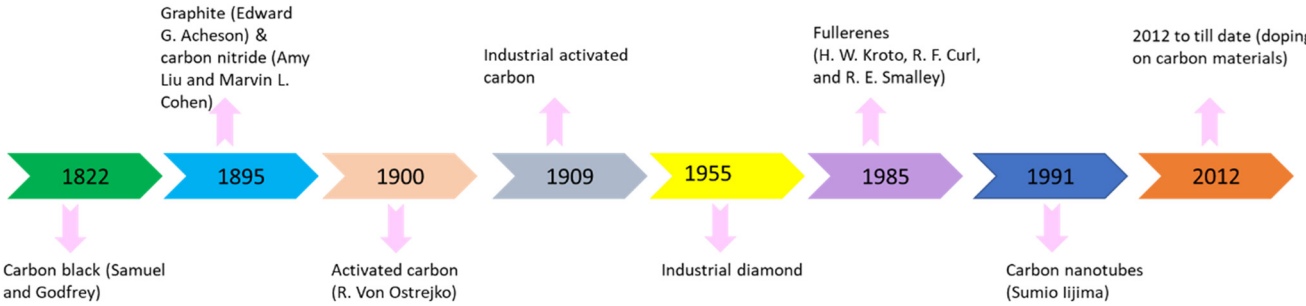

Fig. 3 Discovery of carbons and their use in catalysis.[102,103]

activity and selectivity.[83,121] The incorporation of metal nanoparticles on carbon supports, particularly N-doped carbons, has been notable, with hybrid catalysts combining the advantages of metal and carbon catalysts resulting in improved performance and stability.

2.3. Synthesis of heteroatom-doped carbons

Incorporating heteroatoms such as O, N, P, B, or S into carbons tunes the electronic structure, surface functionality, and chemical activity of the resulting materials.[122] Precise control of the doping process is essential to achieve uniform heteroatom dispersion, optimal activity and tailored structural features, and thus the synthesis method plays a key role in determining the extent and nature of doping. For example, *in situ* methods often result in higher doping levels and uniform dispersion of heteroatoms throughout the carbon matrix,[123] whereas post-functionalisation methods are more effective in modulating surface properties, allowing fine-tuning of active sites on the carbon material.[124] The synthesis and application of heteroatom-doped carbon catalysts are comprehensively reviewed elsewhere for various reactions.[125–127] Carbons can be prepared through various methods, each offering distinct advantages in terms of structural control, scalability, and cost (Fig. 4), including pyrolysis,[128–134] CVD,[135–138] hydrothermal carbonisation (HTC),[139–141] solvothermal route,[140] template-assisted routes,[139,142–148] mechanochemistry,[149–151] and electrochemistry.[152]

The preceding methods enable tailoring of surface area, porosity, morphology, and heteroatom doping to suit specific catalytic applications. Each technique varies in its ability to

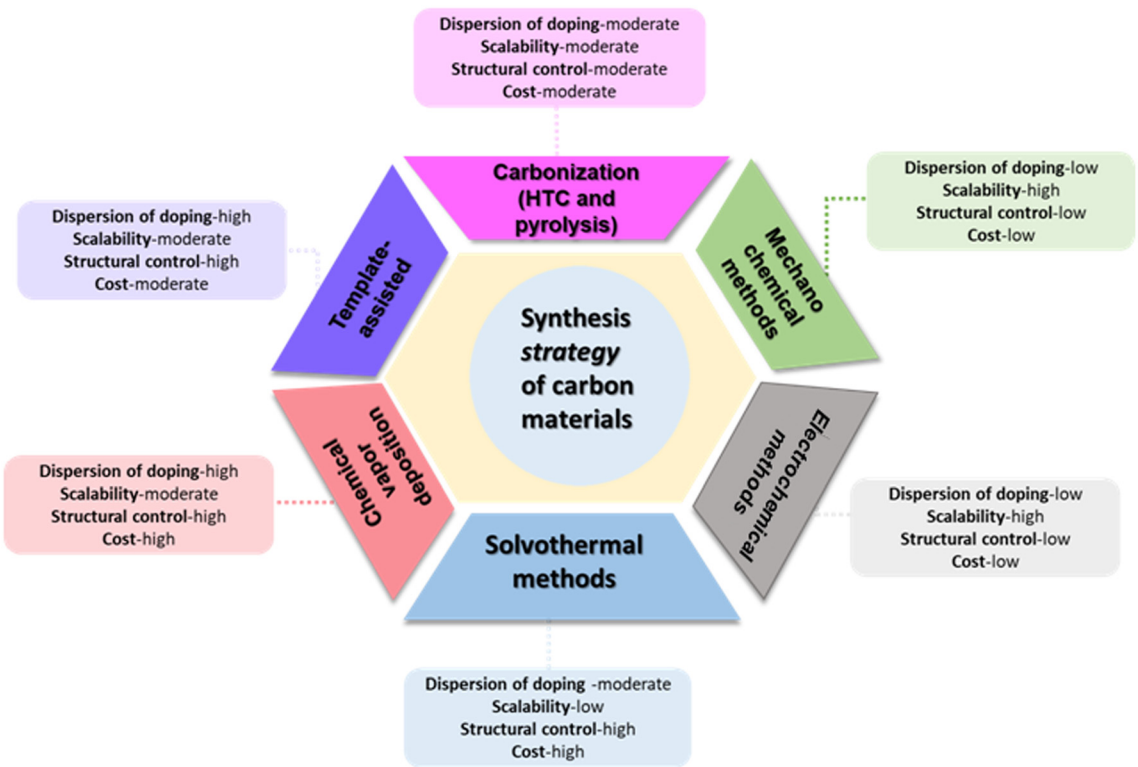

Fig. 4 Comparison of synthetic routes to heteroatom-doped carbons summarising doping efficiency, scalability, and cost.

achieve uniform metal dispersion, a critical factor for catalytic performance. Numerous review articles have comprehensively evaluated these synthesis strategies and merits in terms of metal loading efficiency, economic feasibility, and scalability.[141,153–169] Diverse carbonaceous precursors has been explored for the synthesis of functional carbons, each offering distinct structural and chemical characteristics that influence their catalytic performance (Table 1). Coal and heavy oil residues have long been utilised due to their high carbon content and availability. However, growing environmental concerns have directed interest toward more sustainable and renewable alternatives. Biomass-derived waste materials, including agricultural byproducts such as bagasse, coconut shells, corncob residue, and wheat straw, offer a cost-effective and eco-friendly route to porous carbons with tuneable surface functionalities. Animal-derived wastes such as crab shells (chitin/chitosan) are gaining attention in marine waste valorisation due to their high nitrogen and calcium content, which can aid in heteroatom doping and structural development. More recently, plastic waste has emerged as a non-conventional yet promising carbon precursor, supporting the circular economy by converting environmental pollutants into valuable carbon-based catalysts. The choice of precursor significantly influences the surface area, pore structure, and heteroatom content of the resulting carbon, and hence catalytic performance in oxidative esterification.[153,158,170–173]

Comparative analysis of synthesis routes to N-doped carbons/polymers from melamine and formaldehyde (Table 2) highlights notable differences in physicochemical properties. Mechanochemistry is particularly attractive for high area carbons (1080 $m^2\ g^{-1}$) and high N content (16 wt%). Although HTC delivered the highest N loading (48 wt%), the corresponding surface area is modest (328 $m^2\ g^{-1}$). In contrast, solvothermal routes produce low surface area carbons (205 $m^2\ g^{-1}$) and poor nitrogen retention. Pyrolysis delivers a balanced N content and surface area (657 $m^2\ g^{-1}$), whereas CVD yields the lowest surface area (39 $m^2\ g^{-1}$) albeit with 14 at% N-doping. Chemical activation of biomass feedstocks (bamboo sawdust precursors) achieves a high surface area (1069 $m^2\ g^{-1}$) and N content (13.3 at%). Mechanochemical and biomass activation methods are thus optimal for high surface areas and nitrogen loadings for oxidative esterification.[183]

To elucidate the influence of carbon sources and catalyst supports, Co-containing N-doped carbons and metal oxides (CeO_2, MgO, ZrO_2) were evaluated for the oxidative esterification of 5-HMF to 2,5-furandicarboxylic acid dimethyl ester (2,5 FDCA-DME). Co@CN-Zn12-5 (derived from chitosan) delivering the highest yield of 2,5 FDCA-DME (94%) with an activity of 261 mmol $g_{cat}^{-1}\ h^{-1}$ (Table 3). This performance was attributed to its large surface area (658 $m^2\ g^{-1}$) and accessibility to active sites, and uniform dispersion of Co species promoted by N-doping. In contrast, catalysts derived from sucrose–urea and 1,10-phenanthroline (surface areas of 40 and 369 $m^2\ g^{-1}$, respectively) were less effective. Although the 1,10-phenanthroline-derived catalyst showed an exceptional activity of 1700 mmol $g_{cat}^{-1}\ h^{-1}$, it only afforded only a 52% yield of 2,5 FDCA-DME, suggesting that undesired side reactions occurred under high oxygen pressure, illustrating a trade-off between activity and selectivity. In comparison, Co supported on MgO, ZrO_2, and CeO_2 showed markedly lower performance, with conversions <25% and yields <6%. The lower activities of these oxide systems ($\leq$17 mmol $g_{cat}^{-1}\ h^{-1}$) are likely due to their lower surface areas and poor stabilisation of Co active sites that lead to larger nanoparticles.

2.4. Bimetallic systems

Some binary metal combinations with N-doped carbons promote oxidative esterification, with the second metal either modulating the electronic properties of the principal metal active sites or facilitating key reaction steps (such as oxygen activation, reductive elimination, or hydrogen transfer). Such synergy between metals can improve selectivity and yield in oxidative esterification.[105,174] Incorporating Ni into Co_xNi_y-CNTs (CNT = carbon nanotubes) significantly enhanced catalytic performance by introducing new active sites containing Ni–N bonds. These Ni–N_x sites were proposed to facilitate electron migration between Ni and N atoms and thereby promote O_2 activation. Nickel addition also enhanced the basicity of Co-CNTs, thus favouring β-hydride elimination and the formation of carbonyl intermediates. FTIR identified showing that Ni–N bonds were responsible for substrate adsorption and promoted oxidative esterification.[175] Co_xCu_y-NC catalysts with varying Co : Cu molar ratios (9 : 1, 7 : 3, and 4 : 6) were also reported for the oxidative esterification of 5-HMF; a Co_7Cu_3-NC catalyst achieved a 95% yield of furan-2,5-dimethylcarboxylate. Copper addition was proposed to generate basic Co–N_x sites and hence promote β-hydride elimination of 5-HMF.[176]

Plasma modification has emerged as an effective and versatile strategy to tailor the surface properties of carbon-

Table 1 Carbonaceous precursors to functional carbons and their typical textural properties

Source	Method or activating agent	Surface area/$m^2\ g^{-1}$	Pore volume/$cm^3\ g^{-1}$	Ref.
Cornstalk	NaCI, KCl	1588	1.0	171
Chitin	$KMnO_4$	1488	1.3	171
Corncob residue	Steam	1210	0.7	171
Waste plastics	KOH	3200	3.7	160
Coal tar pitch + petroleum pitch	ZnO	1163	0.6	172
Coal tar	KOH	1215	0.7	172

Table 2 N-doped carbons/polymers from melamine with either formaldehyde or bamboo sawdust

Methods	Surface area/m^2 g^{-1}	Pore volume/cm^3 g^{-1}	N loading/wt% or at%	Treatment	Ref.
Templating	400–600	—	10	Pyrolysis under inert gas	173
Mechanochemical	1080		16	Room temperature ball milling (5–120 min)	177
CVD	39	—	14[a]	800 °C under H_2	178
HTC	328	2.1	48	150 °C	179
Pyrolysis	657	0.7	13	Flowing N_2	180
Solvothermal	205	0.6	—	DMF pretreated at 90 °C	181
Activated melamine/formaldehyde	2140	0.6	5[a]	KNO_3 activator	182
Activated melamine/bamboo sawdust[a,b]	1069	0.6	13	K_2CO_3 activator	183

[a] Atom%. [b] Bamboo sawdust as carbon source; N-doped carbon used for oxidative esterification of 5-HMF.

Table 3 Comparison of N-doped carbon and metal oxide supported Co catalysts for 5-HMF oxidative esterification

Catalyst (carbon source)	Surface area/m^2 g^{-1}	Pore volume/cm^3 g^{-1}	Reaction conditions	Conversion/%	Yield/%	Specific activity/mmol g_{cat}^{-1} h^{-1}	Ref.
Co@CN-Zn12-5 (chitosan)	658	—	0.3 mmol HMF, Co@CN-Zn12-5 (15 mol% Co), 3 mL MeOH, 1 bar O_2, 50 °C, 24 h	100	94	261	184
Sucrose, urea	40	—	0.5 mmol HMF, 100 mg Co/CoN/CN-700 (32 wt% Co), 5 mL MeOH, 1 bar O_2, 80 °C, 5 h	96	92	163	170
Co@NC-2ST	837	—	0.5 mmol HMF, catalyst (2.3 mol% Co), 5 mL CH_3OH, atmospheric air, 80 °C, 3 h	100	96	—	185
Co(1,10-phen)	369	0.50	0.5 mmol HMF, 25 mg Co_xO_y–N@C-800 (3% Co), 10 bar O_2, 60 °C, 12 h	100	52	1700	186
Co@MgO	—	—	0.3 mmol HMF, Co@CN-Zn12-5	12	—	—	184
Co@ZrO_2	—	—	(15 mol% Co), 3 mL MeOH,1 bar O_2,	19	2	5.56	
Co@CeO_2	—	—	50 °C, 24 h	25	6	16.7	

All carbons synthesised by pyrolysis.

based catalysts for oxidation reactions. Techniques such as oxygen, nitrogen, or argon plasma treatment enable the introduction or tuning of surface functional groups, defect density, and electronic structure without significantly altering the bulk properties of the carbon material. For instance, oxygen plasma can introduce oxygen-containing functionalities that act as active sites for oxidation reactions or improve wettability, while nitrogen plasma can incorporate pyridinic and graphitic nitrogen species that enhance electron transfer and facilitate oxygen activation.[187] Plasma treatment also increases surface defects and edge sites, which are often correlated with higher catalytic activity in reactions such as the aerobic oxidation of alcohols or hydrocarbons. Compared to conventional chemical oxidation methods, plasma modification is cleaner, faster, and more controllable, avoiding the use of harsh reagents and minimizing waste generation.[188] However, challenges remain in achieving uniform functionalization and maintaining long-term stability under reaction conditions. Overall, plasma-engineered carbon catalysts have shown improved activity, selectivity, and durability in oxidation processes due to their tunable surface chemistry and enhanced active site accessibility.[189]

2.5. Impact of physicochemical properties of catalyst supports

Hydrophobicity plays a crucial role in determining the activity and selectivity of carbon-based catalysts in oxidation reactions, particularly in aqueous or biphasic systems. Hydrophobic carbon surfaces such as those found in graphitized carbons, carbon nanotubes, or heteroatom-doped carbons tend to preferentially adsorb nonpolar organic substrates while repelling excess water, thereby enhancing substrate–catalyst interactions at active sites. This effect is especially beneficial in liquid-phase oxidations,[190] where water can otherwise block active sites or promote unselective side reactions. Increased hydrophobicity has also been shown to facilitate oxygen activation by stabilizing adsorbed oxygen species and improving electron transfer on the carbon surface.[191] Moreover, tuning the surface functional groups allows control over the hydrophobic–hydrophilic balance, which directly impacts catalytic turnover frequency and resistance to deactivation. However, excessively hydrophobic surfaces may limit accessibility for polar oxidants like hydrogen peroxide, indicating that an optimal balance is required. Overall, tailoring hydrophobicity is a key design

Table 4 Supported Au catalysts for benzyl alcohol (BA) oxidative esterification

Catalyst	Surface area/m^2 g^{-1}	Pore volume/cm^3 g^{-1}	Au loading	Reaction conditions	Conversion/%	Selectivity/%	Specific activity/mmol g_{cat}^{-1} h^{-1}	Ref.
Au/Al_2O_3	—	—	0.4 mol%	0.97 mmol BA, 100 °C, 10 bar O_2, 0.38 mol% catalyst, 1 ml water and 1 ml toluene, 1 h	100	10	2	200
Au/TiO_2			0.1 mol%	29 mmol BA, 0.1 mol% catalyst, 373 K, 10 bar O_2, 8 h	83	23	6	201
Au/CeO_2	39	—	1.0 wt%	2 g BA, 20 mg catalyst, 120 °C, 4 h	3.7	1.2	10	202
Au/Ce(30)–Al	272	12	1.9 wt%	2.5 mmol BA, 10 mg catalyst, 3 mL MeOH, 110 °C, 10 bar O_2, 10 h	85	15	3	203
Au/MgO	41	—	1.3 mol%	2.5 mmol BA, 10 mg catalyst, 2 mL MeOH, 110 °C, 10 bar O_2, 1 h	38	33[a]	31	204
Au/Au25 (PET)/GMS[b]	1738	3	0.33 mol%	5 mg catalyst, 300 mol% NaOH, 2 mL H_2O, 1 bar O_2, 30 °C	86	39	67	193

[a] Benzyl benzoate or methyl benzoate. [b] Aqueous solutions of benzyl alcohol (Au 0.33 mol%).

strategy for improving the efficiency and durability of carbon catalysts in oxidation chemistry.[192]

Gold/carbon catalysts (Table 4), such as partially thiolated Au_{25} nanoclusters in Au_{25}(PET)/carbon mesosponge (CMS) and Au_{25}(PET)/graphene mesosponge (GMS) materials, demonstrate excellent catalytic performance in the oxidative esterification of benzyl alcohol.[193] Au_{25}(PET)/GMS showed the highest catalytic activity, achieving 86% conversion and 39% selectivity under mild conditions (30 °C and 1 bar O_2), outperforming conventional Al_2O_3, TiO_2, CeO_2, Ce(30)–Al, and MgO supports. Although Au/Al_2O_3 showed 100% conversion it was only 10% selective to the ester product; Au/TiO_2 and Au/Ce(30)–Al achieved 83% and 85% conversion with 23% and 15% selectivity, respectively, whereas Au/CeO_2 and Au/MgO displayed significantly lower conversions of 4% and 38% and selectivities of 1% and 33%, respectively. The superior activity and selectivity of the carbon supported catalysts was attributed to their high surface areas (up to 1738 m^2 g^{-1}), dispersion of active gold species, and stability in alkali conditions. Mechanistic investigations revealed that the hydrophobic GMS support improved selectivity by suppressing the nucleophilic attack of hydroxide ions on the aldehyde intermediate and facilitating benzylic anion attack, and inhibiting hydrolytic degradation of the benzyl benzoate product.

To enhance pore order and surface area, mesoporous N-doped carbons synthesised using different sacrificial templates *e.g.*, MCM-41, ZSM-5, and SBA-15, have been used to prepare ordered metal/carbon catalysts denoted as Co-NOPC-M, Co-NOPC-Z, and Co-NOPC-S, respectively (Table 5). A strong correlation was observed between oxidative esterification performance and the presence of pyridinic nitrogen, with the MCM-41-templated catalyst (Co-NOPC-M) exhibiting the highest surface area (532 m^2 g^{-1}), proportion of pyridinic nitrogen, and smallest average Co nanoparticle size (2.8 nm, 2.7 wt% loading). These desirable properties were reflected in the oxidative esterification of furfural to methyl 2-furoate, wherein Co-NOPC-M achieved >99% conversion and a methyl 2-furoate selectivity of 96%. In contrast, Co-NOPC-S (derived from SBA-15) possessed a lower surface area (395 m^2 g^{-1}), pyridinic N content, and larger Co nanoparticles (3.5 nm), and only achieved 65% conversion and 46% selectivity. The lowest area (258 m^2 g^{-1}), and pyridinic N content Co-NOPC-Z catalyst exhibited the lowest Co dispersion (5.7 nm) and activity (43% conversion and 38% selectivity). These observations indicate a strong structure sensitivity, with small Co nanoparticles essential for high aldehyde conversion and ester selectivity. The influence of the N dopant was also investigated for Co@C catalysts. In the absence of nitrogen, a low methyl 2-furoate yield (12%) was observed, which increased to 98% for a N-doped Co@NC catalyst.[194] Comparison of different nitrogen species (pyridinic, pyrrolic, and indolic) identified pyridinic nitrogen as conferring the highest activity, ascribed to its Lewis

Table 5 Physiochemical properties of Co-NOPC catalysts[66]

Sample	Surface area[a]/m^2 g^{-1}	Metal loading[b]/wt%	Co particle size/nm	N content[c]/wt%	Pyridinic N[d]/wt%
Co-NOPC-M	532	2.7	2.8 ± 0.5	9.2	1.24
Co-NOPC-S	395	2.3	3.5 ± 0.7	7.9	0.82
Co-NOPC-Z	258	1.7	5.7 ± 1.4	8.3	0.43

[a] BET. [b] ICP-MS. [c] Organic element analyzer. [d] XPS.

basicity and localised lone electron pair, whereas cobalt coordinated to pyrrolic, graphitic, or pyridine N-oxide species either lacked basicity or exhibited reduced Lewis basicity due to "N" electron delocalisation across the carbon conjugated π-system.[67,195,196] These differing reactivity of N species was highlighted for benzyl alcohol oxidation, with N-doped graphene achieving 4% conversion and 100% benzaldehyde selectivity, whereas undoped graphene and AC showed negligible activity.[197] The chemical nature of N-dopants in carbons is thus as important as their concentration for oxidation catalysis.[198,199]

2.6. Structure–reactivity relationships of heteroatom-doped carbons

Heteroatoms such as N, B, P, and S introduced into carbons can create catalytically active sites for oxidative esterification. X-ray photoelectron spectroscopy (XPS) analysis reveals that N-doped carbons typically comprise four nitrogen species: pyridinic, pyrrolic, graphitic, and quaternary nitrogen (Fig. 5a and b). All these species promote electron transfer, acting as either electron-donors or -acceptors to activate molecular oxygen and organic substrates, or to modulate the electronic properties and stability of metal co-catalysts.[198,205] A study of N-doped carbon analogues for benzyl alcohol oxidative esterification revealed that pyridinic N was active under mild conditions whereas pyrrolic and graphitic N showed poor activity (Fig. 5c).[206] Comparing acridine (AD and pK_a: 5.6), phenanthridine (PAD and pK_a: 5.8), and phenazine (PZ and pK_a: 1.2) revealed AD (with pyridinic nitrogen) as the most active. Catalytic activity increased using larger π-conjugated model catalysts such as quinoline (QL) and dibenz[*a*,*i*]acridine (DBAD), suggesting that extended conjugation enhances electron transfer and substrate activation (Fig. 5d). Variations in edge configurations, such as zigzag *versus* armchair arrangements of pyridinic nitrogen, had minimal impact on the turnover frequency (TOF). The presence of pyridinic nitrogen was more important than its location. Pyridinic nitrogen is believed to promote aldehyde adsorption and the activation of molecular oxygen, while providing Lewis base sites that enhance the reactivity of adjacent carbon atoms for the activation of methylene groups in alcohols.

The role of active sites in N-doped carbon for oxygen activation during the oxidation of styrene to benzaldehyde using N-doped carbon derived from natural eumelanin (Table 6), AC, and the model molecular catalysts phenol (pK_a: 10), indole (containing pyrrolic N and pK_a: 16.2), pyridine (containing pyridinic N and pK_a: 5.2), benzyltrimethylammonium chloride, and cetylpyridinium chloride (containing quaternary N^+).[199] Neither AC nor phenol exhibited any oxidation activity, however indole, pyridine, benzyltrimethylammonium chloride, and cetylpyridinium chloride were active.

The preceding observation is consistent with other studies of alcohol oxidation over N-doped carbon catalysts, wherein nitrogen promoted benzyl alcohol oxidation (Table 7)[197,207] to achieve activities comparable to commercial Pt/C.[207] Pyridinic

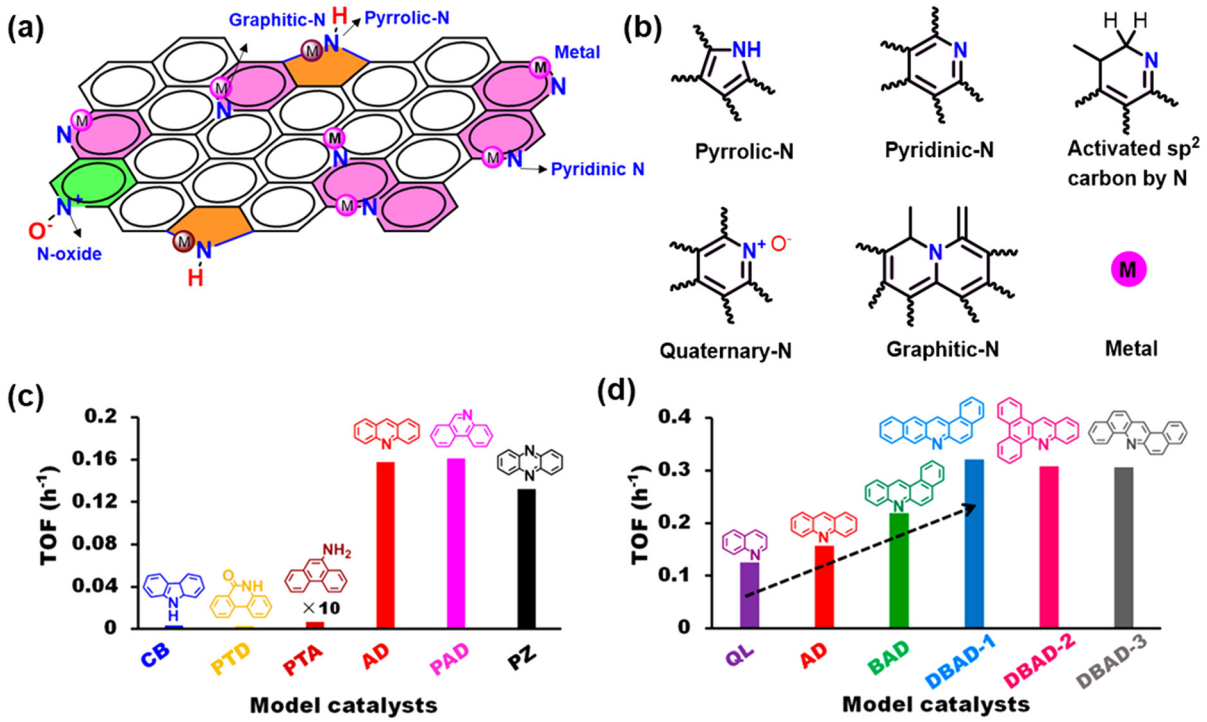

Fig. 5 (a) Nitrogen species present in N-doped carbons and common metal coordination sites, (b) molecular structures of N-species in N-doped carbons, and turnover frequencies (TOFs) of (c) different N-doped carbon (three ring) catalysts, and (d) pyridinic N-doped carbon catalysts (with extended π-conjugation) for the conversion of benzyl alcohol to benzaldehyde. Reaction conditions: 0.2 mmol catalyst, 2.0 mmol Ph-CH_2OH, 2 mmol TBHP, 5 mL ACN, 70 °C, 4 h. Reproduced with permission from ref. 189. Copyright 2019 American Chemical Society.

Table 6 Styrene oxidation to benzaldehyde over N-containing organocatalysts[188]

Entry	Model catalyst	Conversion/%	Selectivity/%			Catalytic activity/mmol g_{cat}^{-1} h^{-1}
			SO	BAL	Others	
1	AC	—	—	—	—	—
2		—	—	—	—	—
3		22	45	55	—	0.96
4	Eumelanin	4	—	48	52	0.15
5	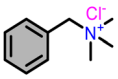	21	42	58	—	0.97
6	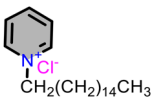	5	63	37	—	0.15
7	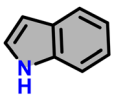	10	—	100	—	0.80
8[a]	PNDC + TEMPO	Trace	—	—	—	—

Reaction conditions: 1 mmol of styrene and 10 wt% of substrate to catalyst was dissolved in 1 mL of 1,4-dioxane for 12 h under 1 atm O_2.[a] TEMPO (1 mmol). SO: styrene oxide, BAL: benzaldehyde.

Table 7 Benzyl alcohol oxidation to benzaldehyde over graphene catalysts[186]

Entry	Substrate	Product	Catalyst	Temperature/°C	Conversion/%	Selectivity/%	Specific activity/mmol g_{cat}^{-1} h^{-1}
1	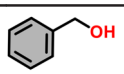	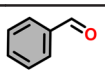	Undoped graphene	70	0.3	100	0.042
2	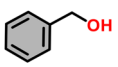		N-doped graphene	70	12.8	100	0.001

Reaction conditions: 30 mg catalyst; 0.1 mmol BA, 80 mL H_2O; 1300 rpm; 10 h.

and quaternary N species were particularly effective, achieving 12% conversion.[208] Mechanistic studies indicate the reaction proceeds *via* epoxide and peroxide intermediates through a radical mechanism. 1-Benzyl-4-cyanopyridin-1-ium bromide, which contains a pyridinium moiety, achieved 39% conversion of *p*-xylene under aerobic oxidation conditions, although tetrabutylammonium bromide (TBAB) only achieved 4% conversion, highlighting the importance of pyridinium functions. Studies of *N*-alkyl pyridinium salts for the aerobic oxidation of methyl aromatic hydrocarbons revealed that *N*-alkyl pyridinium salts enhance the decomposition of peroxide intermediates; 1-benzyl-4-cyanopyridin-1-ium bromide catalyses the decomposition of 35% of TBHP, whereas the uncatalysed reaction achieves only 10% decomposition.[208]

Building on the promise of N-doped carbons for benzyl alcohol oxidation their role in esterification has also been explored. In the absence of noble metals, it is notable that (metal-free) N-doped mesoporous carbon efficiently catalyse the oxidation of various alcohols such as benzyl alcohol, 5-HMF, cyclohexylmethanol, 1-heptanol, and cinnamyl alcohol to the corresponding carbonyl compounds, and tandem oxidative esterification of benzyl alcohol to methyl benzoate in methanol (Table 8).[207] N-doped carbons from biomass-derived bamboo sawdust and melamine can also facilitate the oxidative transformation of HMF to value-added furan derivatives such as 2,5-furandicarboxylic acid (FDCA) and methyl-5-formylfuran-2-carboxylate (MFFC) in the absence of homogeneous base.[183]

Synergies in the oxidative esterification of 5-HMF to dimethyl furan dicarboxylate (DMFDCA) are reported for Co@C–N catalysts (Table 9). Co@C–N was synthesised *via* precipitation of a ZIF-67 precursor and its subsequent pyrolysis at 600–900 °C under an Ar atmosphere (denoted as Co@C–N(600), Co@C–N(700), Co@C–N(800), and Co@C–N(900)). For comparison, a Co@C(800) sample was synthesised by mixing Co and trimesic acid followed by

Table 8 Alcohol oxidation to aldehydes over N-doped carbon and Pt/C catalysts[207]

Entry	Substrate	Product	Catalyst	Time/h	Conversion/%	Selectivity/%	Specific activity/mmol g_{cat}^{-1} h^{-1}
3	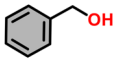		100 mg N-doped carbon	5	23	100	0.25
4	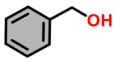		10 mg Pt/C	0.5	7	100	15.4
5	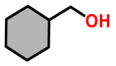		100 mg N-doped carbon	5	0	—	—
6	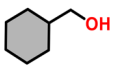		10 mg Pt/C	5	20	—	—
7[a]	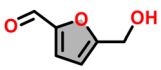	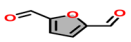	100 mg N-doped carbon	15	24	93	0.16
8[a]	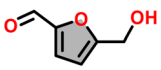	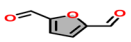	10 mg Pt/C	5	29	0	—

Reaction conditions: 5 mL ethanol, 1.1 mmol alcohol, 120 °C.[a] 80 °C.

Table 9 Oxidative esterification of HMF to DMFDCA over carbon catalysts[72]

Entry	Catalyst	Conversion/%	DMFDCA yield/%	Specific activity/mmol g_{cat}^{-1} h^{-1}
1	—	21	<1	0.01
2	AC	25	<1	0.01
3	C–N	85	12	0.12
4	Co	38	<1	0.01
5	Co + C	28	2	0.02
6	Co + C–N	86	13	0.13
7	Co@C(800)	60	18	0.18
8	Co@C–N(800)	99	98	

Reaction conditions: 100 mg catalyst, 0.5 mmol HMF, 30 mol% Na_2CO_3 (*vs.* HMF), 5 mL MeOH, 2 MPa O_2, 100 °C, 5 h.

pyrolysis at 800 °C for 6 h. The Co@C–N(800) catalyst achieved 99% 5-HMF conversion and 98% selectivity to DMFDCA. Controls without a catalyst or using AC resulted in low 5-HMF conversion and a negligible DMFDCA yield (Table 9, entries 1 and 2). Some activity was retained after treating Co@C–N(800) with *aqua regia* to remove cobalt (Table 9, entry 3), suggesting a contribution from the N-doped carbon or incomplete Co removal. Reduction of Co@C–N(800) at 400 °C under H_2 formed metallic cobalt but suppressed activity (Table 9, entry 4) which may reflect sintering of Co or the need for electron-deficient Co^{n+}. A physical mixture of metallic cobalt and AC also showed poor activity (Table 9, entry 5) whereas combining metallic cobalt with a N-doped carbon improved the DMFDCA yield (Table 9, entry 6), albeit this was not superior to the leached N-doped carbon (Table 9, entry 3). Nitrogen-free Co@C(800) produced 18% DMFDCA (Table 9, entry 7) indicating that unreduced Co species can drive oxidative

Table 10 Catalytic oxidative esterification of furfural over various catalysts[36]

Catalysts	Conversion/%	Selectivity/%		Specific activity/mmol g_{cat}^{-1} h^{-1}
		Methyl 2-furoate	4-Furaldehyde-dimethyl-acetal	
Au/CMK-3	78	97	3	18
Pd/CMK-3	80	92	8	19
Pt/CMK-3	60	88	12	15
Ni/CMK-3	29	100	—	7
Au/SBA-15	73	>99	—	16
Au/graphite	76	87	13	18
Au/graphene	41	85	15	10
Au/MWCNT	73	93	7	18
Au/AC	27	99	1	7
Au/TiO_2	94	80	20	20

Reaction conditions: 300 μL furfural, 3 eq. TBHP, 50 mg catalyst, metal loading 5 wt%, 20 mL MeOH, 393 K, 3 h.

esterification. Understanding the origin of this synergy between metals and N-doped carbons requires further investigation.[72,87,207,209]

3. Oxidative esterification over carbon catalysts

Having outlined the general properties of carbon catalysts for oxidative esterification, the oxidative esterification of aldehydes, alcohols, and olefins over carbons is now critically assessed in more detail.

3.1. Oxidation of aldehydes to esters

The selective oxidation of aldehydes to their corresponding esters is a fundamental chemical transformation in the laboratory and on at industrial scale. Base-free aerobic oxidative esterification of furfural using Co, Ni, and bimetallic $Co_{0.8}Ni_{0.2}$ nanoparticles immobilised on CNTs has been explored.[175] Co-CNTs achieved 75% furfural conversion and a 67% yield of methyl furoate whereas Ni analogues only achieved 26% conversion and 11% yield. However, despite these differences between the individual metals, bimetallic variants ($Co_{0.8}Ni_{0.2}$-CNTs) delivered a 94% yield of methyl furoate attributed to cooperativity between Co–N_x and Ni–N_x sites: Co–N_x was responsible for oxygen activation, with Ni–N_x proposed to enhance basicity and β-hydride elimination, while favouring the adsorption of furfural *via* the aldehyde group. The surface composition of $Co_{0.8}Ni_{0.2}$-CNTs revealed three different N species with photoelectron binding energies of 398.4, 399.9, and 400.9 eV, assigned to pyridinic, pyrrolic, and graphitic N species respectively; the former increased with the Ni content of $Co_{0.8}Ni_{0.2}$-CNTs. Base-free aerobic oxidative esterification of furfural was also studied over Au, Pd, Pt, and Ni doped mesoporous carbons (CMK-3) synthesised by a nanocasting method from SBA-15 hard template. Au/CMK-3 exhibited superior catalytic activity for the oxidative esterification of furfural (Table 10), achieving a 78% conversion and 97% selectivity to methyl 2-furoate. Although Ni/CMK-3 was 100% selective to the desired ester, furfural conversion was only 29%. Comparison with different supports, including graphite, graphene, AC, and TiO_2, confirmed Au/CMK-3 as optimal; despite a high conversion, Au/TiO_2 exhibited poor ester selectivity, producing significant acetal biproduct a likely consequence of its higher support acidity.[36]

Oxidative esterification of furfural over Co–N–C/MgO catalysts attained in 93% and 99% selectivity to methylfuroate (Fig. 6a). To explore the impact of solid base, the catalyst was treated with HCl to remove the MgO support resulting in primarily acetal production (Fig. 6b and c). Investigations under a nitrogen atmosphere confirmed that ester production was dependent on the support material, with MgO facilitating dehydrogenation reactions. Doping the HCl-treated Co–N–C catalyst with MgO restored ester formation, highlighting the importance of support basicity in promoting oxidative esterification over carbons.[66]

Table 11 compares selected literature reports of the catalytic oxidative esterification of aldehydes. Metal free, Au, Cu, and Co carbon catalysts have been studied reported for the oxidative esterification of benzaldehyde, furfural, and 4-methylbenzaldehyde, with Au/carbons exhibiting the highest activities, reaching 58 mmol g_{cat}^{-1} h^{-1} (Table 11, entry 3). In all cases, oxidation was highly selective to the ester. Supporting Co on a N-doped highly (meso)porous carbon (HC) improves it activity to 48 mmol g_{cat}^{-1} h (Table 11, entry 7). However, the high conversions used in these studies prohibit their quantitative comparison as catalysts were operating under mass transport limited conditions. This hinders observation of structure–activity relationships, and for the field to advance future studies must focus on measuring intrinsic catalyst activity and selectivity under (low) iso-conversion of aldehydes. Benchmarking different catalysts is also hindered by the wide range of oxygen pressures and substrate:catalyst concentrations employed, and occasional use of soluble bases. CuC_4/CoN_4@HC catalysts synthesised *via* molten salt assisted pyrolysis followed by a "misplaced deposition" strategy (Fig. 7a) are also reported for the oxidative esterification of furfural with methanol. Monometallic Co and Cu catalysts exhibited lower furfural conversions than bimetallic CuCo counterparts, with CuC_4/CoN_4@HC achieving complete furfural conversion and 100% selectivity to the ester. Density functional theory (DFT) calculations identified the Co sites as responsible for O_2 activation. CuC_4 adsorbed O_2 with a 1.23 Å O═O bond length, insufficient to activate the molecular bond, whereas CoN_4 sites strongly adsorbed O_2 (−0.64 eV) accompanied by a significant stretching of the O═O bond (Fig. 7b). Genesis of CoN_4 sites was essential to achieving high activity in CuC_4/CoN_4@HC catalysts.[210] The effect of N and S dopants on furfural oxidative esterification was explored for hollow carbon-encapsulated Cu/Co_2P nanoparticles (denoted as Cu/Co_2P@C-NS)[211] derived by pyrolysis of a ZIF-67 core coated with a poly(cyclotriphosphazene-*co*-4,4′-sulfonyldiphenol) shell that coordinates Cu^{2+} species. This catalyst achieved high conversion and 99% selectivity towards methyl furoates, attributed to a synergy between Cu and Co_2P components, although the performance of Co@C–N and Co_2P@C-NS controls and Cu/Co_2P@C-NS was compared at >99% conversion under which reactions were diffusion-limited hindering quantitative assessment of the benefits of N/S co-doping.

There are a few reports on the photocatalytic oxidative esterification of aldehydes (Table 11, entries 12–15), and none that provide apparent quantum yields which is critical for quantitative benchmarking to account for different spectral outputs and light fluxes. Inorganic semiconductor photocatalysts are reported for the conversion of benzaldehyde to methyl benzoate using alcohols. A Ag/CeO_2-rGO catalyst achieved 89% conversion and 99% selectivity to methyl

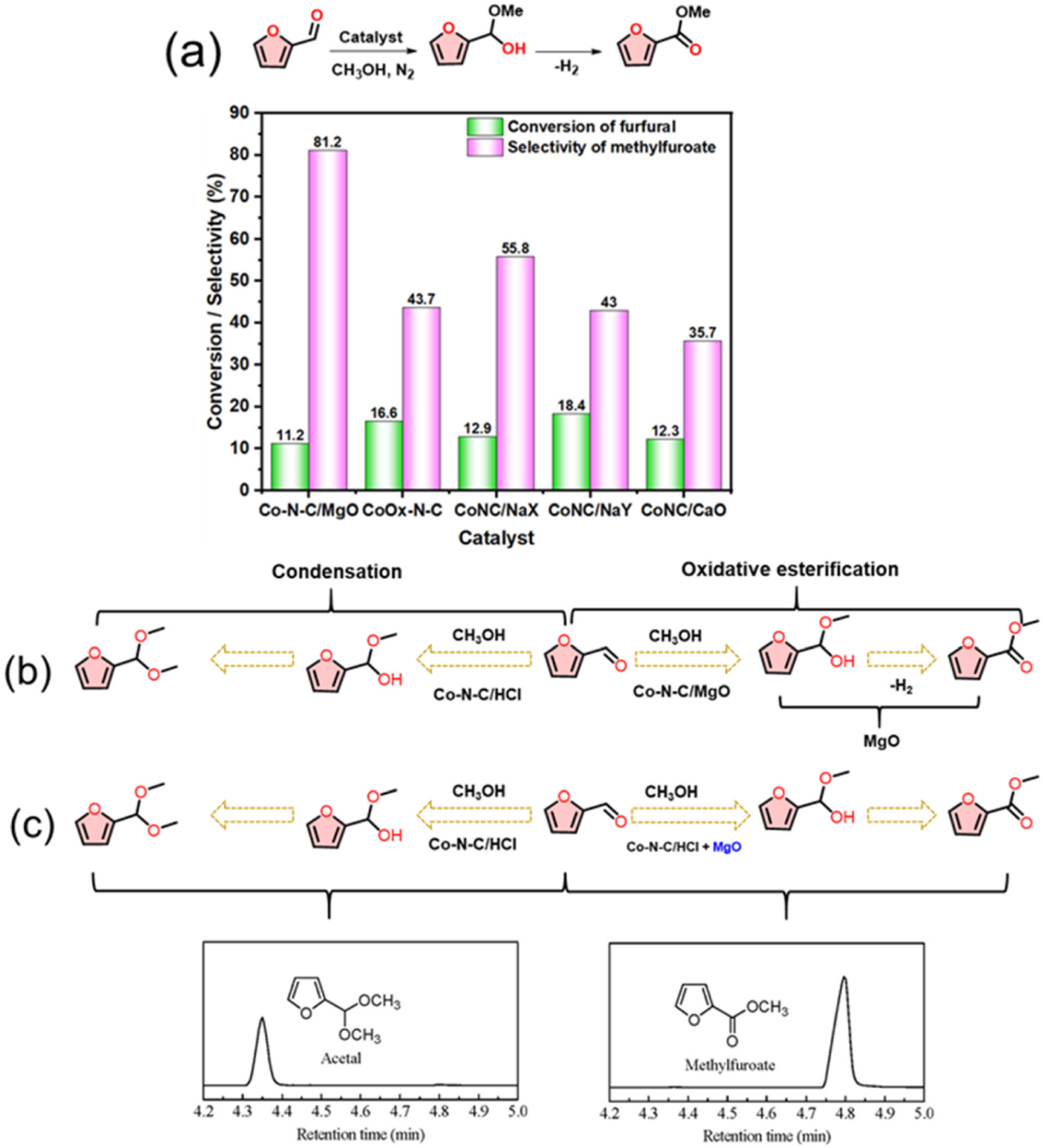

Fig. 6 (a) Dehydrogenative esterification of furfural with methanol. Reaction conditions: 0.5 mmol furfural, 80 mg catalyst, 5 mL MeOH, 100 °C, 0.1 MPa N_2, 12 h. (b and c) Control experiments wherein MgO is leached away by HCl and then replenished.[66] Reproduced with permission from ref. 61. Copyright 2017 Elsevier.

benzoate under visible light (400–800 nm) with a specific activity of 5.39 mmol g_{cat}^{-1} h^{-1} at 25 °C (Table 11, entry 12). Co@npg-C_3N_4 also showed 97% and 96% selectivity to methyl benzoate under visible light, but with a lower activity of 0.78 mmol g_{cat}^{-1} h^{-1} (Table 11, entry 13). In contrast, pristine g-C_3N_4 and mesoporous g-C_3N_4 (mpg-C_3N_4) only afforded 32% and 20% benzyl alcohol conversion respectively, with corresponding activities of 0.08 and 0.33 mmol g_{cat}^{-1} h^{-1} (Table 11, entries 14 and 15). Although metal co-catalysts appear necessary to stabilise separated photoexcited charges, and oxygen activation, for efficient photocatalysis, the modest activity of mpg-C_3N_4 shows the promise of metal-free photocatalyst for the oxidative esterification of aldehydes to esters, with the reaction proposed to proceed *via* the a hemiacetal intermediate (Scheme 3).[218]

3.2. Oxidation of alcohols to esters

The selective oxidation of alcohols can also be used to drive oxidative esterification cascades (Scheme 2); a recent

Table 11 Summary of carbon catalysts for oxidative esterification of aldehydes to esters

Entry	Catalyst	Substrate	Oxidant/additive	Reaction conditions	Conv./%	Sel./%	Specific activity/mmol g_{cat}^{-1} h^{-1}	Ref.
1	$Co_{0.8}Ni_{0.2}$-CNTs	FF	O_2	0.3 mmol furfural, 0.05 g catalyst (2.5 wt% total metal), 3 mL MeOH, 20 bar O_2, 100 °C, 3 h	>99	>99	2	175
2	5% Au/CMK-3	FF	O_2	300 μL furfural, 0.05 g catalyst (5 wt% Au), 20 ml MeOH, 15 bar O_2, 100 °C, 3 h	>99	>99	24	36
3	Au@UiO-66-COOH	FF	O_2/K_2CO_3	0.1 g furfural, 25 mg catalyst (4.6 wt% Au), 15 mL EtOH, 3 bar O_2, 140 °C, 4 h	67	84	58	212
4	CMK-3@PDA/Pd	4-MBz	O_2/K_2CO_3	1 mmol 4-MBz, 0.1 mol% catalyst, 3 mL MeOH, O_2, 80 °C, 8 h	100	96	—	116
5	Co–N–C/MgO	FF	O_2/K_2CO_3	0.5 mmol furfural, 0.05 mmol Co catalyst, 5 mL MeOH, 5 bar O_2, 100 °C, 6 h	93	99	1	66
6	HCP-BzmimCl	FF	O_2/DBU	1 mmol furfural, 1 mmol catalyst, 2 mL MeOH, 5 bar O_2, 120 °C, 4 h	98	100	—	213
7	Co-NOPC-M	FF	O_2	50 mmol furfural, 0.5 g catalyst (4 wt% Co), 500 mmol MeOH, 5 bar O_2, 80 °C, 2 h	>99	96	48	68
8	CuC_4/CoN_4@HC	FF	O_2/K_2CO_3	0.5 mmol furfural, 5 mol% catalyst (1.20 Cu:1.84 Co mol%), 4 mL CH_3OH; 1 bar O_2, 50 °C, 2 h	100	100	—	210
9	Cu/Co_2P@C-NS-36 nm	FF	O_2/K_2CO_3	0.1 mmol furfural, 0.2 g catalyst (25 Cu:5 Co wt%), 2 mL MeOH, 20 bar O_2, 120 °C, 3 h	>99	99	1	211
10	Kaolin@CS-starch	4-MBz	O_2/K_2CO_3	1 mmol 4-MBz, 20 mg catalyst, 3 mL CH_3OH, O_2, 80 °C, 8 h	100	96	6	214
11	Graphite oxide	Bz	Oxone	1 mmol Bz, 0.2 g catalyst, 4 mL MeOH, 1 mmol oxone, 60 °C, 0.5 h	100	90	9	28

Photocatalytic conversion

Entry	Catalyst	Substrate	Light source	Reaction conditions	Conv./%	Sel./%	Specific activity/mmol g_{cat}^{-1} h^{-1}	Ref.
12	Ag/CeO_2-rGO	Bz	W lamp (400–800 nm)	1 mmol Bz, 20 mg catalyst (0.8 wt% Ag), 10 mL MeOH, O_2, RT, 8 h	87	99	5.4	215
13	Co@npg-C_3N_4	Bz	Visible ($\lambda > 400$ nm)	1 mmol Bz, 0.1 g catalyst (1 wt% Co), 5 mL MeOH, O_2, RT, 12 h	97	96	0.8	216
14	Graphitic C_3N_4	Bz	300 W Xe lamp with 420 nm UV cut-off filter	1 mL Bz, 0.1 g catalyst, 8 mL MeOH, 50 °C, 4 h	32	—	0.1	217
15	mpg-C_3N_4	Bz	300 W Xe lamp with 420 nm UV cut-off filter	1 mmol Bz, 50 mg catalyst, 5 mL EtOH; RT, 12 h	20	99	0.3	218

FF: furfural, Bz: benzaldehyde, 4-MBz: 4-methylbenzaldehyde, CNTs – carbon nanotubes, DBU-1, 8-diazabicyclo [5.4.0] under-7-ene, Au@SiO_2/ZA-SiO_2-coated Zn-Al hydrotalcite-supported Au NPs.

perspective on the use of carbons for the catalytic oxidation of HMF provides valuable insight in this regard.[11] Various carbons are demonstrated for the oxidative esterification of alcohols, including graphene, nanotubes, MOF-derived materials, and N, S, and/or P-doped carbons. Cobalt single atoms on N-doped carbons (Table 12, entry 2) exhibit the best performance with a specific activity of 220 mmol g_{cat}^{-1} h^{-1}, with the added advantage of not requiring soluble base (important to avoid the production of base-contaminated liquid waste); the intrinsic basicity of the dopant being sufficient. Nevertheless, most reports employ K_2CO_3 to increase the solution basicity.[195,219] Cobalt is particularly effective in combination with N-doped carbons for oxidative esterification, conferring high activity for benzyl alcohol and selectivity to methylbenzoate, even at 60 °C and 1 bar O_2 or air. However, activity and selectivity were strongly affected by substitution of the benzyl ring, with 4-methyl-, 4-methoxy-, and 4-nitro-substituents favouring high conversion (78%, 96%, and 69%, respectively) over a Co-MOF derived catalyst (Table 12, entry 9),[62] whereas benzyl alcohol and its 4-bromo-, and 4-chloro-analogues only achieved ~50% conversion. High ester selectivity was only attained for Br- (82%), Cl- (100%), and methyl- (78%) substituted benzyl alcohols, with the parent benzyl alcohol only undergoing oxidative

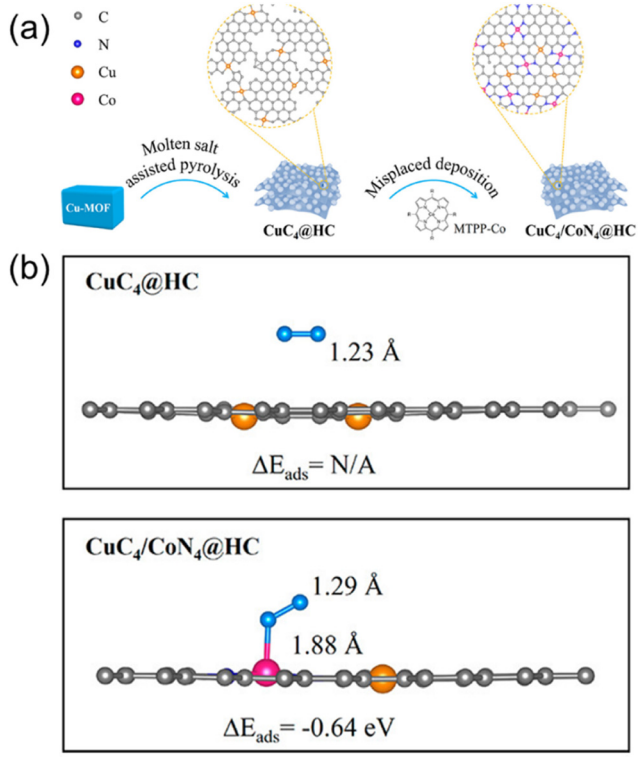

Fig. 7 (a) Schematic of CuC_4/CoN_4@HC synthesis, and (b) computed optimum configurations of molecular oxygen and CuC_4@HC *versus* molecular oxygen adsorbed on CuC_4/CoN_4@HC. O atoms in sky-blue; Cu atoms in orange; Co atoms in pink; carbon atoms in grey.[210] Reproduced with permission from ref. 210. Copyright 2021 American Chemical Society.

dehydrogenation to benzaldehyde. A separate study of 4-nitrobenzyl alcohol oxidative esterification over a different MOF-derived Co/carbon catalyst (Table 12, entry 10) observed a high ester selectivity,[12] although this was conducted using lower oxygen pressure and temperature, a much longer reaction time, and without K_2CO_3 additive. Moderate to high Co loadings are common, spanning 2 wt% (Table 12, entry 5) to 33 wt% (Table 12, entry 6), although there is no evidence of any structure-sensitivity in terms of rate or selectivity. While Au and Pd carbon catalyst have also been investigated, these show no benefits over Co analogues, and indeed the former generally exhibit lower rates, with the notable exception of Au-Pd/graphene prepared by deposition-precipitation of chloride salts (Table 12, entry 16) to yield bimetallic $Au_{2.5}Pd_{0.5}$ nanoparticles on graphene sheets which attained 40 mmol g_{cat}^{-1} h^{-1} at only 25 °C.[32] Reaction profiles indicated that benzyl alcohol was first selectively oxidised to benzaldehyde, with K_2CO_3 subsequently abstracting a hydrogen atom promoting O–H bond cleavage to form metal alkoxide and hydride species. Methanol reacts with benzaldehyde *via* nucleophilic addition reaction to form the hemiacetal intermediate which then undergoes oxidative dehydrogenation to yield methyl benzoate. Excitation of the Au surface plasmon resonance had no impact on reactivity.

Base-free oxidative esterification of alcohols to esters is also reported using a Co/N-doped carbons, wherein electron transfer across the Schottky barrier formed at the metal/N-doped carbon interface (Fig. 8) enhanced the oxidative esterification of alcohols to esters.[195] Nitrogen atoms bound to carbons acted as Lewis base sites, while metal atoms acted as Lewis acid sites. Carbon atoms nitrogen are can also activate small electron-rich molecules such as O_2, facilitating redox reactions.[233]

Bioinspired SACs comprising Fe, Co, Ni or Cu immobilised on N-doped carbons are reported for the base-free, aerobic oxidative esterification of primary alcohols. Their synthesis involved the coordination of metal ions with a phenolic network to form insoluble lignin complexes

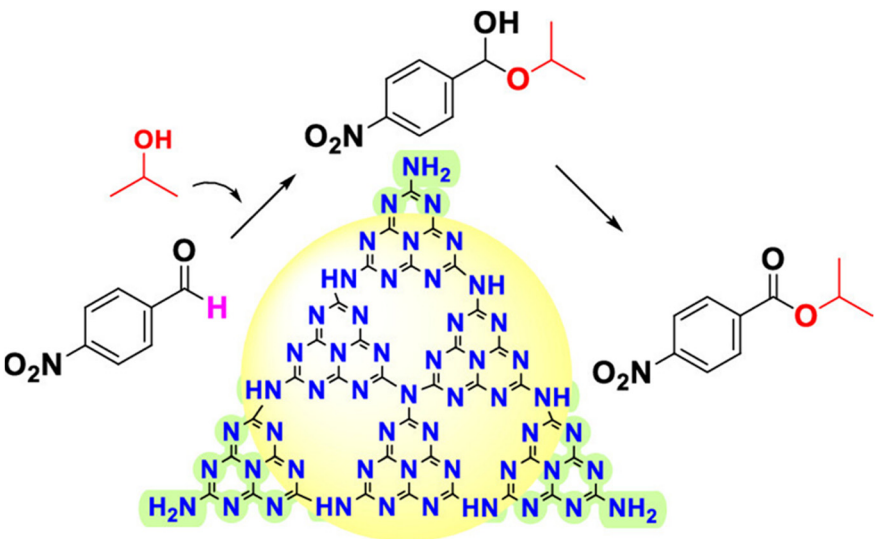

Scheme 3 Proposed mechanism of the photocatalytic 4-nitro benzaldehyde esterification reaction.[218] Reproduced with permission from ref. 218. Copyright 2023 American Chemical Society.

(Fig. 9a and b) whose pyrolysis creates in a homogeneous distribution of metal single atoms (Fig. 9c and d). Experimental and computational studies indicate that isolated metal-N_3C moieties are the active sites.[72]

Table 12 Summary of carbon-based materials for oxidative esterification of alcohols to esters

Entry	Catalyst	Substrate	Oxidant/additive	Reaction conditions	Con./%	Sel./%	Specific activity/mmol g_{cat}^{-1} h^{-1}	Ref.
1	Co@NC-4	BzOH	O_2	0.5 mmol BzOH, 7 mg catalyst (5.5 mol% Co), 1 bar O_2, 4 mL MeOH, 60 °C, 12 h	99	98	5.8	195, 220
2	Co SAs-N@C	BzOH	O_2	0.5 mmol BzOH, 7 mg catalyst, 1 bar O_2, 5 mL MeOH, 60 °C, 3 h	>99	98	220	72
3	Co@NC-Gr7	BzOH	O_2/K_2CO_3	250 mg BzOH, 40 mg catalyst (13 wt% Co), 1 bar O_2, 4 mL MeOH, 60 °C, 12 h	88	96	4.1	219
4	CoCu@NC_2	BzOH	O_2	0.5 mmol BzOH, 40 mg catalyst (9 wt% Co), 1 bar O_2, 5 mL MeOH, 60 °C, 12 h	100	>99	1.0	221
5	CoNC/CNT	BzOH	O_2/K_2CO_3	0.4 mL BzOH, 200 mg catalyst (1.8 wt% Co), 20 bar O_2, 32 mL MeOH, 60 °C, 12 h	88.1	92	1.3	222
6	Co–CoO@NC	BzOH	O_2/K_2CO_3	1 mmol BzOH, 25 mg catalyst (33 wt% Co), 1 bar O_2, 8 mL MeOH, 80 °C, 12 h	100	>99	3.3	223
7	Co-NC	BzOH	Air/K_2CO_3	0.5 mmol BzOH, 25 mg catalyst (9% Co), 1 bar air 4 mL MeOH, 60 °C, 24 h	99.3	>99	0.8	224
8	Co SACs@NG-800-50	BzOH	O_2/K_2CO_3	0.5 mmol BzOH, 20 mg catalyst (10 wt% Co), 1 bar O_2, 4 mL MeOH, 60 °C, 24 h	>99	>99	1.0	224
9	Co-MOFs-800	4-RBzOH	O_2/K_2CO_3	1 mmol 4-RBzOH, 20 mg catalyst (32 wt% Co), 10 bar O_2, 5 mL MeOH, 60 °C, 24 h	50–96	0–100	1.3	62
10	Co@C–N(800)	4-NO_2-BzOH	Air	0.5 mmol 4-NO_2-BzOH, catalyst (15 mol% Co), 1 bar air, 1 mL MeOH, 25 °C, 96 h	>99	>99	0.4	12
11	Au0.05Co@NC	BzOH	O_2/K_2CO_3	0.5 mmol BzOH, 20 mg catalyst (39 wt% Co), 1 bar O_2, 10 mL MeOH, 120 °C, 4 h	100	>99	6.3	226
12	$PdBi_{0.47}Te_{0.09}$	BzOH	O_2/K_2CO_3	0.5 mmol BzOH, 21 mg catalyst (0.1 mol% Pd), 1 bar O_2, MeOH (flow), 60 °C, 8 h	>99	>99	3.0	227
13	Co@NC-2-900	BzOH	Air/K_2CO_3	0.5 mmol BzOH, 30 mg catalyst (5 wt% Co), 10 bar O_2, 4 mL MeOH, 60 °C, 24 h	>99	97	0.7	228
14	Pd_5Bi_5/NCB	BzOH	Air/K_2CO_3	0.5 mmol BzOH, 10 mg catalyst (20 wt% Pd), 1 bar air, 2 mL MeOH, 80 °C, 2 h	>99	96	24	180
15	CoOx-N@C, PAN	BzOH	O_2/K_2CO_3	1 mmol BzOH, 0.15 g catalyst (22 wt% Co), 1 bar air, 4 mL MeOH, 60 °C, 24 h	92	99	0.3	229
16	Au–Pd/graphene	BzOH	O_2/K_2CO_3	2 mmol BzOH, 50 mg catalyst (2.7 wt% Au, 0.3 wt% Pd), 1 bar O_2, 5 mL MeOH, 25 °C, 1 h	100	>99	40	32
17	Co@NOSC	BzOH	O_2	0.5 mmol BzOH, 60 mg catalyst (21 wt% Co), 1 bar O_2, 5 mL MeOH, 60 °C, 24 h	97	>98	0.3	230
18	Au-G nanocatalyst	BzOH	O_2/K_2CO_3	2.5 mmol BzOH, 50 mg catalyst (18 wt% Au), 1 bar O_2, 6 mL MeOH, 45 °C, 6 h	100	97	8.1	231

Photocatalytic conversion

Entry	Catalyst	Substrate	Light source	Reaction conditions	Conv./%	Sel./%	Specific activity/mmol g_{cat}^{-1} h^{-1}	Ref.
19	Co@NC	BzOH	300 W Xe UV-vis	BzOH (0.5 mmol), catalyst (0.01 g), O_2; 0.1 MPa, CH_3OH: 4 mL; 60 °C, 1 h, K_2CO_3	100	>99	50	232

BzOH: benzyl alcohol; 4-NO_2BzOH: 4-nitrobenzyl alcohol; 4-RBzOH: R = CH_3, CH_3O, NO_2, Cl, and Br.

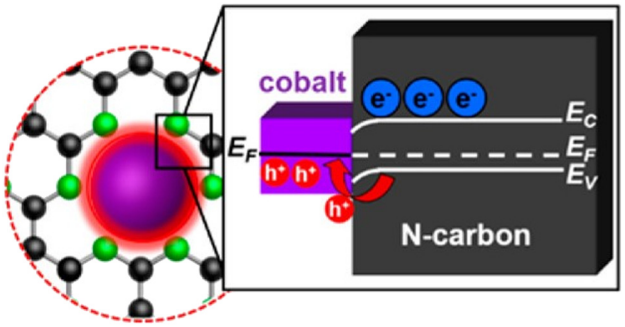

Fig. 8 Mott–Schottky effect in Co single atoms dispersed in N-rich carbons.[195] Reproduced with permission from ref. 180. Copyright 2017 American Chemical Society.

Solvent-free mechanochemical routes to Co@N-doped carbon catalysts have also been developed for the oxidative esterification of benzyl alcohol to methyl benzoate, conferring higher activity than Co@NC-Phen and Co@NC-ZIF based catalysts (Table 11, entry 4).[219] Ball-milling and carbonization provide a low cost route to bimetallic analogues metal ($CoCu@NC_n$) for the base-free oxidative esterification of various alcohols under mild reaction conditions.[221] Mechanical mixing and subsequent pyrolysis of chitosan as a carbon source, with melamine as a nitrogen precursor, and $CoCl_2{\cdot}6H_2O$, and $CuCl_2{\cdot}2H_2O$ metal precursors, yielded a N-doped carbon embedded with cobalt and copper nanoparticles. HRTEM (Fig. 10a–c) demonstrated uniformly dispersed nanoparticles throughout the N-doped carbon matrix (Fig. 10e). Synergy between proximate Cu and Co nanoparticles significantly enhanced the catalytic performance (Fig. 10d) for oxidative esterification of electron donating and withdrawing alcohols with high conversion (up to 100%) and selectivity (up to 100%).

The oxidative esterification of benzyl alcohols over Co@CNT catalysts has also been explored, with Co_3O_4 containing catalyst particularly effective.[222] In contrast, unfunctionalised and N-doped CNTs were inactive. The stability of Co@CNT catalysts was assessed by washing with HCl and HNO_3: only a small activity loss occurred after HCl treatment, however, HNO_3 significantly lowered activity, likely due to leaching (Fig. 11).

Co and CoO nanoparticles incorporated into N-doped MOF-derived carbons are highly effective for the direct oxidation of

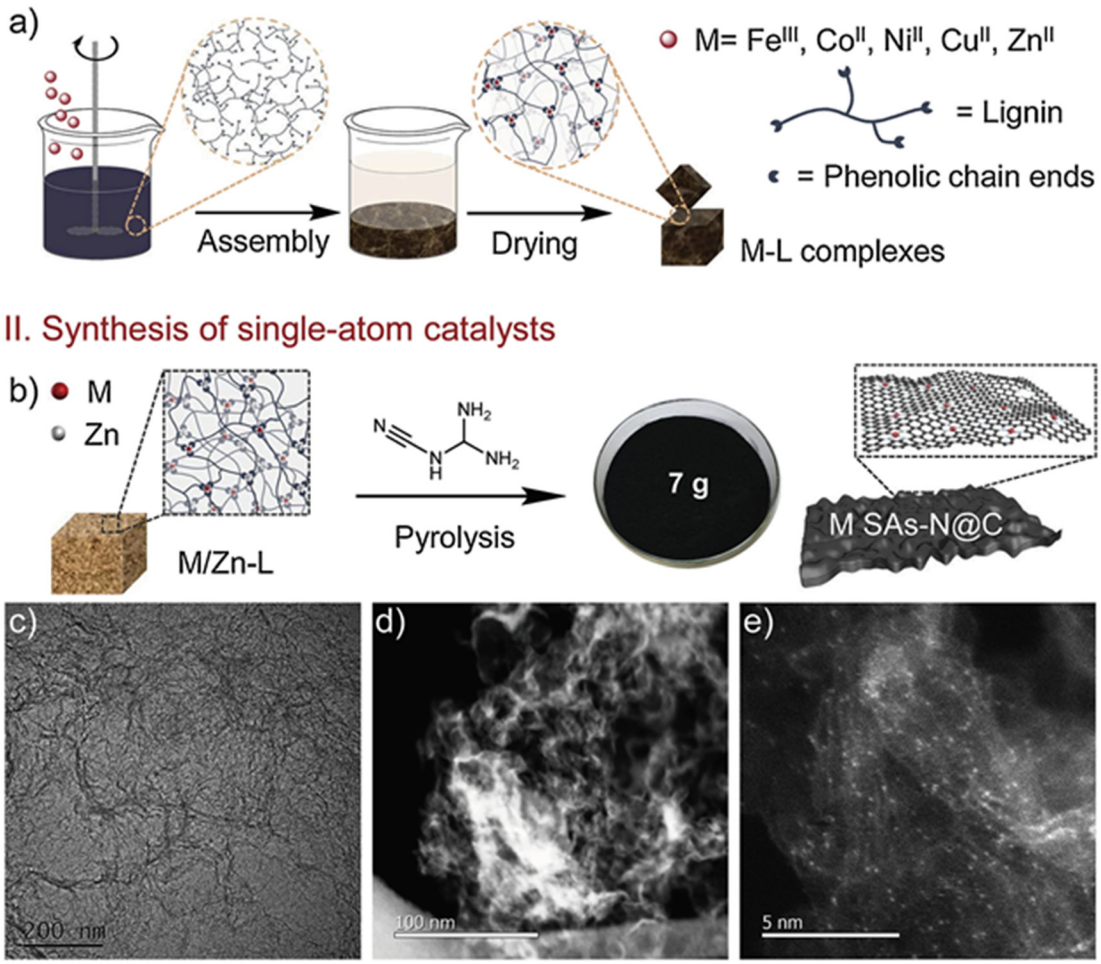

Fig. 9 (a and b) Synthesis of carbon-supported SACs using metal–lignin (M–L) complexes. (c–e) TEM and HAADF-STEM images of Co SAs-N@C.[72] Reproduced with permission from ref. 66. Copyright 2019 Elsevier.

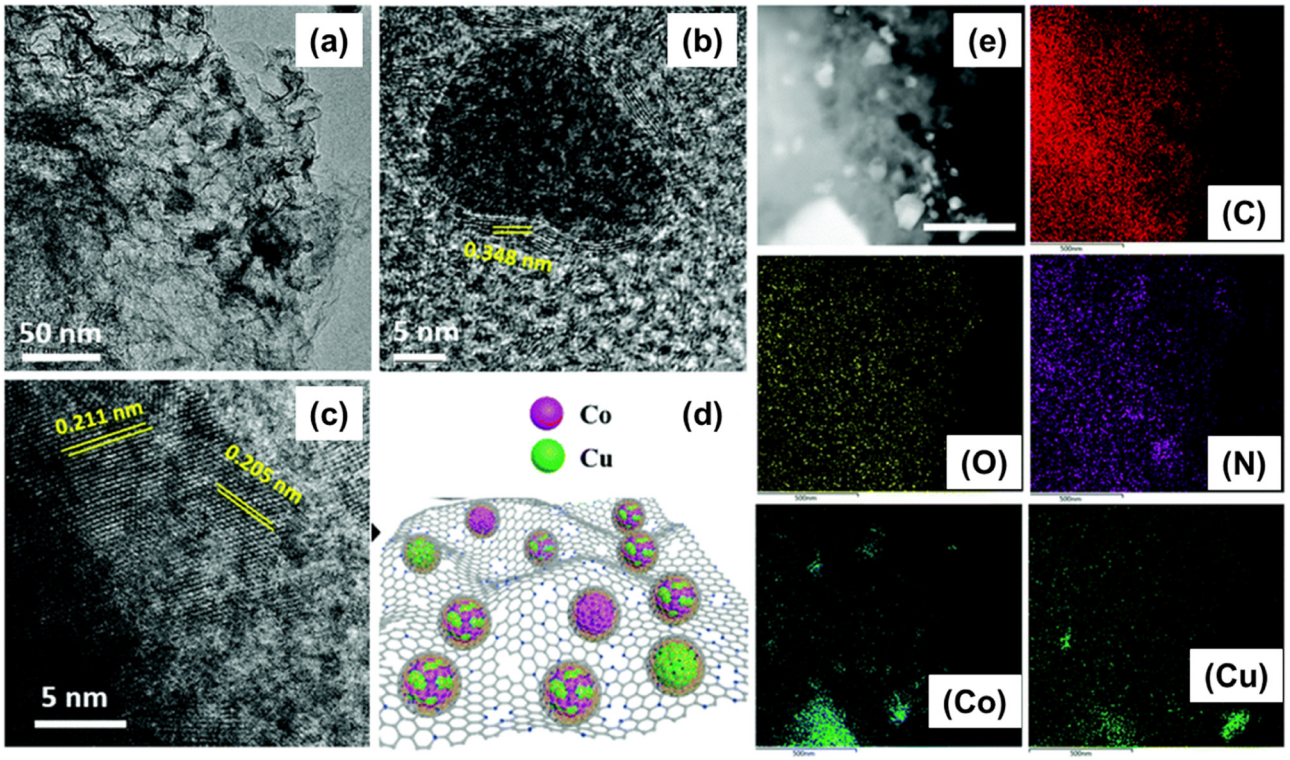

Fig. 10 (a–c) HRTEM images, (d) schematic of $CoCu@NC_2$, and (e) EDS maps of C, O, N, Co, and Cu for $CoCu@NC_2$.[221] Reproduced with permission from ref. 221. Copyright 2020 Royal Society of Chemistry.

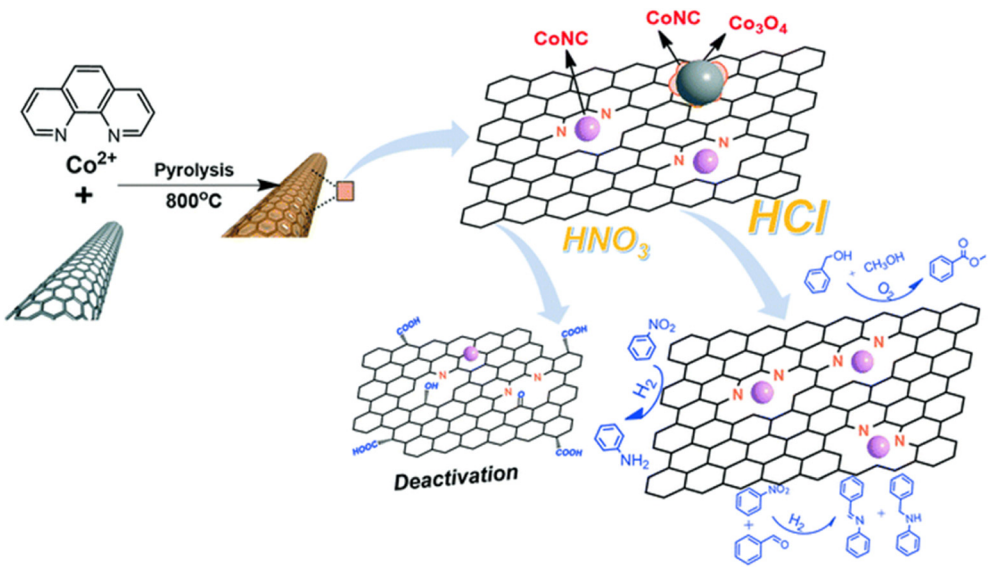

Fig. 11 CoNC catalyst for benzyl alcohol oxidative esterification (and nitrobenzene hydrogenation or the hydrogenated coupling of nitrobenzene with benzaldehyde).[222] Reproduced with permission from ref. 222. Copyright 2016 Royal Society of Chemistry.

alcohols to esters (Fig. 12) due to the rich redox chemistry of cobalt.[223] N-doped carbons help stabilise Co@CoO core–shell nanoparticles, preventing their aggregation and deactivation. Nitrogen-doping also enhances the electronic properties of the carbon support, facilitating alcohol adsorption near active sites. The high porosity and surface area of the carbon also ensures efficient diffusion of reactants/products to/from active sites. Although catalyst recycling was explored, it was performed at high alcohol conversion and hence little can be deduced about catalyst stability.

Co-NC catalysts prepared with and without a salt template have also been compared for the aerobic oxidative

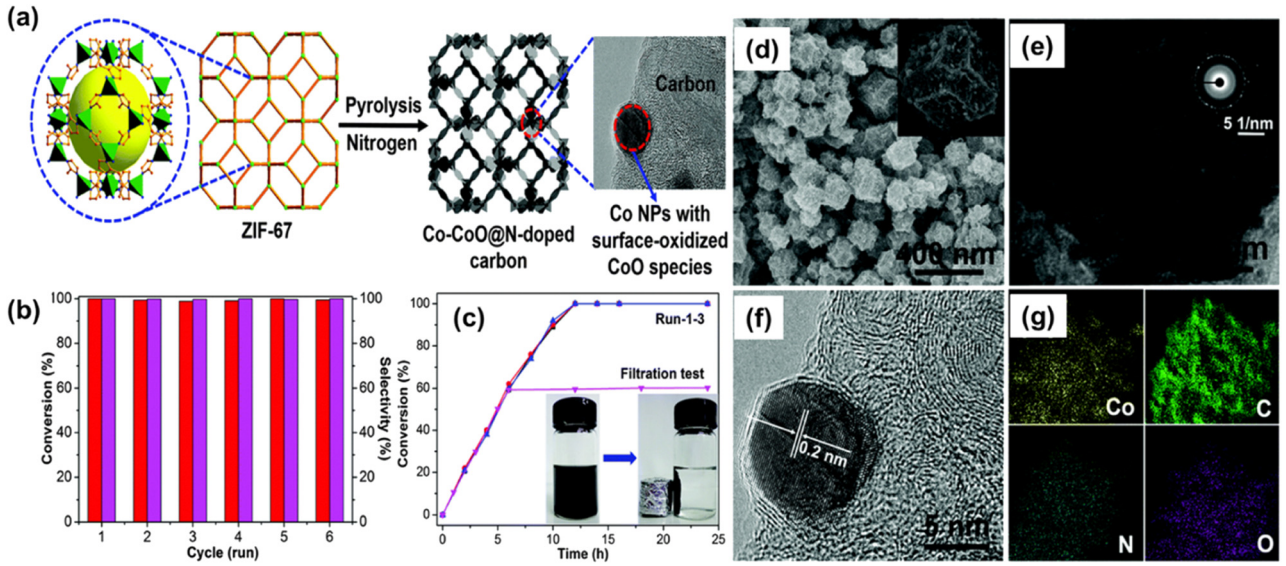

Fig. 12 (a) Schematic synthesis of Co–CoO@N-doped carbons by ZIF-67 pyrolysis (inset, SEM image of Co@CoO particle), (b) conversion and selectivity for benzyl alcohol oxidative esterification with methanol, (c) catalyst recycle and filtration test (inset shows magnetic separation), (d) TEM image of NC-700-3 h, and (e) corresponding SAED pattern, (f) HRTEM image showing lattice fringes of Co nanoparticle and graphitic layers, and (g) elemental maps showing uniform dispersion of Co, C, N and O. Reproduced with permission from ref. 223. Copyright 2015 Royal Society of Chemistry.

esterification of benzyl alcohol with methanol at 60 °C. The salt-templated Co–N–C catalyst possessed a higher surface area (1011 m^2 g^{-1}) and pore volume (1.05 cm^3 g^{-1}) and achieved 99% alcohol conversion and 99% selectivity to methyl benzoate. In contrast, the template-free Co–N–C catalyst (164 m^2 g^{-1} and 0.15 cm^3 g^{-1}) only achieved 30% conversion, and a metal-free N-doped carbon only 6% conversion, highlighting the importance of cobalt and carbon textural properties on performance.[213] Recently, Co SACs@NG-800-50 synthesised using a hard template-assisted (spatial confinement) strategy was reported for the oxidative esterification of aromatic alcohols to esters (Fig. 13A). Cobalt single atoms were identified as the active sites (Fig. 13B), with the formation of CoN_3 species deemed responsible for O_2 activation to form $^{\bullet}O^{2-}$ species which facilitate oxidative esterification. Molecular catalysts such as cobalt phthalocyanine were inactive. The high conversion of benzyl alcohol and selectivity to methyl benzoate over Co SACs@NG-800-50 was attributed to its high surface area and density of Co active sites achieved through the dicyandiamide N-precursor.[225] However, this study did not provide quantitative elemental analysis or information on the dispersion of Co and/or CoN_3 species, hence the assignment of active sites is not definitive and impact of synthesis protocol remains unclear.

Co@C–N prepared by the one-step thermolysis of a Co-containing ZIF-67 (synthesised from Co(MeIM)2, MeIM = 2-methylimidazole) is also reported for the oxidative esterification of *p*-nitrobenzyl alcohol with methanol at 25 °C (Fig. 14).[12] The parent ZIF-67 was inactive under base-free conditions, whereas the pyrolysed material achieved >99% ester yield. Calcination and reduction under hydrogen to remove carbon and nitrogen and reduce CoO_x species to the metal (resulting in a material of ~99 wt% Co) dramatically deactivated the catalyst resulting in only 5% alcohol conversion. Leaching of Co from the Co@C–N catalyst using *aqua regia* to produce metal-free N-doped carbon also resulted in deactivation: both Co and N-doped carbon components were required to activate alcohols. Further insight into the nature of the active site in Co@C–N(800) was obtained from N 1s XPS of the ZIF-67 and derived Co@C–N(600), Co@C–N(700) and Co@C–N(800) catalysts (Fig. 14C). ZIF-67 only possessed pyridinic nitrogen (398.7 eV binding energy) whereas Co@C–N possessed pyridinic and graphitic nitrogen species (401.0–402.0 eV). This observation is at odds with previous studies that suggest pyridinic-N is preferential for oxidative esterification, and reflects incorrect assignment of the N 1s species in the ZIF framework. The parent ZIF-67 contains an imidazole linker (from the pyrrole family) which is weakly basic compared to pyridine as the N lone pair is delocalised across the aromatic system. Nitrogen within the pyrrolic, methyl imidizole linker of Co-ZIF-67 therefore does not provide the optimum basicity for oxidative esterification. The graphitic-N species generated by pyrolysis offer increased basicity for O_2 activation and cooperative interactions. Hence graphitic-N, while inferior to pyridinic-N, is more effective for oxygen activation than pryrrolic-N species.

$Au_{0.05}Co@NC$ has also been investigated, with Au employed to regulate the electronic structure of the catalyst, and Co–N_x sites responsible for O_2 adsorption and activation.[226] Gold hypothesised to increase the electron density on Co–N_x species, supported by CO_2 temperature programmed desorption (CO_2-TPD) measurements (Fig. 15a) which showed a slight increase in the CO_2 desorption

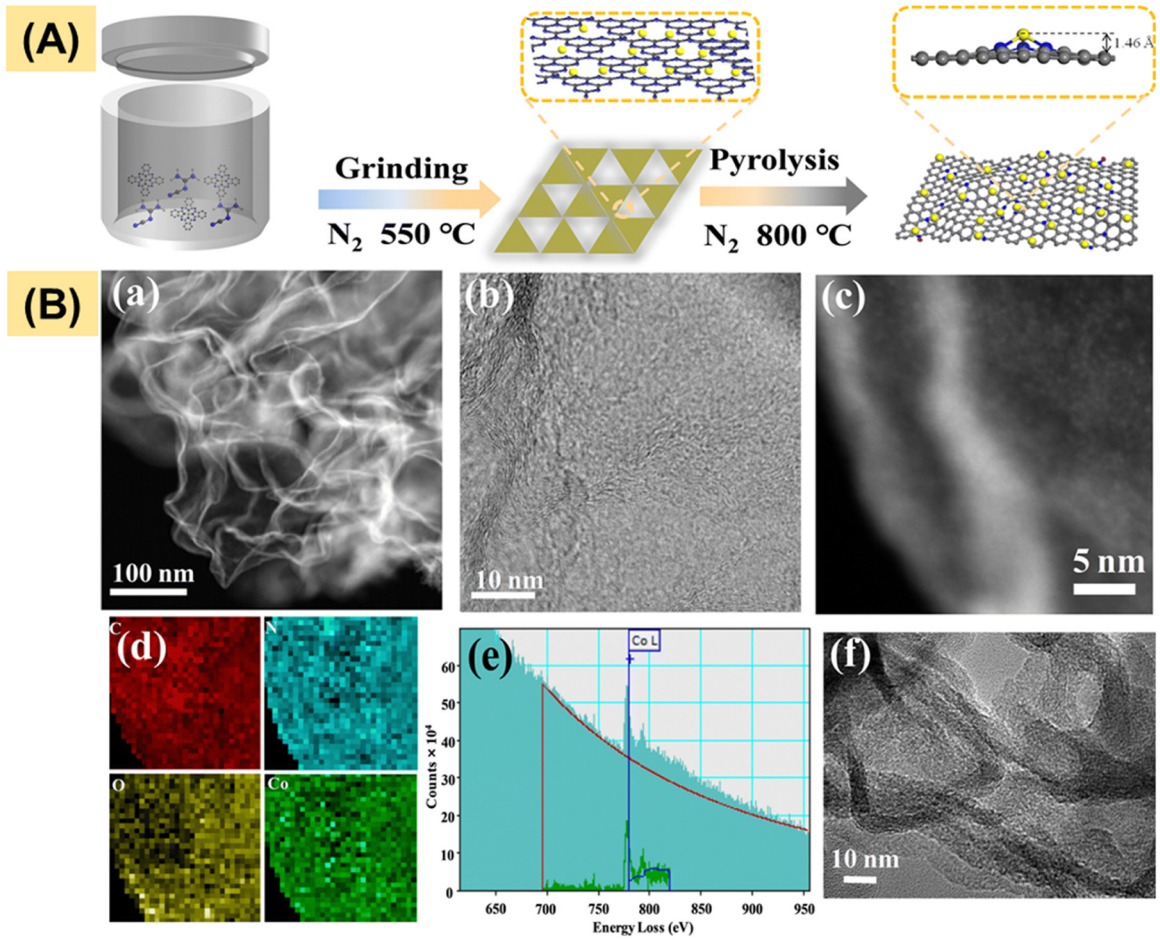

Fig. 13 A) Synthesis of Co SACs@NG-*T*-*n*, B) (a) TEM, (b) HRTEM, (c and d) HAADF-STEM, (d) corresponding elemental maps, and (e) energy loss spectrum of Co SACs@NG-800-50, and (f) HRTEM image of Co0.9Cu0.1@NG-800-50.[225] Reproduced with permission from ref. 210. Copyright 2023 Royal Society of Chemistry.

maxima with increasing Au content. The basicity of Co@NC also increased from 1.54 mmol g^{-1} for Co@NC to 3.29 mmol g^{-1} for Au0.10 Co@NC; the density of base sites was thus enhanced by Au addition (Fig. 15c). Raman spectroscopy was used to identify the defect density of the carbons, with the higher $I_D : I_G$ value of $Au_{0.05}$Co@NC (1.196) *versus* Co@NC (1.107) consistent with surface defect formation (Fig. 15b). Specific activity and TOF (per Co site) for the selective oxidative esterification of benzyl alcohol with methanol both increased with Au content/basicity up to a maximum of 0.00416 mol g^{-1} h^{-1} and 0.626 mol mol^{-1} h^{-1}, respectively, for $Au_{0.05}$Co@NC. A moderate enhancement of basicity improves methanol activation and stabilises reaction intermediates, thereby promoting selectivity toward methyl benzoate. Further increases in Au content and basicity may lowered performance, possibly due to destabilisation of active sites or the promotion of side reactions. Unfortunately, catalyst testing was again performed under diffusion-limited conditions, making it impossible to unequivocally comment on the origin of Au promotion. Reported activities based on 100% benzyl alcohol conversion may also be an underestimate, and further studies at low iso-conversion are needed to extract kinetic data. TOFs based solely on the surface Co may also be misleading as Au itself is active for oxidative esterification, and it would be more meaningful to consider the total surface metal content.

Approximately 400 metal salt were screened in combination with Pd/C undertake to identify optimal catalysts for the oxidative esterification of 1-octanol with methanol (Fig. 16),[227] with Bi and Te identified as the most effective promoters. Subsequent synthesis of $PdBi_{0.47}Te_{0.09}$/C and $PdBi_{0.35}Te_{0.21}$/C *via* wet impregnation yielded active catalysts for the oxidative esterification, with $PdBi_{0.35}Te_{0.21}$/C showing superior activity to $PdBi_{0.47}Te_{0.09}$/C. Further testing with various primary alcohol substrates showed that $PdBi_{0.35}Te_{0.21}$/C was a versatile catalyst achieving yields ~90% for all primary alcohols tested.

Heteroatom-doped Co/carbon nanotubes containing N, S, and O (Co@NOSC, Co@NC and Co@OSC) were explored for the oxidative esterification of alcohols. Tri-doped carbons prepared by direct mixing and freezing drying of precursors followed by carbonisation at 900 °C show excellent conversions (up to 97%) for alcohols with ester selectivity up to 99%.[230] However, the Co contents varied significantly

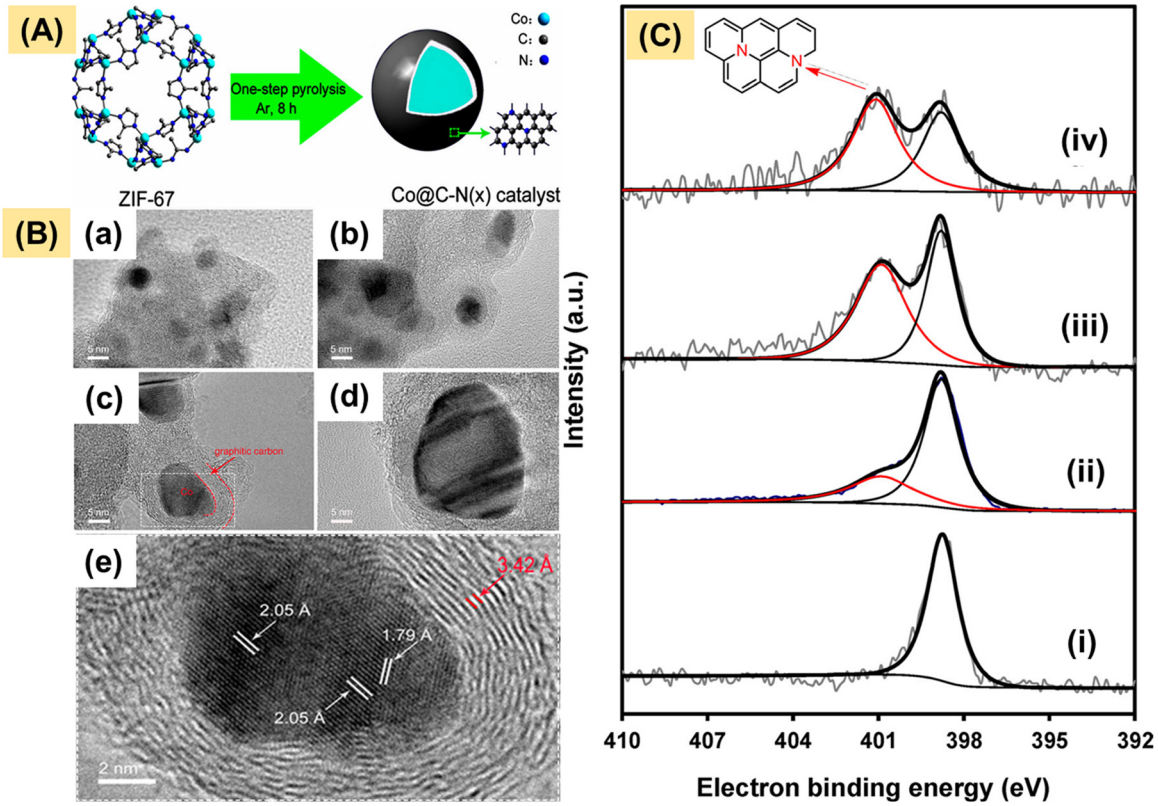

Fig. 14 (A) Schematic of a Co/N-doped graphite catalyst prepared by one-step pyrolysis of ZIF-67, (B) HRTEM images of (a) Co@C–N(600), (b) Co@C–N(700), (c) Co@C–N(800), and (d) Co@C–N(900). Red lines in (c) indicate a Co nanoparticle encapsulated by graphite layers (shown enlarged in panel (e)), and (C) N 1s spectra of (i) ZIF-67, (ii) Co@C–N(700), (iii) Co@C–N(800), and (iv) Co@C–N(900).[12] Reproduced with permission from ref. 12. Copyright 2015 American Chemical Society.

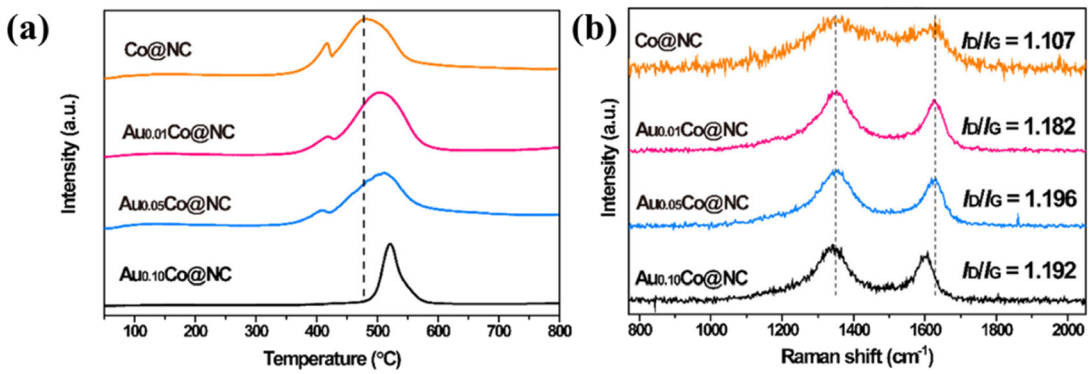

(c)

Sample	Basic sites (mmol g^{-1})	Conversion (%)	Selectivity (%)	Catalytic activity (mol g cat^{-1} h^{-1})	TOF (mol.mol-1.h-1)
Co@NC	1.54	100	67.6	0.00282	0.419
Au0.01Co@NC	1.87	100	75.6	0.00315	0.481
Au0.05Co@NC	2.56	100	99.9	0.00416	0.626
Au0.10Co@NC	3.29	100	84.2	0.00351	0.527

Catalytic activity of various catalysts in the selective oxidative esterification of benzyl alcohol and methanol, reaction conditions: 10 mL of methanol, 0.5 mmol benzyl alcohol, 30 mg of K_2CO_3, 1 atm O_2, 120 °C, 4 h. TOF based on Co content on the materials

Fig. 15 (a) CO_2 TPD profiles, (b) Raman spectra, and (c) relationship between Au content and catalyst basicity and performance for $Au_xCo@NC$ catalysts.[226] Reproduced with permission from ref. 226. Copyright 2022 American Chemical Society.

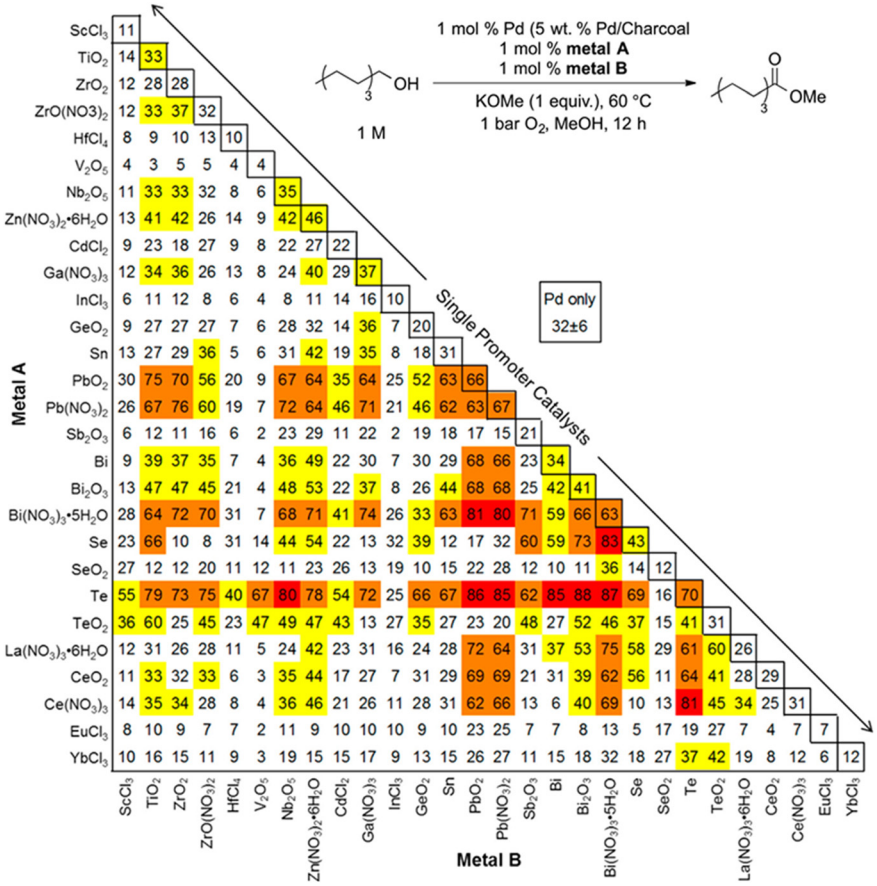

Fig. 16 Admixture screening (methyl octanoate yields) for the aerobic oxidation of 1-octanol with catalysts composed of Pd/charcoal in combination with one or two additives. Colour code reflects methyl octanoate yields: <Pd (white), >Pd (yellow), >60% (orange), and ≥80% (red).[227] Reproduced with permission from ref. 227. Copyright 2017 American Chemical Society.

across these catalyst families, from 21 wt% in Co@NOSC, to 37 wt% in Co@OSC, and 61 wt% in Co@NC which may be responsible for observed performance differences. Although efforts were made to record Co : benzyl alcohol ratios, these also varied significantly across samples, and the impact of Co particle size and presence of different Co phases (*e.g.* metallic Co in Co@NC, metallic Co and 23% Co_9S_8 in Co@NOSC, and metallic Co with 70% Co_9S_8 in Co@OSC) was also not considered. Particle sizes (of ~40 nm) for Co metal and Co_9S_8 were reported for Co@NOSC, but corresponding values were not reported for Co@NC or Co@OSC. Furthermore, Co in Co@CN (synthesised from a urea based gel) was only partially encapsulated by a carbon shell, whereas that in Co@OSC and Co@NOSC was embedded in a heteroatom rich shell. The latter suggests that using carrageenan as the gelling medium during catalyst synthesis conferred a more uniform Co distribution. It remains unclear whether S directly contributes to the reaction, or simply aids the synthesis to produce more stable/active forms of Co.

Co@NC has also been investigated for the photocatalytic oxidative esterification of benzyl alcohol to methyl benzoate under UV-visible light irradiation (300 W). This catalyst achieved complete conversion of benzyl alcohol to methyl benzoate, with a specific activity of 50 mmol g_{cat}^{-1} h^{-1} at room temperature (Table 12, entry 19), highlighting the potential of graphitic carbon-based photocatalysts in driving oxidative esterification of alcohol (albeit in the presence of K_2CO_3) with minimal energy input.

3.3. Oxidation of alkenes to esters

The synthesis of carbonyl compounds (aldehydes, ketones, esters, and acids) from alkenes is highly desirable due to their extensive use as synthons in the pharmaceutical industry. These transformations facilitate the production of essential intermediates for a wide range of chemical processes and drug manufacture.[234] However, the conversion of generally inactive olefins to carbonyl compounds presents significant challenges requiring highly efficient and selective catalysts to achieve the desired transformations under mild conditions. There are relatively few reports on the conversion of olefins to esters using carbon catalysts. Recent studies have shown that carbons doped with metals (*e.g.*, Fe) and nitrogen are effective for the oxidative esterification of alkenes.[235] Incorporating iron into N-doped carbon was recently reported for the oxidative esterification of olefins using molecular O_2 or TBHP as oxidants. High-resolution transmission electron microscopy showed that the catalyst comprised metallic Fe and Fe_3C nanoparticles encapsulated by

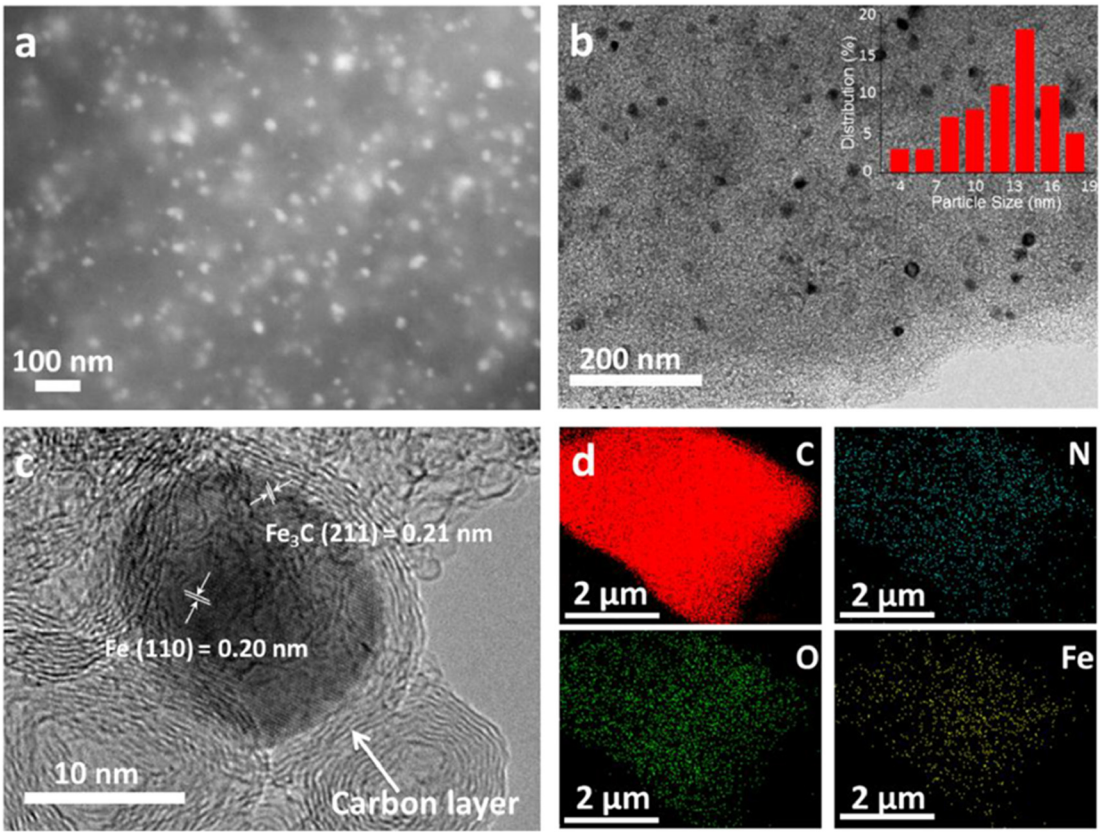

Fig. 17 Electron microscopy analysis of Fe-NC-900. (a) SEM images under BED-C mode. (b) TEM image (the inset is the particle size distribution of nanoparticles) and (c) HRTEM image. (d) Elemental mapping images.[235] Reproduced with permission from ref. 235. Copyright 2022 Elsevier.

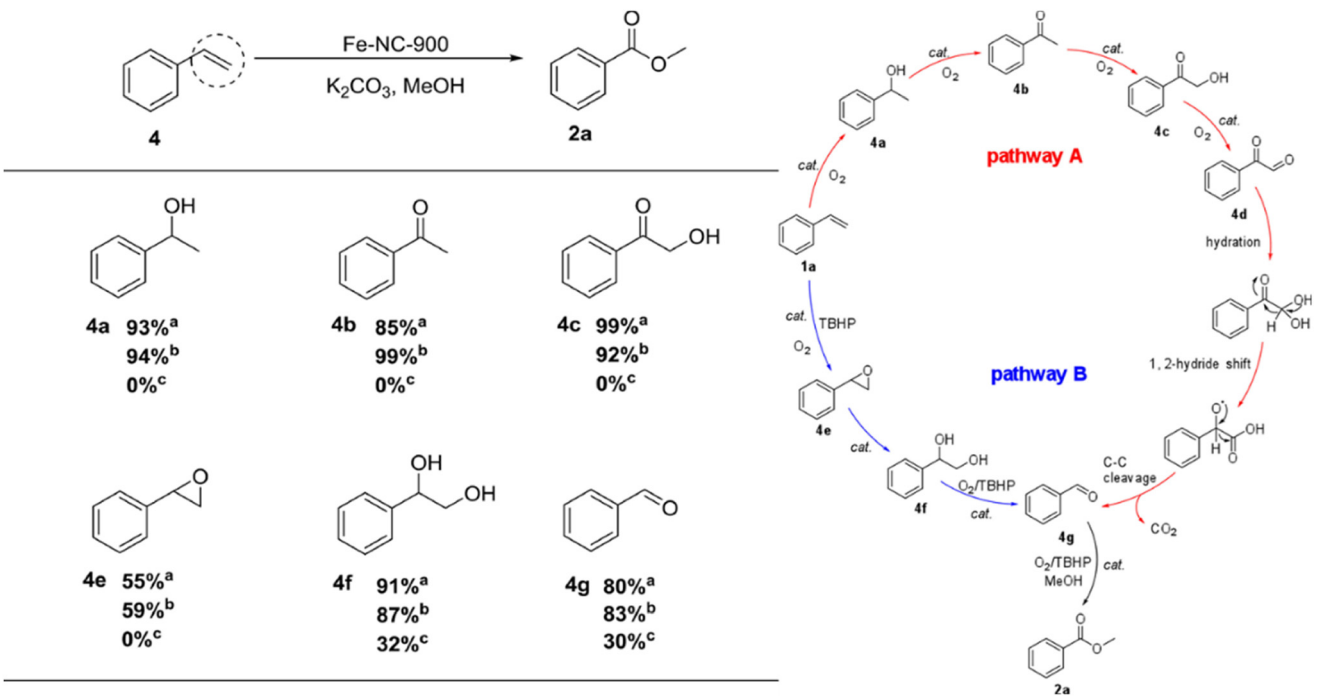

Scheme 4 Proposed reaction pathways for the oxidative cleavage of C═C bonds to esters over Fe-NC-900.[235] Reproduced with permission from ref. 235. Copyright 2022 Elsevier.

graphitic carbon with lattice spacings of 0.2 nm and 0.21 nm, respectively, and nanoparticle sizes of 5 and 20 nm (Fig. 17a–d). Mechanistic studies indicated that the reaction involved radicals in a cascade process with both Fe nanoparticles and the N-doped carbon playing important roles; radical scavengers (BHT or TEMPO) inhibited oxidative esterification. Trace amounts of **4a**, **4b**, **4e**, and **4g** (Scheme 4) were detected during the oxidative cleavage of styrene, and these molecules proved suitable starting materials for oxidative esterification suggesting that they are intermediates in cascades **A** and **B**. The catalyst was particularly effective for the oxidative esterification of halogenated aryl olefins which exhibited good to moderate conversions without the formation of dehalogenation products. Functional groups on the aromatic ring had little effect on catalytic activity, demonstrating its versatility.[235]

The hydroxyl-mediated oxidative esterification of various alkenes is reported using tubular carbon nitride (TCN) as a photocatalyst under 250 W Xe lamp irradiation. TCN achieved good yields of aromatic esters (48% to 89%), however the valence band potential of TCN was too small to activate aliphatic olefins (Fig. 18a and b). The TCN photocatalyst exhibited good reusability, maintaining activity for four cycles, before conversion dropped to ~60% due to corrosion of the g-C_3N_4 support by acid by-products.[236]

3.4. Oxidation of alkynes to esters

Significant progress has been made in the catalytic cleavage of –C–C– and –C═C– bonds, however the activation of –C≡C– bonds remains challenging due to their high bond dissociation energy (>200 kcal mol^{-1}).[237,238] Nevertheless, the oxidative cleavage of –C≡C– to form esters using molecular oxygen has been reported over a Co@NC-800 catalyst.[239] HRTEM analysis revealed a metallic cobalt core surrounded by graphitic carbon layers, with Co–N_x coordination sites in the carbon shell (Fig. 19a and b). The oxidative esterification of phenylacetylene with methanol resulted in a 93% yield of methyl benzoate. Treatment of Co@NC-800 with *aqua regia* removed cobalt nanoparticles (Fig. 19c and d). The acid-treated Co/NC-800-H^+ material was inactive for oxidative esterification of alkynes, confirming the critical role of cobalt. Mechanistic studies showed that ketones were formed as reaction intermediates (Fig. 20), suggesting that cobalt nanoparticles were essential for activating molecular oxygen and oxygen insertion.

Photocatalytic oxidative esterification of alkynes was also explored using a recyclable, carbon nitride semiconductor (potassium/sodium poly(heptazine imide), K,Na-PHI) under 7 W UV LED light in the presence of O_2.[240] The catalytic system was effective for activating substrates with electron-withdrawing and electron-donating groups. Electron-withdrawing substrates resulted in lower ester yields compared to electron-donating substrates. Control experiments and electron paramagnetic resonance (EPR) analysis highlighted the role of superoxide radicals in the reaction mechanism. Reactions performed with either H_2O^{18} or $^{18}O_2$ resulted in ^{18}O labeled esters, suggesting that the oxygen originates from water and dioxygen. Replacing the

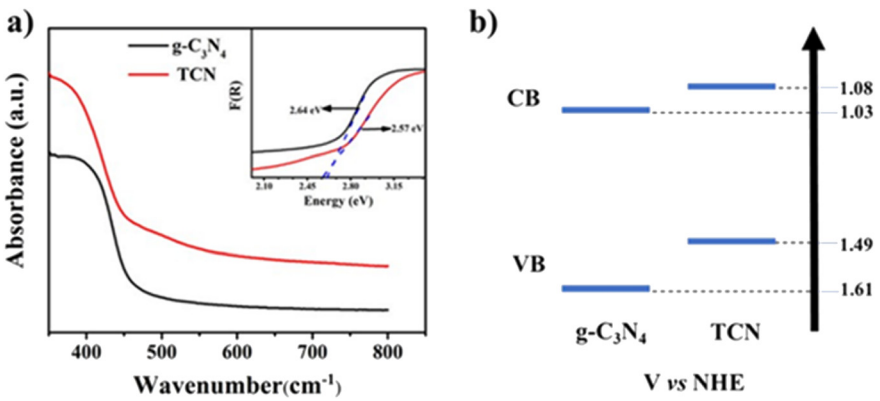

Fig. 18 (a) UV-visible absorption spectra of g-C_3N_4, TCN (inset shows band gap energies), and (b) their band structure alignments.[236] Reproduced with permission from ref. 236. Copyright 2021 Royal Society of Chemistry.

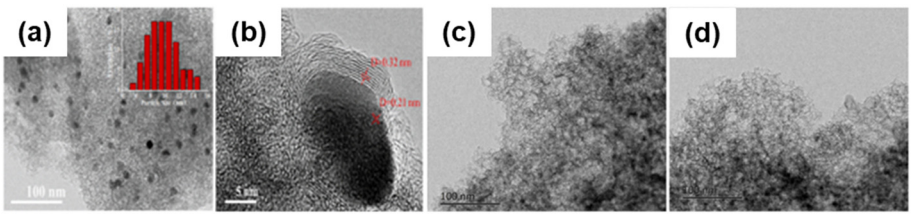

Fig. 19 TEM images of (a and b) Co/NC-800 (inset shows particle size distribution), and (c and d) Co/NC-800-H^+.[239] Reproduced with permission from ref. 239. Copyright 2023 Elsevier.

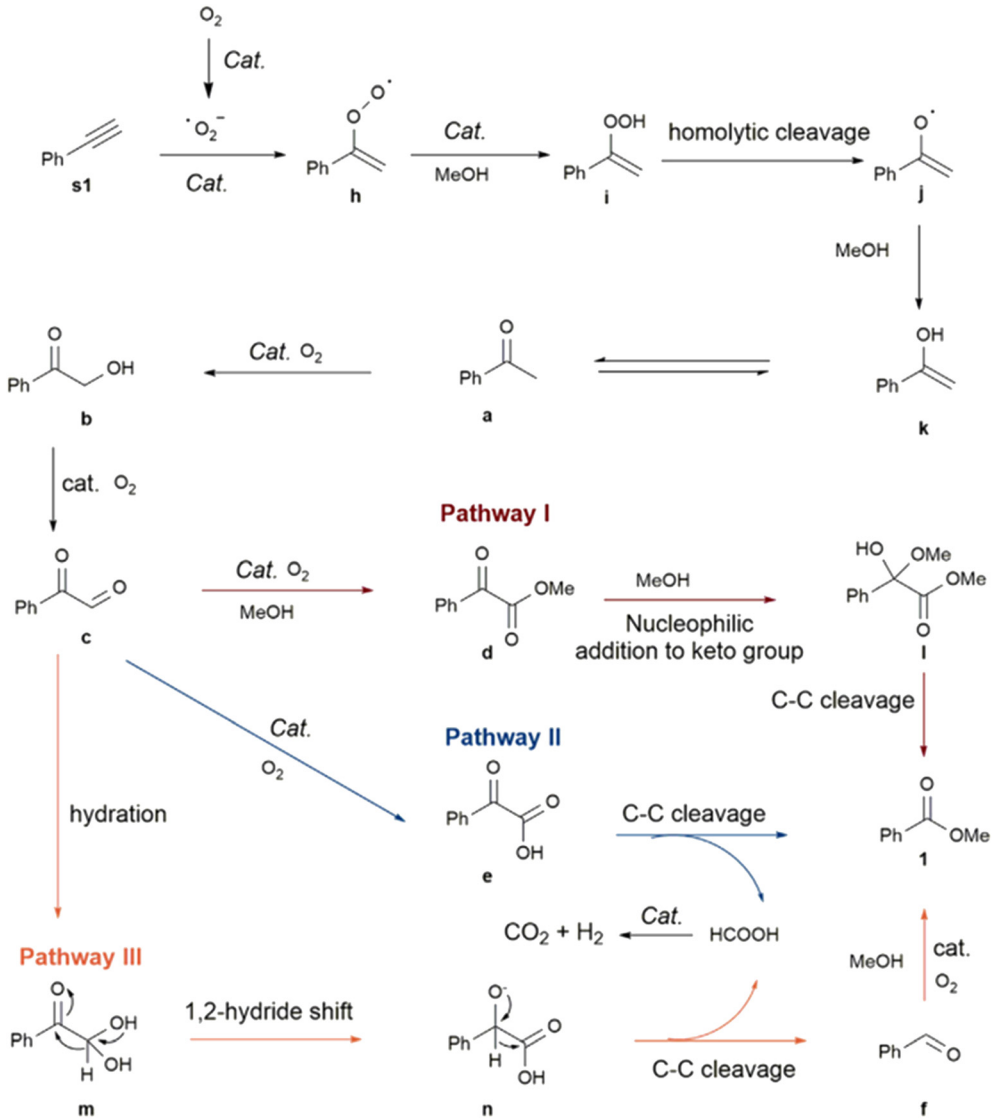

Fig. 20 Possible pathway for the oxidative esterification of alkynes.[239] Reproduced with permission from ref. 239. Copyright 2023 Elsevier.

alkyne with an aldehyde gave a 92% ester yield of esters, whereas replacing it for an acid did not give any ester product, indicating aldehyde as a reactive intermediate. However, when methionine was used as a trap to identify the dioxetane intermediate no diol formation was observed, suggesting that the reaction does not proceed *via* dioxetane (Fig. 21A and a–f). Evidence for a radical pathway was provided by using 2,2,6,6-tetramethyl-1-piperidinyloxyl (TEMPO) as a radical trap, which resulted in only trace oxygenated products during phenylacetylene oxidation. EPR confirmed the presence of hydroxyl and superoxide radicals when reactions were performed in the presence of *p*-benzoquinone and tertiary butanol as superoxide and hydroxyl radical scavengers (Fig. 21B and C). Finally, control experiments using CCl_4 and $HCOONH_4$, as scavengers of photoexcited electrons and holes respectively, showed a significant decrease in the yield of oxygenated products (to 27% and 35% respectively), confirming that reaction was light-driven; photogenerated hydroxyl radicals act as a green oxidant in the esterification according to a putative mechanism for photocatalytic oxidative cleavage of alkynes (Fig. 21D) Although this water-soluble catalyst was recyclable, its recovery requires CH_2Cl_2 extraction, whose use is now banned by the US Environmental Protection agency in industrial applications.[241] Alternative separation protocols are thus required for such molecular carbon catalysts.

The photocatalytic aerobic oxidative cleavage of –C≡C– bonds has also been demonstrated for electron-withdrawing and electron-donating aromatic alkynes, with diazonium salts as an aryl radical initiator, over porous graphitic carbon nitride (p-g-C_3N_4). This approach can be driven by solar irradiation, with results comparable to those under a Xe lamp for the aerobic oxidative conversion of phenylacetylene and diazonium salts. Use of solar energy is essential for large-scale ester production (Fig. 21E).[242]

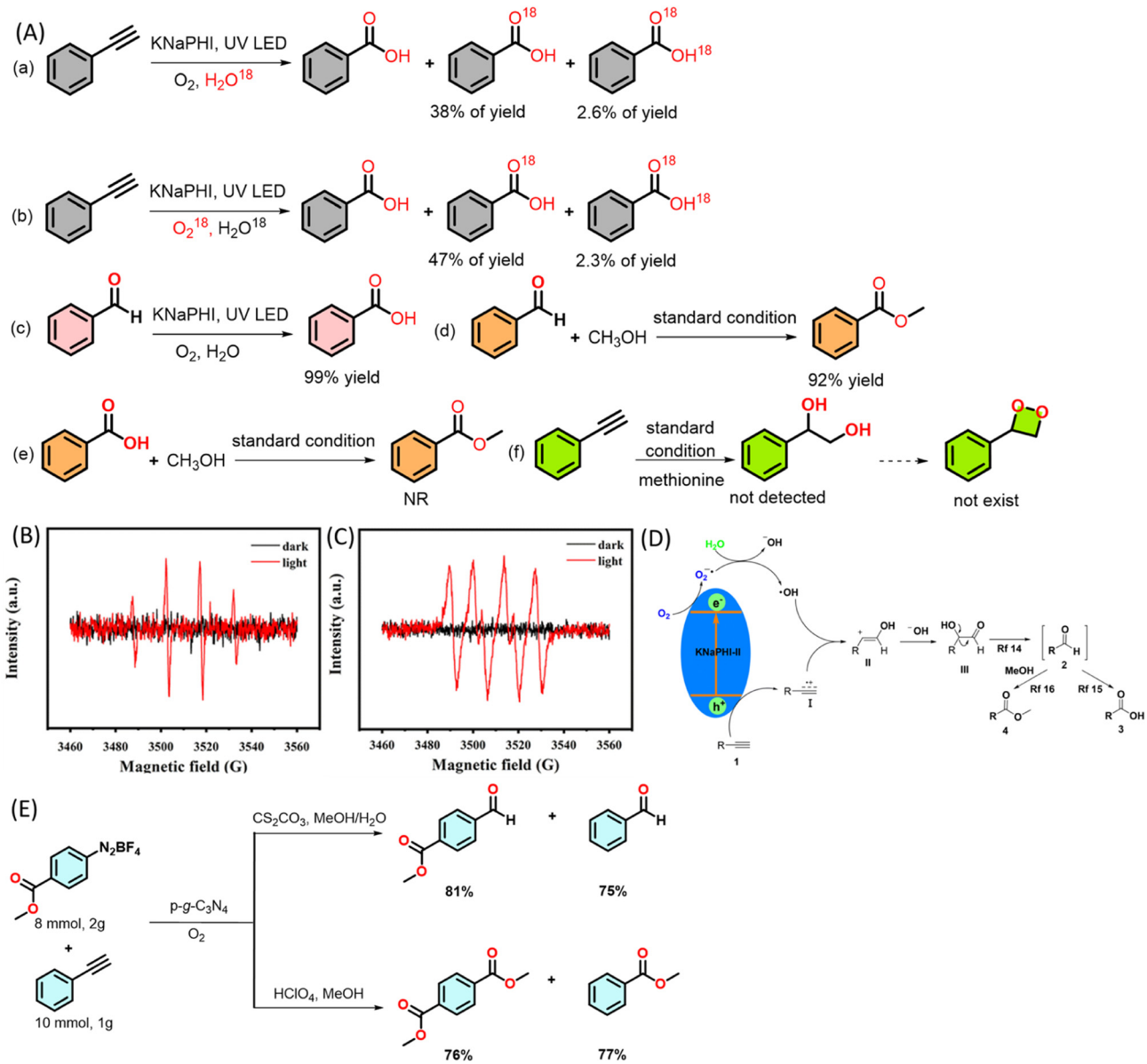

Fig. 21 (A) Oxidative esterification of phenylacetylene over K,Na-PHI using oxygen isotopes, and control reactions using benzaldehyde or benzoic acid. ESR spectra of KNaPHI with/without visible light irradiation to detect (B) $O_2^{\bullet-}$, and (C) $^{\bullet}OH$ radicals, (D) plausible reaction mechanism, and (E) direct solar energy mediated –C≡C– bond cleavage on the gram scale.[240] Reproduced with permission from ref. 240. Copyright 2022 Royal Society of Chemistry.

4. Progress and challenges in the oxidative esterification of alkynes and alkenes

Gold and palladium supported on solid acid catalysts have been extensively studied for the oxidative esterification of aldehydes and alcohols, demonstrating high efficiency and selectivity. More recently, cobalt catalysts have attracted attention for oxidative esterification reactions due to the redox properties of cobalt. Despite progress in the oxidative esterification of aldehydes and alcohols, the direct one-pot conversion of alkenes or alkynes to esters remains a formidable challenge which requires further investigation.

4.1. Challenges

The principal challenges associated with oxidative esterification of alkenes and alkynes are: (i) the low reactivity of alkenes and alkynes which hampers their selective thermal activation under oxidative conditions; (ii) competing pathways such as epoxidation, hydration, oxidative dehydrogenation, and polymerisation, which lower the yield of desired esters; (iii) poor catalyst efficiency for both

oxidation and esterification steps under the same conditions (required for a one-pot cascade).

4.2. New strategies

While the oxidative esterification of alkenes to esters is reported over core-shell Fe and Fe_3C nanoparticles supported on graphitic carbon with TBHP as an oxidant, there are no reports of corresponding aerobic oxidation which is necessary to ensure environmental sustainability and process safety.[235] A different approach to the tandem aerobic oxidative esterification of alkenes was recently reported for a bifunctional Cu-Al-SBA-15 catalyst wherein the copper activated molecular oxygen and the acidic Al-SBA-15 support catalysed esterification.[234] Such bifunctional, heterogeneous catalysts may exploit spatial compartmentalisation of metal and acid active sites, *e.g.*, through hierarchical pore networks, to separate each step of the cascade and exploit substrate-channeling.[243,244] This strategy would ensure that alkenes/alkynes are partially oxidised by co-adsorbed atomic oxygen at metal sites in large pores before encountering acid sites localised within smaller pores. Alternatively, if the lifetime of partially oxidised reactive intermediates is on the order of seconds, continuous flow reactors could be exploited: contiguous dual-beds would permit alkene/alkyne oxidation over a first metal catalyst bed, with any residual oxygen separated from the solution prior to contacting the aldehyde/ketone intermediate with a second acid catalyst bed.[245,246] Such catalytic cascades would streamline process efficiency and productivity (and the latter permit different reaction temperatures for steps 1 and 2 of Scheme 2). Overcoming these challenges in oxidative esterification will not only broaden the scope of this powerful transformation but also enable sustainable and efficient synthesis of esters directly from hydrocarbons such as alkenes and alkynes, reducing dependency on pre-functionalised substrates like aldehydes or alcohols.

5. Mechanistic insights into the oxidative esterification of aldehydes, alcohols, alkenes, and alkynes

The oxidative esterification of alcohols, and aldehydes (and to a lesser extent alkenes and alkynes) has been extensively studied to elucidate mechanistic pathways, and the nature of active sites and synergies therein.

5.1. Synergies between metals and metal oxides

Cooperative effects between metals and metal oxides on carbons have been most studied for cobalt catalysts containing *e.g.*, Co_3O_4 and Co nanostructures. For example, catalysts prepared by pyrolysing Co-based precursors on carbon supports at 300 °C were subsequently air-exposed to partially oxidise the Co nanoparticle surface to Co_3O_4

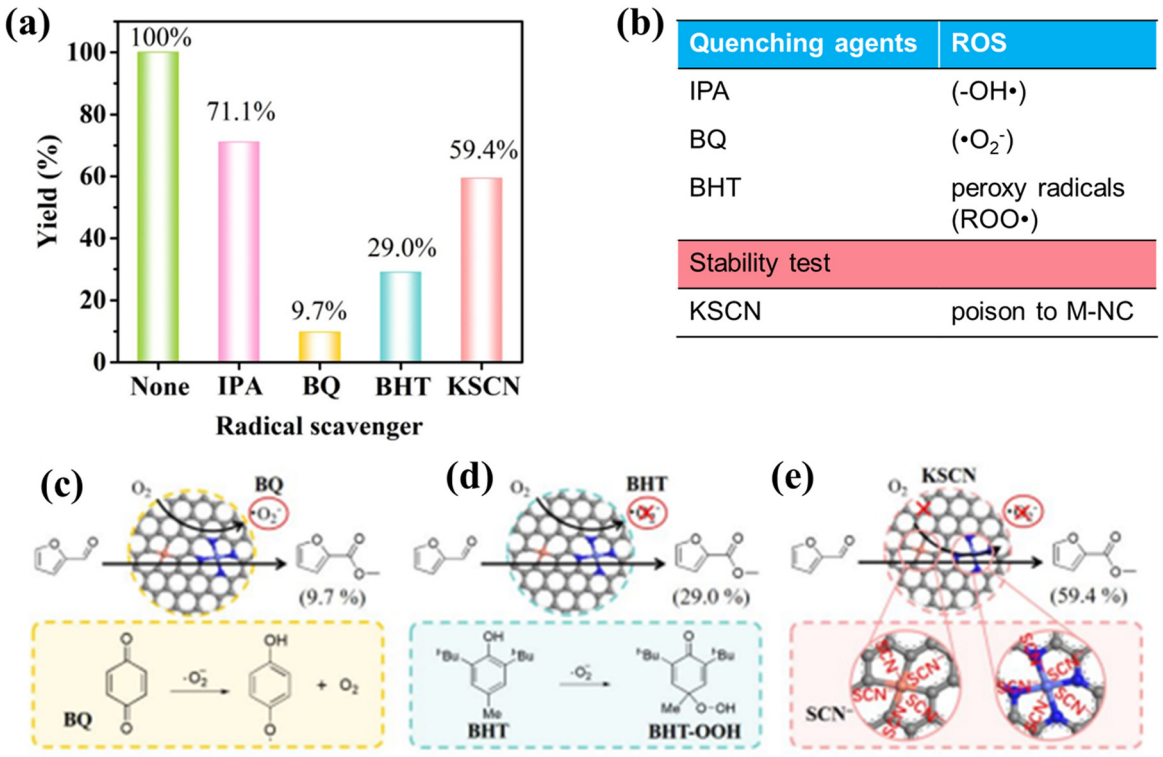

Fig. 22 (a and b) MF yields over CuC_4/CoN_4@HC in the presence of different radical traps. Reaction conditions: 0.5 mmol furfural, 5 mol% metal, 0.1 mmol K_2CO_3, 4 mL CH_3OH, 1 bar O_2, 50 °C, 6 h. Schematic of FFA oxidative esterification over CuC_4/CoN_4@HC in the presence of (c) BQ, (d) BHT, or (e) SCN^-.[210] Reproduced with permission from ref. 210. Copyright 2021 American Chemical Society.

(confirmed by powder X-ray diffraction).[247] Pure Co_3O_4 nanoparticles only showed 4% conversion for the oxidative esterification of alcohols, whereas Co_3O_4/Co nanoparticles achieved 99% conversion. This synergy was attributed to electron transfer from metal nanoparticles to the (large work function) heteroatom-doped carbon support, the resulting Mott–Schottky junction permits the Co nanoparticle core to serve as an electron source (Lewis base), enable the reaction to proceed in the absence of soluble bases.

5.2. Effect of acidic and basic supports

The choice of acidic or basic supports significantly impacts on oxidative esterification. For example, acidic Al_2O_3 is less effective than basic MgO (or soluble bases) for the oxidative esterification of HMF.[85] To understand the role of nitrogen atoms in carbon materials, pure carbon, N-doped carbon, and physical mixtures of cobalt with both carbon types were compared for the oxidative esterification of 5-HMF (Table 3).[64] The most basic N-doped carbon exhibited the highest conversion and selectivity.

5.3. Role of radicals in reaction pathways

Radical scavengers suppress oxidative esterification, confirming the involvement of radical species such as the superoxide anion radical ($^{\bullet}O_2^-$) in the mechanism. Electron paramagnetic resonance spectroscopy provides direct evidence for radical-mediated pathways involving intermediates such as carbocations, carbanions, and free radicals, with the superoxide anion radical ($^{\bullet}O_2^-$) identified as critical to high conversion.[210,248] Quenching experiments (Fig. 22a and b) over a CuC_4/CoN_4@HC catalyst using 1,4-benzoquinone (BQ), and butylated hydroxytoluene (BHT) identified the formation of peroxide radicals, while isopropyl alcohol (IPA) evidenced hydroxyl radicals. In the oxidative esterification of furfural to methyl 2-furoate (MF), BQ and BHT addition suppressed the MF yield to 10% and 29%, respectively, suggesting that both superoxide and peroxy radicals are important oxidants (Fig. 22c and d). In contrast, IPA had little effect on the MF yield which remained ~71%, suggesting that hydroxyl radicals are less important. Addition of KSCN was also explored to test catalyst stability (Fig. 22e), with minimal loss of activity observed, however the relevance of this test to thermal oxidative esterification is unclear as this additive is mainly exploited in electrocatalytic oxygen reduction wherein low valence sulfur species can poison anodic oxidation.[237]

5.4. General mechanistic aspects

The general pathway for oxidative esterification involves the initial chemisorption of dissolved oxygen at the catalyst surface resulting to form $^{\bullet}O_2$ radicals (Scheme 5).[88,215,239,240] Co-adsorbed organic substrates react with the superoxide radical *via* the C=C or C≡C bond in alkenes or alkynes, resulting in the formation of aldehydes (from alkenes) and ketones (from alkynes). Under basic conditions, alcohols readily undergo hydrogen abstraction or dehydrogenation to form aldehydes. Aldehydes are further converted to hemiacetal intermediates in the presence of alcohols,[88,235,240] and soluble bases (such as Na_2CO_3, KOH, or K_2CO_3) or basic supports (such as N-doped carbons). However, aldehydes can also be oxidised to carboxylic acids, which can be converted to esters over acidic supports. Although the formation of acids during the reaction can potentially deactivate the catalyst, the presence of soluble bases or basic supports helps to neutralise these thereby maintaining catalytic activity. For alkynes, the reaction proceeds through the formation of ketones, which are then converted to hemiacetal intermediates, whose subsequent oxidation forms ketoesters. Ketoesters are converted to esters *via* a 1,2-hydride shift or C–C bond cleavage (Fig. 20).[239] This mechanism highlights the role of both radicals and non-radical intermediates in the oxidative esterification process, as well as the importance of bases or basic supports in facilitating various reaction steps and neutralising by-products.

6. Conclusions and future perspectives

The oxidative esterification of aldehydes, alcohols, alkenes and alkynes has emerged as a versatile and sustainable approach to ester synthesis, particularly with the development of heterogeneous carbon catalysts which offer recyclability, low by-product formation, and reduced environmental impact. Carbons such as graphene, mesoporous carbons, and N-doped carbon have shown promise due to their high surface area, stability, and tuneable basicity. Among these, N-doped carbons with pyridinic or graphitic N-species exhibit the optimal basicity. In contrast, acidic carbon materials, particularly those doped with P or B, have received considerably less attention. This limited exploration may be attributed to the challenges in precisely tuning the acidity of these materials to suppress side reactions such as acetal formation. Investigating and optimising the acidic properties of P and B doped carbon materials could open new avenues for enhancing catalytic efficiency and selectivity in oxidative esterification processes. In addition, the use of molecular oxygen as a green oxidant is consistent with the principles of green chemistry and provides a more sustainable route to ester production. Oxidative esterification using carbon-based materials has been extensively explored under thermocatalytic conditions (Fig. 23). Thermocatalysis offers well-established reaction pathways, good substrate scope, and high selectivity when using functionalised carbons (*e.g.*, doped graphene or activated carbon) as supports. Currently, most oxidative esterification reactions focus on aldehydes and alcohols, which are typically derived from alkenes and alkynes. However, the relatively low reactivity of alkenes and alkynes in oxidative esterification has limited their exploration in this field. Given their synthetic potential, further research in this area could lead to the development of novel methodologies and expanded industrial applications.

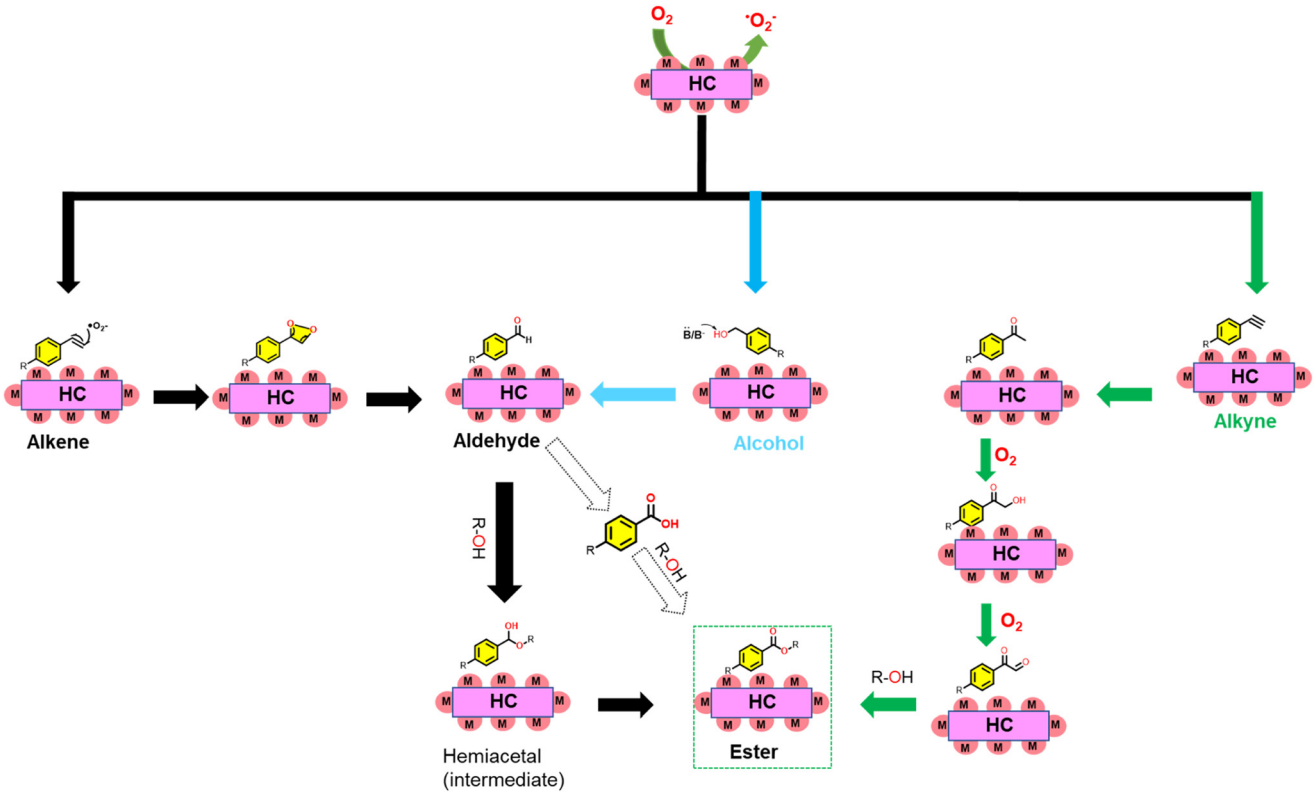

Scheme 5 General reaction pathways for the oxidative esterification of alkenes, alkynes, alcohols, and aldehydes.

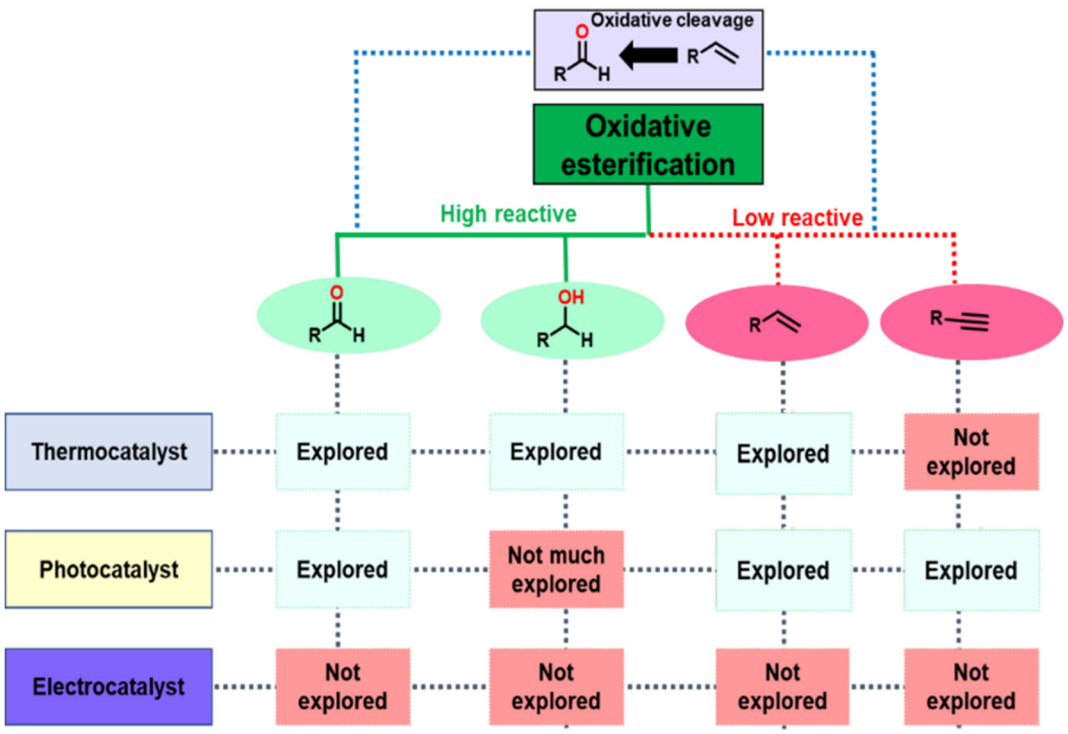

Fig. 23 Catalytic approaches for the oxidative esterification of aldehydes, alcohols, alkenes and alkynes using carbons.

Doped carbons benefit from thermal stability, tuneable surface functionalities, and compatibility with metal co-catalysts. However, the requirement of elevated temperatures often leads to high energy consumption and possible over-

oxidation, especially with sensitive substrates like alkenes or alkynes. Au/carbon catalysts are predominantly employed in the oxidative esterification of alcohols to esters, owing to their high selectivity and ability to activate oxygen under mild conditions. In contrast, Co/carbon catalysts are widely utilised for the oxidative esterification of bio-derived aldehydes such as furfural and 5-HMF to their corresponding esters. Notably, the incorporation of N dopants into the carbon support enhances catalytic performance by modulating the electronic environment of metal (*e.g.*, Au or Co) nanoparticles. The electron-donating nature of N-doped carbons facilitates charge transfer to the metal (Au, Co) centres, thereby tuning their oxidative properties and improving overall catalytic activity and selectivity. However, the conversion of hemiacetal intermediates to esters remains both kinetically challenging and thermodynamically unfavourable, particularly when employing bulky alcohols.

Photo-oxidative esterification using carbon-based photocatalysts remains relatively underexplored, with only a few reports demonstrating activity under UV or visible light. These approaches offer greener alternatives by utilising solar energy and mild conditions, yet they are limited by poor light absorption, fast electron–hole recombination, and challenges in selectively activating both the oxidant and the substrate. Electrochemical processes driven by renewable electricity are viewed as a promising way to decarbonize the chemical industry.[249] However, to date, electrochemical oxidative esterification using carbon catalysts has not been reported, likely due to the complexity of managing multiple electron-transfer steps, the need for selective coupling between intermediates, and insufficient understanding of reaction kinetics at the electrode interface. This highlights a significant research gap and an opportunity for innovation in the development of mild, selective, and energy-efficient electro-oxidative esterification protocols. Electrochemical oxygen reduction reaction has been extensively studied using heteroatom-doped carbon materials in combination with redox-active molecules, with the role of metals in N-doped carbons recently reviewed.[250] Electrochemical esterification has emerged as a promising reaction, with the electrochemical dehydration of carboxylic acids with alcohols using trimethoxy-*N*-phenylphenothiazine as a catalyst reported.[251] Oxidative coupling of aldehydes and alcohols using tetrabutylammonium fluoride (TBAF) as an electrolyte and methanol solvent is also possible at room temperature (Fig. 24).[252]

Despite these advances, carbon-based electrocatalysts, which have been widely used in oxygen reduction reactions, have not been extensively applied to electrochemical oxidative esterification reactions, making this an exciting area for future development. As illustrated in recent mechanistic analyses (Fig. 24a and b), a key challenge in catalytic esterification lies in reconciling the opposing electronic demands of the catalytic cycle. The electron-poor conditions favour acid activation and nucleophilic acyl substitution, while electron-rich conditions promote catalyst turnover through water elimination. Electrochemical approaches offer a unique opportunity to overcome this limitation by dynamically modulating the oxidation state of the catalyst during the reaction. For instance, electrochemical

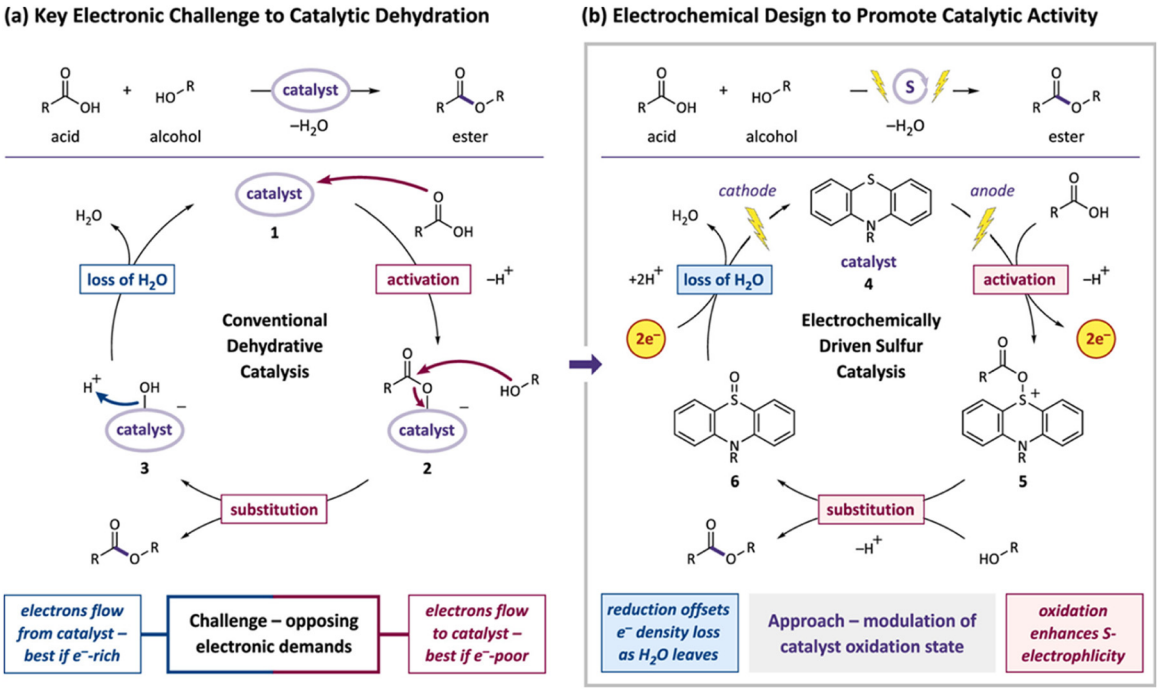

Fig. 24 (a) Conventional catalytic esterification is complicated by opposing electronic demands on the catalyst electron density in different steps of its cycle. (b) Electrochemical processes may overcome this challenge by modulating the catalyst oxidation states.[247] Reproduced with permission from ref. 236. Copyright 2023 American Chemical Society.

oxidation can generate electron-deficient catalytic species to facilitate acyl activation, while subsequent reduction restores electron richness to enable dehydration and catalyst regeneration. Extending this redox-switchable concept to carbon-based electrocatalysts such as N-doped carbon and mesoporous carbon could provide tuneable electronic environments, high stability, and scalable platforms for sustainable oxidative esterification processes. The potential of carbon materials in electrochemical esterification is significant due to their low cost, structural diversity, and tuneable properties. However, a critical aspect to consider with "metal-free" carbon materials is whether residual metal impurities play a role in the reaction. At low concentrations, these impurities are often difficult to detect using conventional techniques such as XPS and energy dispersive X-ray spectroscopy (EDX). However, it has been shown how metal residues can enhance catalytic activity in electrochemical oxygen reduction reactions, raising an important question regarding the true metal-free nature of certain carbon-based catalysts.[253]

This review has highlighted the critical role of catalyst supports and their influence on oxidative esterification reactions, with the importance of using systematic control experiments to identify the nature of active sites in heteroatom-doped carbon materials. Even though significant progress has been made in this area, important challenges remain, notably improvements in the activation of molecular oxygen, control of reaction selectivity and long-term stability of carbon-based catalysts are required. In addition, the development of high-performance base metal catalysts as alternatives to precious metals could improve cost effectiveness and sustainability. A deeper understanding of the specific roles that different carbon structures and functional groups play in catalysis will be critical in designing next generation carbon materials with improved selectivity, durability, and efficiency. However, to achieve this requires a change in the way many studies are reported with more emphasis on detailed characterisation and control over the particle size and accessibility of metal/metal oxide dopants. Many studies operate under reaction conditions that are focussed on high conversion and consequently diffusion limited making it impossible to discern trends in catalytic activity and identify the nature of the active site for optimisation. Without accurate kinetic studies to determine activity and productivity, the ability to identify structure–activity–basicity relationships and inform optimisation of next generation catalysts will continue to falter.

Flow oxidative esterification presents a scalable and sustainable route for ester synthesis, particularly when leveraging advanced catalyst systems. A recent study has demonstrated a continuous-flow method utilising *in situ* generated persulfuric acid for aldehyde esterification, effectively mitigating the hazards associated with batch use of strong oxidants while achieving high conversion of aldehydes (82–100%) and selectivity of various aromatic esters (44–99%) under controlled conditions.[254] Similarly, a base-free oxidative esterification of allylic, aliphatic and benzylic alcohols using H_2O_2 and Au/TiO_2 catalysts has been reported in flow, where reaction selectivity could be tuned simply through temperature adjustments, offering flexibility and safety for industrial adaptation. The oxidative esterification of 1-decanol was conducted at >70 °C achieving 100% selectivity towards esters,[255] with further advances demonstrating the efficacy of Au/ZnO for the oxidative esterification of octanal and 1-octanol with ethanol in both batch and flow systems, highlighting the improved reaction control and scalability afforded by flow reactors.[256]

Use of bimetallic metal nanoparticles can offer additional synergy, with Co and Ru deposited on N-doped ordered porous carbon (Co_xO_y–N + RuO_x–N@C-irregular), achieving outstanding activity and selectivity in the base-free oxidative esterification of HMF. Additionally, under flow conditions a 15-fold increase in FDCM production was observed compared to batch reactions.[257] Complementing this a bimetallic Co_7Fe_3-NC catalyst has been reported that efficiently converted HMF to FDMC with high yield and formation rate under mild conditions, attributing its performance to synergistic metal interactions and the basicity of the nitrogen-doped carbon support.[55] Future research should focus on refining carbon support architectures through heteroatom doping, pore design, and surface functionalization and on integrating these catalysts into continuous-flow systems. Such advancements align well with green chemistry and circular economy goals, positioning carbon-based flow catalysis as a transformative approach for sustainable ester synthesis.

Conflicts of interest

The authors declare no competing interests.

Data availability

No primary research results, software or code have been included and no new data were generated or analysed as part of this review.

Acknowledgements

This research study was funded by the Deutsche Forschungsgemeinschaft (DFG, German Research Foundation, project number 388390466 TRR 247). This study was supported by the "Center for Solvation Science ZEMOS" funded by the German Federal Ministry of Education and Research (BMBF) and by the Ministry of Culture and Research of North Rhine-Westphalia. K. W. and A. F. L. acknowledge funding from the Australian Research Council (DP200100204, DP200100313, and LP190100849).

References

1 F. Oppong, C. S. Xu, X. L. Li and Z. Y. Luo, *Fuel Process. Technol.*, 2022, **229**, 107185.
2 R. Petibon, C. P. Aiken, L. Ma, D. Xiong and J. R. Dahn, *Electrochim. Acta*, 2015, **154**, 287–293.
3 I. Ambat, V. Srivastava and M. Sillanpää, *Renewable Sustainable Energy Rev.*, 2018, **90**, 356–369.
4 L. Lomba, B. Giner, I. Bandrés, C. Lafuente and M. R. Pino, *Green Chem.*, 2011, **13**, 2062–2070.
5 A. d. N. de Oliveira, D. T. de Oliveira, R. S. Angélica, E. H. d. A. Andrade, J. K. d. R. da Silva, G. N. d. Rocha Filho, N. Coral, L. H. d. O. Pires, R. Luque and L. A. S. do Nascimento, *React. Kinet., Mech. Catal.*, 2020, **130**, 633–653.
6 E. Garcia Sega and J. Clarke, *J. Chem. Educ.*, 2013, **90**, 1658–1661.
7 G. D. Yadav and M. S. M. M. Rahuman, *Org. Process Res. Dev.*, 2002, **6**, 706–713.
8 C. S. M. Pereira, V. M. T. M. Silva and A. E. Rodrigues, *Green Chem.*, 2011, **13**, 2658–2671.
9 M. Muszyński, J. Nowicki, A. Krasuska, E. Nowakowska-Bogdan, M. Bartoszewicz, M. Długosz, M. Zygadło and G. Dudek, *Polym. Degrad. Stab.*, 2023, **218**, 110592.
10 Z. Khan, F. Javed, Z. Shamair, A. Hafeez, T. Fazal, A. Aslam, W. B. Zimmerman and F. Rehman, *J. Ind. Eng. Chem.*, 2021, **103**, 80–101.
11 C. Xie, Z. W. Jiang, Y. Y. Pang, C. L. Xiao and J. L. Song, *Green Chem.*, 2024, **26**, 6886–6899.
12 W. Zhong, H. L. Liu, C. H. Bai, S. J. Liao and Y. W. Li, *ACS Catal.*, 2015, **5**, 1850–1856.
13 M. Zare, M. T. Golmakani and A. Sardarian, *Green Chem. Lett. Rev.*, 2020, **13**, 83–92.
14 J. H. Steele, M. X. Bozor and G. R. Boyce, *J. Chem. Educ.*, 2020, **97**, 4127–4132.
15 https://www.futuremarketinsights.com/reports/esters-market.
16 https://www.marketsandresearch.biz/report/211277/global-ester-market-2021-by-manufacturers-regions-type-and-application-forecast-to-2026.
17 https://www.verifiedmarketreports.com/product/methyl-benzoate-market/.
18 https://www.verifiedmarketreports.com/product/methyl-salicylate-market/.
19 https://www.verifiedmarketreports.com/product/ethyl-levulinate-market-size-and-forecast/.
20 https://www.verifiedmarketreports.com/product/methyl-levulinate-market/.
21 S. Munawar, A. F. Zahoor, S. M. Hussain, S. Ahmad, A. Mansha, B. Parveen, K. G. Ali and A. Irfan, *Heliyon*, 2024, **10**, e23416.
22 S. Tang, J. Yuan, C. Liu and A. Lei, *Dalton Trans.*, 2014, **43**, 13460–13470.
23 S. Gaspa, A. Porcheddu and L. De Luca, *Tetrahedron Lett.*, 2016, **57**, 3433–3440.
24 F. E. A. Van Waes, J. Drabowicz, A. Cukalovic and C. V. Stevens, *Green Chem.*, 2012, **14**, 2776–2779.
25 H. Yang, Y. Jiao, G. Zhang, P. Gao and F. Chen, *J. Catal.*, 2025, **447**, 116154.
26 A. Abiko, J. C. Roberts, T. Takemasa and S. Masamune, *Tetrahedron Lett.*, 1986, **27**, 4537–4540.
27 P. Sundararaman, E. C. Walker and C. Djerassi, *Tetrahedron Lett.*, 1978, 1627–1628.
28 M. Mirza-Aghayan, S. Zonoubi, M. Molaee Tavana and R. Boukherroub, *Ultrason. Sonochem.*, 2015, **22**, 359–364.
29 P. Li, J. J. Zhao, R. Lang, C. G. Xia and F. Li, *Tetrahedron Lett.*, 2014, **55**, 390–393.
30 J. J. Wang, F. Jiang, C. F. Tao, H. Yu, L. Ruhlmann and Y. G. Wei, *Green Chem.*, 2021, **23**, 2652–2657.
31 K. Wilson and J. H. Clark, *Pure Appl. Chem.*, 2000, **72**, 1313–1319.
32 R. Y. Wang, H. Liu, C. Y. Fan, J. Gao, C. M. Chen and Z. F. Zheng, *Mol. Catal.*, 2020, **484**, 110687.
33 C. P. Ferraz, A. H. Braga, M. N. Ghazzal, M. Zieliński, M. Pietrowski, I. Itabaiana, F. Dumeignil, L. M. Rossi and R. Wojcieszak, *Catalysts*, 2020, **10**, 430.
34 Y. Li, Y. Zheng, L. Wang and Z. Fu, *ChemCatChem*, 2017, **9**, 1960–1968.
35 E. Lam and J. H. T. Luong, *ACS Catal.*, 2014, **4**, 3393–3410.
36 R. Radhakrishnan, S. Thiripuranthagan, A. Devarajan, S. Kumaravel, E. Erusappan and K. Kannan, *Appl. Catal., A*, 2017, **545**, 33–43.
37 Y. Zheng, C. Huang, Y. Li, Y. Yang and R. Xu, *ChemCatChem*, 2024, **16**, e202300976.
38 L. J. Ding, P. Z. Su, Y. L. Shi, H. Huang, L. Zhu, H. J. Zhang and B. H. Wang, *Ind. Eng. Chem. Res.*, 2024, **63**, 18667–18698.
39 M. Manzoli, F. Menegazzo, M. Signoretto and D. Marchese, *Catalysts*, 2016, **6**, 107.
40 D. Y. Zhao, T. Su, C. Len, R. Luque and Z. L. Yang, *Green Chem.*, 2022, **24**, 6782–6789.
41 K. Ekoue-Kovi and C. Wolf, *Chemistry*, 2008, **14**, 6302–6315.
42 Z. H. Zhang and K. J. Deng, *ACS Catal.*, 2015, **5**, 6529–6544.
43 M. Caporaso, G. Cravotto, S. Georgakopoulos, G. Heropoulos, K. Martina and S. Tagliapietra, *Beilstein J. Org. Chem.*, 2014, **10**(1), 1454–1461.
44 K. Nakajima, M. Hara and S. Hayashi, *J. Am. Ceram. Soc.*, 2007, **90**(12), 3725–3734.
45 T. Targel, P. Ramesh and M. Portnoy, *Eur. J. Org. Chem.*, 2018, **2018**, 3017–3021.
46 J. C. Craig and E. C. Horning, *J. Org. Chem.*, 1960, **25**, 2098–2102.
47 E. Gopi, E. Gravel and E. Doris, *Nanoscale Adv.*, 2019, **1**, 1181–1185.
48 N. Mori and H. Togo, *Tetrahedron*, 2005, **61**, 5915–5925.
49 Y. Tamaru, Y. Yamada, K. Inoue, Y. Yamamoto and Z. Yoshida, *J. Org. Chem.*, 1983, **48**, 1286–1292.
50 C. Liu, J. Wang, L. Meng, Y. Deng, Y. Li and A. Lei, *Angew. Chem., Int. Ed.*, 2011, **50**, 5144–5148.
51 N. Yamamoto, Y. Obora and Y. Ishii, *J. Org. Chem.*, 2011, **76**, 2937–2941.
52 H. Miyamura, T. Yasukawa and S. Kobayashi, *Green Chem.*, 2010, **12**, 776–778.

53 B. A. Yusuf, W. Yaseen, J. M. Xie, A. A. Babangida, A. I. Muhammad, M. Xie and Y. G. Xu, *Nano Energy*, 2022, **104**, 107959.
54 A. Abad, P. Concepción, A. Corma and H. García, *Angew. Chem., Int. Ed.*, 2005, **44**, 4066–4069.
55 N. Zheng and G. D. Stucky, *Chem. Commun.*, 2007, 3862–3864, DOI: 10.1039/B706864F.
56 I. S. Nielsen, E. Taarning, K. Egeblad, R. Madsen and C. H. Christensen, *Catal. Lett.*, 2007, **116**, 35–40.
57 S. S. R. Gupta, A. Vinu and M. L. Kantam, *J. Catal.*, 2020, **389**, 259–269.
58 W. Z. Xie, B. L. Chen, W. L. Jia, H. Liu, Z. Li, S. L. Yang, X. Tang, X. H. Zeng, Y. Sun, X. X. Ke, T. Y. Li, H. Y. Fang and L. Lin, *J. Energy Chem.*, 2022, **75**, 95–108.
59 A. Salazar, P. Hünemörder, J. Rabeah, A. Quade, R. V. Jagadeesh and E. Mejia, *ACS Sustainable Chem. Eng.*, 2019, **7**, 12061–12068.
60 T. W. Van Deelen, C. Hernández Mejía and K. P. de Jong, *Nat. Catal.*, 2019, **2**, 955–970.
61 K. T. Højholt, A. B. Laursen, S. Kegnæs and C. H. Christensen, *Top. Catal.*, 2011, **54**, 1026.
62 P. Mekrattanachai, L. Zhu, N. Setthaya, C. Chindawong and W. G. Song, *Catal. Lett.*, 2022, 1–12.
63 X. Wan, W. Deng, Q. Zhang and Y. Wang, *Catal. Today*, 2014, **233**, 147–154.
64 T. T. Ge, X. R. Liu, J. Tang, C. Liu and J. H. Huang, *Catalysts*, 2023, **13**, 1430.
65 X. Wang, R. Wang, J. Wang, C. Fan and Z. Zheng, *Phys. Chem. Chem. Phys.*, 2020, **22**, 1655–1664.
66 N. Huo, H. Ma, X. Wang, T. Wang, G. Wang, T. Wang, L. Hou, J. Gao and J. Xu, *Chin. J. Catal.*, 2017, **38**, 1148–1154.
67 T. Wang, H. Ma, X. Liu, Y. Luo, S. Zhang, Y. Sun, X. Wang, J. Gao and J. Xu, *Chem. – Asian J.*, 2019, **14**, 1515–1522.
68 D. Yin, Y. Zheng, L. Yang, S. Li, D. Zhu, Y. Guo, C. Zuo, Y. Li, H. Huang and M. Wang, *RSC Adv.*, 2021, **11**, 3280–3287.
69 V. Panwar, A. Al-Nafiey, A. Addad, B. Sieber, P. Roussel, R. Boukherroub and S. L. Jain, *RSC Adv.*, 2015, **5**, 88567–88573.
70 M. M. Titirici, R. J. White, N. Brun, V. L. Budarin, D. S. Su, F. del Monte, J. H. Clark and M. J. MacLachlan, *Chem. Soc. Rev.*, 2015, **44**, 250–290.
71 J. L. Fiorio, M. A. S. Garcia, M. L. Gothe, D. Galvan, P. C. Troise, C. J. r. Conte, P. Vidinha, P. H. C. Camargo and L. M. Rossi, *Coord. Chem. Rev.*, 2023, **481**, 215053.
72 H. Zhou, S. Hong, H. Zhang, Y. T. Chen, H. H. Xu, X. K. Wang, Z. Jiang, S. L. Chen and Y. Liu, *Appl. Catal., B*, 2019, **256**, 117767.
73 C. Xie, Q. Hou, H. Qian, Y. Tang, R. Lai, X. Bai, G. Yu, S. Lv, T. Xia, Z. Liu, X. Huang, X. Shen and M. Ju, *ChemSusChem*, 2025, **18**, 202402553.
74 C. Wang, Q. Wan, J. Cheng, S. Lin, A. Savateev, M. Antonietti and X. Wang, *J. Catal.*, 2021, **393**, 116–125.
75 S. Ncube, Z. Tian, J. Lin, H. Zhang, S. Wang and W. Tian, *Small*, 2025, **21**, 2504746.
76 L. H. Yu, S. Kasipandi, H. Chen, Y. Y. Li, X. L. Ma, Z. Wen and Y. D. Li, *React. Chem. Eng.*, 2022, **7**, 1191–1198.
77 Y. Wu, Y. Luo, S. Huang, J. Wang, J. Xu, X.-K. Gu and M. Ding, *ACS Catal.*, 2025, **15**, 1704–1714.
78 B. Wang, W. Ran, W. Sun and K. Wang, *Ind. Eng. Chem. Res.*, 2012, **51**, 3932–3938.
79 N. Dimitratos, A. Villa, D. Wang, F. Porta, D. S. Su and L. Prati, *J. Catal.*, 2006, **244**, 113–121.
80 L. Y. Wang, J. Li, W. Dai, Y. Lv, Y. Zhang and S. Gao, *Green Chem.*, 2014, **16**, 2164–2173.
81 X. Guo, Y. Si, Y. Huang, J. Zhang, X. Lyu, Y. Cheng and X. Li, *Ind. Eng. Chem. Res.*, 2023, **62**, 16309–16318.
82 L. L. Chng, J. Yang and J. Y. Ying, *ChemSusChem*, 2015, **8**, 1916–1925.
83 Y. Feng, W. Jia, G. Yan, X. Zeng, J. Sperry, B. Xu, Y. Sun, X. Tang, T. Lei and L. Lin, *J. Catal.*, 2020, **381**, 570–578.
84 H. Weerathunga, S. Sarina, H.-Y. Zhu and E. R. Waclawik, *ACS Omega*, 2021, **6**, 4740–4748.
85 M. S. Abaee, R. Sharifi and M. M. Mojtahedi, *Org. Lett.*, 2005, **7**, 5893–5895.
86 S. Sayama and T. Onami, *Synlett*, 2004, **2004**, 2739–2745.
87 J. Li, S. Wang, H. Li, Y. Tan and Y. Ding, *Int. J. Mol. Sci.*, 2021, **22**, 8668.
88 L. Jiang, Y. Diao, J. Han, R. Yan, X. Zhang and S. Zhang, *Chin. J. Chem. Eng.*, 2014, **22**, 1098–1104.
89 S. Singh and A. Patel, *Catal. Lett.*, 2014, **144**, 1557–1567.
90 S. Mahmood, T. Li, B. H. Xu, Y. F. Guo and S. J. Zhang, *Asian J. Org. Chem.*, 2017, **6**, 768–774.
91 D. Yin, Y. Zheng, L. Yang, S. Li, D. Zhu, Y. Guo, C. Zuo, Y. Li, H. Huang and M. Wang, *RSC Adv.*, 2021, **11**, 3280–3287.
92 S.n.-S.n. Ángela, S.r.-G.a. FabiÁn, M. n.-A. Amelia and T. n. Juan, *ACS Appl. Mater. Interfaces*, 2014, **6**(23), 21237–21247.
93 N. D. Lysenko, P. S. Yaremov, M. V. Ovcharova and V. G. Ilyin, *J. Mater. Sci.*, 2012, **47**, 3089–3095.
94 M. B. Plutschack, B. Pieber, K. Gilmore and P. H. Seeberger, *Chem. Rev.*, 2017, **117**(18), 11796–11893.
95 S. A. Dastgheib, H. Salih, T. Ilangovan and J. Mock, *ACS Omega*, 2020, **5**(33), 21172–21180.
96 A. K. Ipadeola, M. Chitt, A. Abdelgawad, K. Eid and A. M. Abdullah, *Int. J. Hydrogen Energy*, 2023, **48**(46), 17434–17467.
97 https://doi.org/10.1039/9781782622567-00001.
98 W. Guan, T. F. Fang, Y. L. Zhang, S. W. Xu, M. L. Jia, B. Liu and Z. H. Zhang, *Green Chem.*, 2024, **26**, 3139–3145.
99 R. C. Contreras, B. Guicheret, B. F. Machado, C. Rivera-Cárcamo, M. A. C. Alvarez, B. V. Salas, M. Ruttert, T. Placke, A. F. Réguillon, L. Vanoye, C. de Bellefon, R. Philippe and P. Serp, *J. Catal.*, 2019, **372**, 226–244.
100 D. N. Bikiaris, D. S. Achilias, D. J. Giliopoulos and G. P. Karayannidis, *Eur. Polym. J.*, 2006, **42**, 3190–3201.
101 C. M. Domínguez, P. Ocón, A. Quintanilla, J. A. Casas and J. J. Rodriguez, *Appl. Catal., B*, 2014, **144**, 599–606.
102 M. Sankar, Q. He, R. V. Engel, M. A. Sainna, A. J. Logsdail, A. Roldan, D. J. Willock, N. Agarwal, C. J. Kiely and G. J. Hutchings, *Chem. Rev.*, 2020, **120**(8), 3890–3938.
103 G. Collin, *Industrial Carbon and Graphite Materials, Volume I: Raw Materials, Production and Applications*, 2021, vol. 1, pp. 33–43.

104 J.-L. K. Gbe, K. Ravi, M. Singh, S. Neogi, M. Grafouté and A. V. Biradar, *J. CO2 Util.*, 2022, **65**, 102222.
105 K. Ravi, J. H. Advani, B. D. Bankar, A. S. Singh and A. V. Biradar, *New J. Chem.*, 2020, **44**, 18714–18723.
106 X.-H. Li and M. Antonietti, *Chem. Soc. Rev.*, 2013, **42**, 6593–6604.
107 R. Kalusulingam, K. Ravi, S. Mathi, N. Yadhav, A. S. Mikheykin, A. V. Biradar, K. Srinivasan and T. Myasoedova, *Mater. Today Sustain.*, 2024, **27**, 100864.
108 Q. Zhai, H. Huang, T. Lawson, Z. Xia, P. Giusto, M. Antonietti, M. Jaroniec, M. Chhowalla, J. B. Baek, Y. Liu, S. Qiao and L. Dai, *Adv. Mater.*, 2024, **36**, e2405664.
109 M. M. Titirici and M. Antonietti, *Chem. Soc. Rev.*, 2010, **39**, 103–116.
110 C. Xie, L. F. Lin, L. Huang, Z. X. Wang, Z. W. Jiang, Z. H. Zhang and B. X. Han, *Nat. Commun.*, 2021, **12**, 4823.
111 P. González-García, *Renewable Sustainable Energy Rev.*, 2018, **82**, 1393–1414.
112 M. S. Ahmed, D. S. Mannel, T. W. Root and S. S. Stahl, *Org. Process Res. Dev.*, 2017, **21**, 1388–1393.
113 C. A. Wilde, Y. Ryabenkova, I. M. Firth, L. Pratt, J. Railton, M. Bravo-Sanchez, N. Sano, P. J. Cumpson, P. D. Coates, X. Liu and M. Conte, *Appl. Catal., A*, 2019, **570**, 271–282.
114 M. Zheng, Z. N. Xu and M. L. Fu, *J. Environ. Chem. Eng.*, 2022, **10**, 107932.
115 U. Habib, F. Ahmad, M. Awais, N. Naz, M. Aslam, M. Urooj, A. Moqeem, H. Tahseen, A. Waqar and M. Sajid, *J. Chem. Environ.*, 2023, **2**, 14–53.
116 H. Veisi, F. Khorasani, T. Tamoradi, S. G. Saremi, M. Noroozi, S. Hemmati and B. Karmakar, *Inorg. Chem. Commun.*, 2024, **160**, 111869.
117 X. Z. Yu, L. Ni, E. S. Bai, M. Miao, X. Y. Tang and L. Y. Wang, *Mol. Catal.*, 2024, **569**, 114526.
118 P. Kumar, G. Singh, X. Guan, J. Lee, R. Bahadur, K. Ramadass, P. Kumar, M. G. Kibria, D. Vidyasagar, J. Yi and A. Vinu, *Chem. Soc. Rev.*, 2023, **52**, 7602–7664.
119 W. Guan, Y. L. Zhang, Y. N. Wei, B. Li, Y. H. Feng, C. H. Yan, P. W. Huo and Y. S. Yan, *Fuel*, 2020, **278**, 118362.
120 K. B. Patel, B. Parmar, K. Ravi, R. Patidar, G. R. Bhadu, J. C. Chaudhari and D. N. Srivastava, *Appl. Surf. Sci.*, 2023, **616**, 156499.
121 L. Yu, H. Chen, Y. Li, Z. Wen and Y. Li, *Catal. Today*, 2023, **408**, 58–63.
122 W. Xue, Q. Zhou, X. Cui, S. Jia, J. Zhang and Z. Lin, *Nano Energy*, 2021, **86**, 106073.
123 Y. Wu, Z. W. Zhuang, C. Chen, J. Z. Li, F. X. Xiao and C. Chen, *Chem Catalysis*, 2023, **3**, 100586.
124 V. Z. Radkevich, T. L. Senko, K. Wilson, L. M. Grishenko, A. N. Zaderko and V. Y. Diyuk, *Appl. Catal., A*, 2008, **335**, 241–251.
125 W. Al-Hajri, Y. De Luna and N. Bensalah, *Energy Technol.*, 2022, **10**, 2200498.
126 Q. Zhang, D. Zhang, Y. Zhou, J. Qian, X. Wen, P. Jiang, L. Ma, C. Lu, F. Feng and X. Li, *ChemistrySelect*, 2022, **7**, 202102581.
127 H. Wang, Y. Shao, S. Mei, Y. Lu, M. Zhang, J. K. Sun, K. Matyjaszewski, M. Antonietti and J. Yuan, *Chem. Rev.*, 2020, **120**, 9363–9419.
128 R. Kalusulingam, K. Ravi, S. Mathi, T. S. Mikhailova, K. Srinivasan, A. V. Biradar and T. N. Myasoedova, *Colloids Surf., A*, 2024, **692**, 133959.
129 J. H. Advani, K. Ravi, D. R. Naikwadi, H. C. Bajaj, M. B. Gawande and A. V. Biradar, *Dalton Trans.*, 2020, **49**, 10431–10440.
130 S. J. Yu, L. Z. Wang, Q. H. Li, Y. G. Zhang and H. Zhou, *Mater. Today Sustain.*, 2022, **19**, 100209.
131 S. Tian, Y. S. Wang, T. H. Cai, D. Q. Kong, D. D. Wang, H. Ren and W. Xing, *Appl. Surf. Sci.*, 2020, **534**, 147635.
132 C. T. Nguyen and D.-P. Kim, *J. Mater. Chem.*, 2011, **21**, 14226–14230.
133 H. Y. Cheng, X. M. Wu, X. C. Li, Y. Y. Zhang, M. M. Feng, Z. H. Fan and G. H. He, *J. Catal.*, 2021, **395**, 63–69.
134 G. L. Liu, Z. M. Liu, J. L. Li, M. Zeng, Z. Y. Li, L. He and F. W. Li, *Carbon*, 2018, **137**, 68–77.
135 T. S. Zhou, Y. Zhou, R. G. Ma, Z. Z. Zhou, G. H. Liu, Q. Liu, Y. F. Zhu and J. C. Wang, *Carbon*, 2017, **114**, 177–186.
136 J. Campos-Delgado, I. O. Maciel, D. A. Cullen, D. J. Smith, A. Jorio, M. A. Pimenta, H. Terrones and M. Terrones, *ACS Nano*, 2010, **4**, 1696–1702.
137 M. W. Li, X. Wu, J. H. Zeng, Z. H. Hou and S. J. Liao, *Electrochim. Acta*, 2015, **182**, 351–360.
138 Y. M. Manawi, Ihsanullah, A. Samara, T. Al-Ansari and M. A. Atieh, *Materials*, 2018, **11**, 822.
139 M. Möller, P. Nilges, F. Harnisch and U. Schröder, *ChemSusChem*, 2011, **4**, 566–579.
140 L. Ndlwana, N. Raleie, K. M. Dimpe, H. F. Ogutu, E. O. Oseghe, M. M. Motsa, T. A. M. Msagati and B. B. Mamba, *Materials*, 2021, **14**, 5094.
141 S. A. Nicolae, H. Au, P. Modugno, H. Luo, A. E. Szego, M. Qiao, L. Li, W. Yin, H. J. Heeres, N. Berge and M. M. Titirici, *Green Chem.*, 2020, **22**, 4747–4800.
142 M. T. Gilbert, J. H. Knox and B. Kaur, *Chromatographia*, 1982, **16**, 138–148.
143 P. Wang, G. Zhang, W. Chen, Q. Chen, H. Jiao, L. Liu, X. Wang and X. Deng, *ACS Omega*, 2020, **5**, 23460–23467.
144 M. A. Ferry, J. Maruyama, T. A. Asoh and H. Uyama, *Electrochemistry*, 2022, **90**, 077004.
145 L. Chuenchom, R. Kraehnert and B. M. Smarsly, *Soft Matter*, 2012, **8**, 10801–10812.
146 M. Xu, A. Wang, Y. Xiang, A. Ejaz and J. Niu, *Ind. Crops Prod.*, 2022, **176**, 114291.
147 X. Wang, X. Wang, X. Zhou, X. Yang, X. Wu, P. Zhou, J. Zhou and S. Zhuo, *J. Energy Storage*, 2023, **57**, 106221.
148 M. Ovcharov, N. Shcherban, S. Filonenko, A. Mishura, M. Skoryk, V. Shvalagin and V. Granchak, *Mater. Sci. Eng., B*, 2015, **202**, 1–7.
149 F. Hajiali, T. Jin, G. Yang, M. Santos, E. Lam and A. Moores, *ChemSusChem*, 2022, **15**, e202102535.
150 V. Ambrogi, G. Gentile, C. Ducati, M. C. Oliva and C. Carfagna, *Polymer*, 2012, **53**, 291–299.

151 F. Shen, X. N. Xiong, J. Y. Fu, J. R. Yang, M. Qiu, X. H. Qi and D. C. W. Tsang, *Renewable Sustainable Energy Rev.*, 2020, **130**, 109944.
152 H. J. Wu, Z. D. Li, D. Q. Ji, Y. Liu, L. L. Li, D. D. Yuan, Z. H. Zhang, J. W. Ren, M. Lefler, B. H. Wang and S. Licht, *Carbon*, 2016, **106**, 208–217.
153 F. Gao, Y. H. Zang, Y. Wang, C. Q. Guan, J. Y. Qu and M. B. Wu, *New Carbon Mater.*, 2021, **36**, 34–45.
154 M. Ni, L. Zhou, Y. Liu and R. Ni, *Front. Chem.*, 2023, **11**, 1205280.
155 Z. Wei, Z. Yanfei and W. Jiao, *Front. Mater.*, 2025, **12**, 1548671.
156 L. Li, S. Lu, L. Fang, Y. J. Wei and S. L. Yang, *Energy Fuels*, 2023, **37**, 18485–18501.
157 T. X. Li, X. F. An and D. Fu, *Energy Fuels*, 2023, **37**, 8160–8179.
158 Y. Yin, Q. Liu, Y. Zhao, T. Chen, J. Wang, L. Gui and C. Lu, *Energy Fuels*, 2023, **37**, 3523–3554.
159 Z. Li, L. Y. Liu, Z. Wang, P. Gao and G. K. Li, *Energy Fuels*, 2023, **37**, 3413–3427.
160 K. H. Cao, S. B. Zhang, Y. W. Shi, X. Y. Diao, R. H. Wei and N. Ji, *ACS Nano*, 2025, **19**, 12734–12761.
161 S. Kundu, T. Khandaker, M. A. M. Anik, M. K. Hasan, P. K. Dhar, S. K. Dutta, M. A. Latif and M. S. Hossain, *RSC Adv.*, 2024, **14**, 29693–29736.
162 X. S. Zhang, T. Q. Cao, G. Y. Zhang, Q. Liu, G. Kong, K. J. Wang, Y. Jiang, X. Zhang and L. J. Han, *J. Mater. Chem. A*, 2024, **12**, 4996–5039.
163 G. Y. Zhang, X. Liu, L. Wang and H. G. Fu, *J. Mater. Chem. A*, 2022, **10**, 9277–9307.
164 H. F. Zhang, Y. H. Zhang, L. Q. Bai, Y. G. Zhang and L. Sun, *J. Mater. Chem. A*, 2021, **9**, 12521–12552.
165 T. Khandaker, T. Islam, A. Nandi, M. A.-A. M. Anik, M. S. Hossain, M. K. Hasan and M. S. Hossain, *Sustainable Energy Fuels*, 2025, **9**, 693–723.
166 K. Liang, Y. L. Chen, D. Wang, W. C. Wang, S. Y. Jia, N. Mitsuzakic and Z. D. Chen, *Sustainable Energy Fuels*, 2023, **7**, 3541–3559.
167 J. Wang, P. Nie, B. Ding, S. Y. Dong, X. D. Hao, H. Dou and X. G. Zhang, *J. Mater. Chem. A*, 2017, **5**, 2411–2428.
168 Q. Chen, X. F. Tan, Y. G. Liu, S. B. Liu, M. F. Li, Y. L. Gu, P. Zhang, S. J. Ye, Z. Z. Yang and Y. Y. Yang, *J. Mater. Chem. A*, 2020, **8**, 5773–5811.
169 W. Xin and Y. H. Song, *RSC Adv.*, 2015, **5**, 83239–83285.
170 Y. Feng, S. Long, G. Yan, W. Jia, Y. Sun, X. Tang, Z. Zhang, X. Zeng and L. Lin, *J. Catal.*, 2021, **397**, 148–155.
171 C. Wang, D. Wu, H. Wang, Z. Gao, F. Xu and K. Jiang, *J. Mater. Chem. A*, 2018, **6**, 1244–1254.
172 H. Liu, N. Ding, J. Wei, X. Tang, X. Zeng, Y. Sun, T. Lei, H. Fang, T. Li and L. Lin, *ChemSusChem*, 2020, **13**, 4151–4158.
173 C. Liu, Y. Q. Hu, Y. F. Yu, Y. Zhang, Y. Y. Wang and A. B. Chen, *Adv. Mater. Res.*, 2012, **554**, 778–782.
174 Y. Hu, J. Xia, J. Li, H. Li, Y. Li, S. Li, C. Duanmu, B. Li and X. Wang, *J. Mater. Sci.*, 2021, **56**, 7308–7320.
175 X. Yu, X. Huang, W. Jia, J. Chen, S. Yang, L. Peng, Y. Sun, X. Tang, X. Zeng and S. Yang, *Mol. Catal.*, 2023, **546**, 113197.
176 H. Liu, N. Ding, J. Wei, X. Tang, X. Zeng, Y. Sun, T. Lei, H. Fang, T. Li and L. Lin, *ChemSusChem*, 2020, **13**, 4151–4158.
177 M. E. Casco, S. Kirchhoff, D. Leistenschneider, M. Rauche, E. Brunner and L. Borchardt, *Nanoscale*, 2019, **11**, 4712–4718.
178 A. Hachimi, B. Merzougui, A. Hakeem, T. Laoui, G. M. Swain, Q. Chang, M. Shao and M. A. Atieh, *J. Nanomater.*, 2015, **2015**, 453725.
179 T. Q. Bui, L. J. Konwar, A. Samikannu, D. Nikjoo and J.-P. Mikkola, *ACS Sustainable Chem. Eng.*, 2020, **8**, 12852–12869.
180 B. Hu, L. Warczinski, X. Li, M. Lu, J. Bitzer, M. Heidelmann, T. Eckhard, Q. Fu, J. Schulwitz and M. Merko, *Angew. Chem., Int. Ed.*, 2021, **60**, 6807–6815.
181 M. M. Abdelnaby, M. Aliyu, M. A. Nemitallah, A. M. Alloush, E.-H. M. Mahmoud, K. M. Ossoss, M. Zeama and M. Dowaidar, *Polymers*, 2023, **15**, 2475.
182 M. Qian, Z. Wang, Z. Li, J. Xu, P. Sun, J. Lin, T. Lin and F. Huang, *Microporous Mesoporous Mater.*, 2019, **286**, 18–24.
183 K. T. V. Rao, Y. Hu, Z. Yuan, Y. Zhang and C. C. Xu, *Chem. Eng. J.*, 2021, **404**, 127063.
184 Y. Lin, G.-P. Lu, X. Zhao, X. Cao, L. Yang, B. Zhou, Q. Zhong and Z. Chen, *Mol. Catal.*, 2020, **482**, 110695.
185 X. Zhao, L. Xiao, F. Wang, Z. Shen, R. Fang and Y. J. A. J. Li, *AIChE J.*, 2024, **70**, e18537.
186 J. Deng, H. J. Song, M. S. Cui, Y. P. Du and Y. Fu, *ChemSusChem*, 2014, **7**, 3334–3340.
187 X. Sun, J. Bao, K. Li, M. D. Argyle, G. Tan, H. Adidharma, K. Zhang, M. Fan and P. Ning, *Adv. Funct. Mater.*, 2021, **31**(7), 2006287.
188 C. Du, J. Mo and H. Li, *Chem. Rev.*, 2015, **115**(3), 1503–1542.
189 M. Santos, M. M. M. Bilek and S. G. Wise, *Biosurf. Biotribol.*, 2015, **1**(3), 146–160.
190 D. Davies, S. Golunski, P. Johnston, G. Lalev and S. H. Taylor, *ACS Catal.*, 2018, **8**(4), 2730–2734.
191 K. Gong, F. Du, Z. Xia, M. Durstock and L. Dai, *Science*, 2009, **323**(5915), 760–764.
192 X. Liu and L. Dai, *Nat. Rev. Mater.*, 2016, **1**(11), 16064.
193 K. Sakamoto, K. Chida, S. Masuda, T. Yoshii, H. Nishihara and T. Tsukuda, *Green Chem.*, 2025, **27**, 8133–8142.
194 F. Mao, Z. Qi, H. Fan, D. Sui, R. Chen and J. Huang, *RSC Adv.*, 2017, **7**, 1498–1503.
195 H. Su, K.-X. Zhang, B. Zhang, H.-H. Wang, Q.-Y. Yu, X.-H. Li, M. Antonietti and J.-S. Chen, *J. Am. Chem. Soc.*, 2017, **139**, 811–818.
196 Z.-M. Xu, J.-Y. Luo and Y.-B. Huang, *Green Chem.*, 2022, **24**, 3895–3921.
197 J. L. Long, X. Q. Xie, J. Xu, Q. Gu, L. M. Chen and X. X. Wang, *ACS Catal.*, 2012, **2**, 622–631.
198 G. Wen, Q. Gu, Y. Liu, R. Schlögl, C. Wang, Z. Tian and D. S. Su, *Angew. Chem., Int. Ed.*, 2018, **57**, 16898–16902.
199 V. A. Ghadge, K. Ravi, D. R. Naikwadi, P. B. Shinde and A. V. Biradar, *Green Chem.*, 2023, **25**, 2863–2871.
200 S. Rautiainen, O. Simakova, H. Guo, A.-R. Leino, K. Kordás, D. Murzin, M. Leskelä and T. Repo, *Appl. Catal., A*, 2014, **485**, 202–206.

201 X. Yang, X. Wang, C. Liang, W. Su, C. Wang, Z. Feng, C. Li and J. Qiu, *Catal. Commun.*, 2008, **9**, 2278–2281.
202 M. Alhumaimess, Z. Lin, W. Weng, N. Dimitratos, N. F. Dummer, S. H. Taylor, J. K. Bartley, C. J. Kiely and G. J. Hutchings, *ChemSusChem*, 2012, **5**, 125–131.
203 E. Smolentseva, V. V. Costa, R. F. Cotta, O. Simakova, S. Beloshapkin, E. V. Gusevskaya and A. Simakov, *ChemCatChem*, 2015, **7**, 1011–1017.
204 M. Estrada, V. V. Costa, S. Beloshapkin, S. Fuentes, E. Stoyanov, E. V. Gusevskaya and A. Simakov, *Appl. Catal., A*, 2014, **473**, 96–103.
205 H. B. Yang, J. Miao, S. F. Hung, J. Chen, H. B. Tao, X. Wang, L. Zhang, R. Chen, J. Gao, H. M. Chen, L. Dai and B. Liu, *Sci. Adv.*, 2016, **2**, e1501122.
206 Y. Lin, Z. Liu, Y. Niu, B. Zhang, Q. Lu, S. Wu, G. Centi, S. Perathoner, S. Heumann, L. Yu and D. S. Su, *ACS Nano*, 2019, **13**, 13995–14004.
207 H. Watanabe, S. Asano, S. Fujita, H. Yoshida and M. Arai, *ACS Catal.*, 2015, **5**, 2886–2894.
208 Q. Zhang, H. He, H. Wang, Z. Zhang and C. Chen, *RSC Adv.*, 2019, **9**, 38891–38896.
209 M. A. Patel, F. Luo, M. R. Khoshi, E. Rabie, Q. Zhang, C. R. Flach, R. Mendelsohn, E. Garfunkel, M. Szostak and H. He, *ACS Nano*, 2016, **10**, 2305–2315.
210 X. Zhao, F. Wang, X. P. Kong, R. Fang and Y. Li, *J. Am. Chem. Soc.*, 2021, **143**, 16068–16077.
211 Y. Dong, G. Chen, X. Zuo, J. Li, J. Yu, G. Zhang, J. Kuang, I. Akpinar, L. Peng, X. Tang, J.-C. Dong, L. Lin, P. Lyu, S. Yang and J.-F. Li, *ACS Catal.*, 2024, **14**, 6565–6576.
212 L. M. Ning, S. Y. Liao, X. G. Liu, P. F. Guo, Z. Y. Zhang, H. G. Zhang and X. L. Tong, *J. Catal.*, 2018, **364**, 1–13.
213 B. Fuerte-Díez, E. Rangel-Rangel, M. Iglesias and E. M. Maya, *Appl. Catal., A*, 2023, **654**, 119088.
214 H. Veisi, Z. Ebrahimi, B. Karmakar, Z. Joshani and T. Ozturk, *Int. J. Biol. Macromol.*, 2021, **191**, 465–473.
215 Y. Wang, C.-y. Lu and Z.-f. Yin, *Mater. Lett.*, 2020, **270**, 127723.
216 A. Kumar, P. Kumar, A. K. Pathak, A. N. Chokkapu and S. L. Jain, *ChemistrySelect*, 2017, **2**, 3437–3443.
217 L. Song, S. Zhang, X. Wu, H. Tian and Q. Wei, *Ind. Eng. Chem. Res.*, 2012, **51**, 9510–9514.
218 R. P. Gaikwad, D. R. Naikwadi, A. V. Biradar and M. B. Gawande, *ACS Appl. Nano Mater.*, 2023, **6**, 1859–1869.
219 T. V. Astrakova, V. I. Sobolev and K. Y. Koltunov, *Catal. Commun.*, 2020, **137**, 105952.
220 Y. Zhang, Q. Xiao, Y. Bao, Y. Zhang, S. Bottle, S. Sarina, B. Zhaorigetu and H. Zhu, *J. Phys. Chem. C*, 2014, **118**, 19062–19069.
221 J. S. Jiang, X. Li, S. Y. Du, L. C. Shi, P. P. Jiang, P. B. Zhang, Y. M. Dong and Y. Leng, *New J. Chem.*, 2020, **44**, 7780–7785.
222 T. Y. Cheng, H. Yu, F. Peng, H. J. Wang, B. S. Zhang and D. S. Su, *Catal. Sci. Technol.*, 2016, **6**, 1007–1015.
223 Y.-X. Zhou, Y.-Z. Chen, L. Cao, J. Lu and H.-L. Jiang, *Chem. Commun.*, 2015, **51**, 8292–8295.
224 Z. Y. Long, X. W. Chen, P. Lu, S. Liu, G. J. Chen, M. M. Tong, L. M. Sun, W. W. Zhan and F. M. Huang, *Catal. Lett.*, 2019, **149**, 3160–3168.
225 H. He, S. Liu, Y. Liu, L. Zhou, H. Wen, R. Shen, H. Zhang, X. Guo, J. Jiang and B. Li, *Green Chem.*, 2023, **25**, 9501–9542.
226 R. Wang, K. Lu, J. Zhang, X. Li and Z. Zheng, *ACS Catal.*, 2022, **12**, 14290–14303.
227 D. S. Mannel, M. S. Ahmed, T. W. Root and S. S. Stahl, *J. Am. Chem. Soc.*, 2017, **139**, 1690–1698.
228 Q. Zhu, F. Wang, F. Zhang and Z. Dong, *Nanoscale*, 2019, **11**, 17736–17745.
229 V. Panwar, S. S. Ray and S. L. Jain, *Mol. Catal.*, 2017, **427**, 31–38.
230 D. Nandan, G. Zoppellaro, I. Medrik, C. Aparicio, P. Kumar, M. Petr, O. Tomanec, M. B. Gawande, R. S. Varma and R. Zboril, *Green Chem.*, 2018, **20**, 3542–3556.
231 P. Mondal, N. Salam, A. Mondal, K. Ghosh, K. Tuhina and S. M. Islam, *J. Colloid Interface Sci.*, 2015, **459**, 97–106.
232 Q. Hao, Z. Li, Y. Shi, R. Li, Y. Li, L. Wang, H. Yuan, S. Ouyang and T. Zhang, *Angew. Chem., Int. Ed.*, 2023, **62**, e202312808.
233 E. Lepre, S. Rat, C. Cavedon, P. H. Seeberger, B. Pieber, M. Antonietti and N. Lopez-Salas, *Angew. Chem., Int. Ed.*, 2023, **62**, e202211663.
234 K. Ravi, Y. S. Dalal, A. C. Sabu, M. S. A. Khalifa and A. V. Biradar, *Catal. Sci. Technol.*, 2024, **14**, 1653–1665.
235 X. Yu, Z. Zhao, L. Zhu, S. Tan, W. Fu, L. Wang and Y. An, *Mol. Catal.*, 2022, **519**, 112152.
236 H. Wang, R. Jia, M. Hong, H. Miao, B. Ni and T. Niu, *Green Chem.*, 2021, **23**, 6591–6597.
237 S. Rani, S. Aslam, K. Lal, S. Noreen, K. A. M. Alsader, R. Hussain, B. Shirinfar and N. Ahmed, *Chem. Rec.*, 2024, **24**, e202300331.
238 Z.-Y. Wang, S. Wang, N.-N. Dai, Y. Xiao, Y. Zhou, W.-C. Tian, D. Sun, Q. Li, Y. Wang and W.-T. Wei, *Nat. Commun.*, 2025, **16**, 993.
239 Y. Li, H. Luo, S. Wang, L. Li, G. Li and W. Dai, *iScience*, 2023, **26**, 107608.
240 R. Jia, J. Wang, Y. Jiang, B. Ni and T. Niu, *Org. Biomol. Chem.*, 2022, **20**, 8305–8312.
241 https://www.chemistryworld.com/news/ban-on-most-uses-of-dichloromethane-finalised-in-us/4019449.article.
242 J. Wang, B. Ni, T. Niu and F. Ji, *Catal. Sci. Technol.*, 2020, **10**, 8458–8464.
243 C. M. A. Parlett, M. A. Isaacs, S. K. Beaumont, L. M. Bingham, N. S. Hondow, K. Wilson and A. F. Lee, *Nat. Mater.*, 2016, **15**, 178–182.
244 M. A. Isaacs, C. M. A. Parlett, N. Robinson, L. J. Durndell, J. C. Manayil, S. K. Beaumont, S. Jiang, N. S. Hondow, A. C. Lamb, D. Jampaiah, M. L. Johns, K. Wilson and A. F. Lee, *Nat. Catal.*, 2020, **3**, 921–931.
245 L. J. Durndell, M. A. Isaacs, C. e. Li, C. M. A. Parlett, K. Wilson and A. F. Lee, *ACS Catal.*, 2019, **9**, 5345–5352.
246 A. Merenda, S. A. Orr, Y. Liu, B. Hernández Garcia, A. Osatiashtiani, G. Morales, M. Paniagua, J. A. Melero, A. F. Lee and K. Wilson, *ChemSusChem*, 2023, **15**, e202201224.
247 D. Xu, J. F. Li, B. Y. Li, H. C. Zhao, H. H. Zhu, J. F. Kou, F. W. Zhang, Z. P. Dong and J. T. Ma, *Chem. Eng. J.*, 2022, **434**, 134545.

248 Q. Wang, Z.-Y. Zhou, Y.-J. Lai, Y. You, J.-G. Liu, X.-L. Wu, E. Terefe, C. Chen, L. Song, M. Rauf, N. Tian and S.-G. Sun, *J. Am. Chem. Soc.*, 2014, **136**, 10882–10885.
249 D. S. Mallapragada, Y. Dvorkin, M. A. Modestino, D. V. Esposito, W. A. Smith, B.-M. Hodge, M. P. Harold, V. M. Donnelly, A. Nuz, C. Bloomquist, K. Baker, L. C. Grabow, Y. Yan, N. N. Rajput, R. L. Hartman, E. J. Biddinger, E. S. Aydil and A. D. Taylor, *Joule*, 2023, **7**, 23–41.
250 J. Masa, W. Xia, M. Muhler and W. Schuhmann, *Angew. Chem., Int. Ed.*, 2015, **54**, 10102–10120.
251 J. Han, C. A. Haines, J. J. Piane, L. L. Filien and E. D. Nacsa, *J. Am. Chem. Soc.*, 2023, **145**, 15680–15687.
252 D. Smeyne, K. Verboom, M. Bryan, J. LoBue and A. Shaikh, *Tetrahedron Lett.*, 2021, **68**, 152898.
253 J. Masa, A. Q. Zhao, W. Xia, Z. Y. Sun, B. Mei, M. Muhler and W. Schuhmann, *Electrochem. Commun.*, 2013, **34**, 113–116.
254 B. S. Nagy, G. Fu, C. A. Hone, C. O. Kappe and S. B. Ötvös, *ChemSusChem*, 2023, **16**, e202201868.
255 F. J. Roberts, C. Richard, F. W. Zemichael, K. K. Hii, K. Hellgardt, C. Brennan and D. A. Sale, *React. Chem. Eng.*, 2018, **3**, 942–948.
256 A. Taketoshi, T. Ishida, T. Murayama, T. Honma and M. Haruta, *Appl. Catal., A*, 2019, **585**, 117169.
257 A. Salazar, A. Linke, R. Eckelt, A. Quade, U. Kragl and E. Mejía, *ChemCatChem*, 2020, **12**, 3504–3511.